NASA TM- 85870

NASA Technical Memorandum 85870

A Study of Helicopter Gust Response Alleviation by Automatic Control

Shigeru Saito

December 1983

NASA
National Aeronautics and
Space Administration

NASA Technical Memorandum 85870

A Study of Helicopter Gust Response Alleviation by Automatic Control

Shigeru Saito, Ames Research Center, Moffett Field, California

National Aeronautics and
Space Administration

Ames Research Center
Moffett Field, California 94035

SYMBOLS

a	lift slope, or nondimensional distance between midchord of the wing and elastic axis (positive aft)
b	semichord, $c/2$
$C, C_{\Delta\theta}, C_o$	coefficients in equations (73) and (80)
C'	lift deficiency function, equation (B6)
C_{do}	airfoil profile drag coefficient
C_H, C_Y, C_T	horizontal force, side force, and thrust coefficients
C_{MX}, C_{MY}, C_{MZ}	rolling, pitching, and yawing moment coefficients
C_ζ	lag damper coefficient
c	chord length
D_i	induced drag
$E(\ )$	expectation of ( )
e	distance between elastic axis and feathering axis at blade root
e_o	distance between mass center and elastic axis of blade cross section
F_{ax}, F_{ay}, F_{az}	aerodynamic loads on the wing section, equation (B11)
F_X, F_Y, F_Z	net hub forces equal to (H,Y,T)
$\mathbf{F}_\ell$	hub forces vector of the ℓth blade, $(F_x, F_x, F_z)^T_\ell$
f_G	gust frequency
g	gravitational acceleration or the gust velocity vector
H	horizontal force in the rotor frame = $\rho(R\Omega)^2(\pi R^2)C_H$
h	plunging motion of wing cross section
I_β	moment of inertia of a blade about flapping hinge = $\int_{r_\beta}^{R} (r - r_\beta)^2 m\, dr$
i	imaginary unit = $\sqrt{-1}$
i_S	shaft inclination angle (positive fore)
J	quadratic performance function, equation (72)
J_n	Bessel function of the nth order

K_w, K_v, K_ϕ	feedback gain vectors, equation (26)
k	polar radius of gyration of a blade per unit span
k_n	Kalman gain at n time-cycle
L	blade lift per unit span
M	blade pitching moment per unit span
M_{ax}, M_{ay}, M_{az}	aerodynamic moments on the wing section, equation (B12)
M_n	variance of the error before the measurement at n time-cycle
M_X	net rolling moment = $\rho(R\Omega)^2(\pi R^2)RC_{MX}$
M_Y	net pitching moment = $\rho(R\Omega)^2(\pi R^2)RC_{MY}$
M_Z	net yawing moment = $\rho(R\Omega)^2(\pi R^2)RC_{MZ}$
M_β	mass moment of blade = $\int_{r_\beta}^{R} r(r - r_\beta)m\, dr$
M_ℓ	hub moments vector of the ℓth blade, $(M_x, M_y, M_z)_\ell^T$
m	mass per unit span
m_j	generalized mass of the jth mode, equation (2a)
N	number of blades
P	angular velocity of a rotor along the X_B-axis
P_n	variance of the error after the measurement at n time-cycle
Q	angular velocity of a rotor along the Y_B-axis, Floquet transition matrix, variance of the process noise, or hub inertia moment vector in equation (B3)
Q_j	generalized force of the jth mode, equation (2c)
q_j	generalized coordinate of the jth mode
$\hat{q}_k$	kth constant coefficient in the solution of Δq, equation (7)
Δq	perturbation generalized coordinate vector, equation (5)
R	rotor radius
R'	angular velocity of rotor along the Z_B-axis
r	radial coordinate of blade or variance of the measurement noise
r_β	position of flapping hinge
r_ζ	position of lag damper

T	thrust in the rotor frame = $\rho(R\Omega)^2(\pi R^2)C_T$ or period
T_C	transfer function matrix
$\mathbf{T}$	matrix, equation (59)
t	time
U	velocity of rotor along the X_B-axis
U_T, U_P, U_R	tangential, normal, and radial components of velocity at a blade element
u	radial deflection of a blade; process noise
u_G	horizontal component of gust velocity
V	velocity of a rotor along the Y_B-axis
v	lead-lag deflection of a blade; measurement noise
v_G	lateral component of gust velocity
W	velocity of a rotor along the Z_B-axis; gross weight
$W_z, W_\theta, W_{\Delta\theta}$	weighting matrices, equation (72)
w	flap deflection of a blade
w_G	vertical component of gust velocity
w_{Go}	gust amplitude
w_o'	precone angle
x	nondimensional radial coordinate = r/R
Y	side force in the rotor frame = $\rho(R\Omega)^2(\pi R^2)C_Y$
z	measurements
α	angle of attack
γ	Lock number = $\rho acR^4/I_\beta$
Δ	perturbation from a steady value, or small increment
δ	Kronecker delta function
θ	blade trim pitch input = $\theta_0 + \theta_t(x - 0.75) + \theta_{1c}\cos\psi + \theta_{1s}\sin\psi$
θ_t	blade twist rate
θ_0	collective pitch control
θ_{1c}	lateral pitch control

θ_{1s}	longitudinal pitch control
θ	control vector, equation (59)
$\Delta\theta$	control inputs, equation (57)
λ	inflow ratio = $(\nu_S + V \sin i_S)/R\Omega$
μ	advance ratio = $U \cos i_S/R\Omega$
ν_S	mean induced velocity
ρ	air density
σ	solidity = $Nc/\pi R$
ϕ	torsional deflection of a blade, inflow angle, or phase angle
ϕ_I, ϕ_{II}	phase shift in figure 17
ψ	azimuthal angle
Ω	rotor rotational speed
ω_G	gust angular velocity = $2\pi f_G$
ω_j	jth natural frequency of a blade
ω_L	lag frequency of a blade

Subscripts:

B	body frame
b	blade frame
C	control or cosine element
G	gust
H	rotational hub frame
I	inertial frame
j	jth mode
ℓ	ℓth blade
n	n time-cycle
R	rotor frame
S	sine element
0	initial value, amplitude, uncontrolled value, or origin

Superscripts:

$\bar{(\ )}$	trimmed value
$\dot{(\ )}$	d( )/dt
$\hat{(\ )}$	estimate of ( )
$(\ )'$	d( )/dX
$(\ )^T$	transpose of ( )

SUMMARY

Two control schemes designed to alleviate gust-induced vibration are analytically investigated for a helicopter with four articulated blades. One is an individual blade pitch control scheme. The other is an adaptive blade pitch control algorithm based on linear optimal control theory. In both controllers, control inputs to alleviate gust response are superimposed on the conventional control inputs required to maintain the trim condition. A sinusoidal vertical gust model and a step gust model are used. The individual blade pitch control, in this research, is composed of sensors and a pitch control actuator for each blade. Each sensor can detect flapwise (or lead-lag or torsionwise) deflection of the respective blade. The actuator controls the blade pitch angle for gust alleviation. Theoretical calculations to predict the performance of this feedback system have been conducted by means of the harmonic method. The adaptive blade pitch control system is composed of a set of measurements (oscillatory hub forces and moments), an identification system using a Kalman filter, and a control system based on the minimization of the quadratic performance function. Calculations for the individual blade pitch control system show that the thrust fluctuation can be reduced by more than 50% in the low gust frequency range. In addition, it was found that the adaptive blade pitch control system can also be useful for high frequency gusts.

1. INTRODUCTION

The helicopter has the capability of flying close to the ground where the motion of the atmosphere may be thought of as turbulent flow. To avoid structural vibrations and unfavorable dynamic characteristics in flying and riding qualities caused by gusty winds, it is necessary to analyze the gust response of a rotary wing aircraft and to develop a scheme to alleviate such responses.

Studies on the gust response of a helicopter rotor are reported in references 1-9. Many different assumptions were considered in those analyses: for example, quasi-steady or unsteady aerodynamics; constant or variable induced velocity distribution; rigid or flexible blades, with or without hub motion; and sudden or gradual penetration into the gust. In references 5 and 9 the wind tunnel response of a rotor encountering a vertical gust was experimentally investigated. Experimental data for vertical gusts show that the rotor thrust response is most sensitive to the gust amplitude and frequency. For the sinusoidal gust with frequency ω_G, the thrust response characteristics have not only a frequency ω_G component, but also $(\omega_G + n\Omega)$ $(n = \pm 1, \pm 2, \ldots)$ components in the fluctuation, where Ω is the rotor rotational speed. In this thrust response, the ω_G component of the oscillatory characteristics is dominant in the comparatively low gust frequency range $(\omega_G << \Omega)$. Other researchers have investigated the influence of atmospheric turbulence on rotor aeromechanical stability. In references 10-18, rotor stability analyses are reported for the case of a rotor encountering a gust. Typically the turbulence is a random gust with stochastic properties.

Attempts to alleviate gust-induced vibration have been made in the work described in references 19-37. Among them, Briczinski and Cooper (ref. 19) and Briczinski (ref. 20) investigated the effect of a rotor/vehicle state feedback system on the handling qualities of a helicopter, specifically the characteristics concerned with gust response. It was found that the feedback scheme of the rotor tip-path-plane or body-state was very useful as a means of gust suppression. Frick and Johnson (ref. 21) and Johnson (ref. 22) studied the performance of an optimal control system applied to proprotor/wing response to vertical gusts. In that investigation, the von Kármán model or the Markov-process gust model were assumed as gust models, and linearized state equations were assumed to govern the motion of the rotor and wing for the rotor model. Optimal feedback inputs were determined by using linear optimal control theory, and state variables were estimated by a Kalman-Bucy filter. Significant and simultaneous reduction in the rotor and wing response was achieved. Ham et al. (ref. 23) and other investigators (refs. 24-26) have dealt with a classic parameter optimization method to alleviate the gust response of the tilt rotor aircraft. A von Kármán gust model was also used in these studies. Zwicke et al. (ref. 27) and Taylor et al. (ref. 28) investigated the performance of the optimal sampled-data feedback system on the gust response. Zwicke also studied a suboptimal feedback system derived from the above control system; a significant reduction in the gust response was achieved by using this suboptimal feedback system. Ham and McKillip (ref. 29) and Ham (ref. 30) developed an individual blade control (IBC) design for gust response alleviation, which has also been applied to suppressing blade stall-induced vibration, lag damping augmentation, and other dynamic problems (refs. 31-36). Saito et al. (ref. 37) have also studied a simple feedback system to alleviate rotor gust response. In their control scheme, individual blade pitch angle control, using scheduled feedback gains derived from analytical calculation, was used.

There has been significant progress in vibration reduction techniques for helicopters, theoretically and experimentally, in the past decade (refs. 37-83). In these vibration reduction systems, control schemes, known as multicyclic (ref. 45), or higher harmonic control (ref. 61), were applied to reducing the inherent vibratory response of a helicopter. Pitch inputs at harmonics of the rotor rotational speed are used. Typically, the helicopter is represented by a linear, quasi-static frequency domain model. The relationship between control inputs, θ, and outputs, z (which can include loads, vibrations, and rotor performance parameters) are modeled by a transfer matrix T_C. Theoretical and experimental results show that the level of vibration in a helicopter can be significantly reduced by using controllers in which the transfer matrix is updated by a Kalman filtering scheme. These vibration reduction systems are reviewed in detail in reference 70. Investigations have recently been extended to the analysis of nonlinear effects on controller performance (refs. 71 and 72). Other researchers investigated structural modification of the rotor blade or the fuselage body for vibration reduction (refs. 79-83).

In this report, a gust alleviation system is studied using two control schemes: first, an individual blade pitch control scheme, and second, an adaptive blade pitch control scheme based on linear optimal control theory. The emphasis is on the application of these controllers to alleviate gust response as measured by blade flapping and hub oscillatory forces and moments. In this study, the local momentum theory (LMT) (ref. 84) is used to calculate timewise vibratory airloadings and moments at the rotor hub. The LMT is based on the instantaneous balance between the fluid momentum and the blade elemental lift at a local station in the rotor rotational plane. Therefore, this theory can be used to evaluate timewise variation of airloading, aerodynamic moments, and the induced velocity distribution along a blade span. The LMT has been applied to study many rotary wing phenomena (refs. 9, 37, 85-87). An H-34 rotor model with four articulated blades is used. The blades have full

flexibility in the flap, lead-lag, and torsion directions. The perturbational motion of the fuselage is not considered, and the shaft inclination angle i_S is assumed to be zero (perpendicular to the flight direction).

The author expresses his great gratitude to Dr. Wayne Johnson and Dr. William Warmbrodt for their review and valuable suggestions. Further thanks are extended to the late Mr. John L. McCloud III and to Mr. Stephen A. Jacklin for their kind and encouraging discussions. The author also acknowledges computer operation support by the people of NASA Ames Research Center. This study was made possible by the National Research Council Associateship.

2. INDIVIDUAL BLADE PITCH CONTROL

In this section, an individual blade pitch control scheme is studied as a gust alleviation system. First, the harmonic method is applied to the theoretical calculations of the rotor gust response with a simple feedback control system for blade pitch. A similar feedback control system for an individual blade was investigated for a rigid blade in reference 37. The analysis is extended here to include elastic blades; therefore, sensors to detect blade deflection (flap, lead-lag, torsion) are considered to study the sensitivity of the control system. A blade stability analysis with the feedback control system was made using Floquet theory. Finally, for a specified feedback gain, this control system is validated for a rotor penetrating into a vertical gust.

Theoretical Calculation by the Harmonic Method

Theoretical calculations of rotor response to vertical gusts in forward flight have been made by using the harmonic method. Derivation of the isolated blade equations of motion and method of solution are based on references 88-95 with the exceptions that the hub motion (U, V, W, P, Q, R') is replaced by a vertical gust velocity w_G. Coordinate systems used in this study are briefly explained in appendix A. The displacements of an elastic blade are expressed as follows:

$$w = \sum_{j=1}^{\infty} \bar{w}_j q_j \ , \qquad v = \sum_{j=1}^{\infty} \bar{v}_j q_j \ , \qquad \phi = \sum_{j=1}^{\infty} \bar{\phi}_j q_j \tag{1}$$

where q_j is the generalized coordinate of the jth coupled mode and $\bar{w}_j$, $\bar{v}_j$, and $\bar{\phi}_j$ are the corresponding jth coupled mode shapes. When the associated jth modal frequency is denoted by ω_j, the following equation can be derived according to the Rayleigh-Ritz approach (ref. 96):

$$m_j \ddot{q}_j + \omega_j^2 m_j q_j = Q_j \qquad (j = 1, 2, 3, \ldots) \tag{2a}$$

where

$$m_j = \int_0^R [(k^2\bar{\phi}_j + e\bar{w}_j - e\theta\bar{v}_j)\bar{\phi}_j + (\bar{w}_j + e\bar{\phi}_j)\bar{w}_j + (\bar{v}_j - e\theta\bar{\phi}_j)\bar{v}_j]m \, dr \tag{2b}$$

$$Q_j = \int_o^R \Big(\{M_{ax} - m[eg + k^2(\ddot{\theta} + \Omega^2\theta + 2\Omega\theta\dot{v}') + e\theta(e_o\Omega^2 - 2\Omega\dot{u})]\}\bar{\phi}_j$$

$$+ [F_{az} - m(g + e\ddot{\theta} - e\Omega^2\theta) - 2m\Omega w_o'\dot{v}]\bar{w}_j + \{F_{ay} + m[-2\Omega\dot{u} + 2e\Omega(\dot{v}' + \theta\dot{w}')$$

$$+ e\theta\ddot{\theta} + \Omega^2(e_o + 2e)] - 2m\Omega\dot{u}\}\bar{v}_j\Big)dr \tag{2c}$$

In this study, the radial extension of the blade is neglected in the blade equations. However, to take account of the Coriolis force caused by the flapping, u is approximated as

$$u = \left\{r - \int_o^r [1 + (v_o' + v')^2 + (w_o' + w')^2]dr\right\} - \left[r - \int_o^r (1 + v_o'^2 + w_o'^2)dr\right]$$

$$= -1/2 \int_o^r (v'^2 + w'^2)dr - \int_o^r (v_o'v' + w_o'w')dr$$

$$= \sum_{j=1}^{\infty} \bar{u}_j q_j \tag{3a}$$

where

$$\bar{u}_j \cong -\int_o^r w_o'w' \, dr \tag{3b}$$

and w_o' is the time-averaged flap displacement. The lead-lag displacement is omitted in equation (3). More detailed expressions of M_{ax}, F_{az}, F_{ay}, etc., shown in equation (2), are given in appendix B. For this study, consider the vertical gust component w_G as an external exciting source. By introducing w_G into the aerodynamic loads and eliminating W in reference 89, the blade equation of motion, including gust excitation, can be obtained. Equation (2) yields a set of simultaneous differential equations for q_j. A trimmed value of q_j can be obtained by setting all perturbing values from trim condition to be zero. When the gust velocity defined in the rotor frame

$$w_G = w_{Go} \exp[i(\omega_G t + \phi)] \tag{4}$$

is superimposed on the trim condition, additional blade motion will occur, where w_{Go} is a constant real number. If the gust-induced blade response amplitude is assumed to be small, the incremental blade motion can be described by a small perturbation Δq_j from the trim value $\bar{q}_j$. Furthermore the perturbation generalized coordinate vector, $\Delta\mathbf{q}$, is defined as

$$\Delta\mathbf{q} = (\Delta q_1, \Delta q_2, \Delta q_3, \ldots)^T \tag{5}$$

It is then easy to show that $\Delta\mathbf{q}$ can be described by a set of second-order linear differential equations. Hereinafter, all quantities (i.e., elastic deflections,

aerodynamic forces, and moments, etc.) should be considered as perturbed values from a trim position.

In forward flight, coefficients of the differential equations become time-varying and can be written as follows:

$$\sum_{m=-3}^{3} \{[\mathbf{A}_m \exp(im\psi)]\Delta\ddot{q} + [\mathbf{B}_m \exp(im\psi)]\Delta\dot{q} + [\mathbf{C}_m \exp(im\psi)]\Delta q\} = \sum_{n=-\infty}^{\infty} \mathbf{F}_n \exp[i(\omega_G t + n\psi)] \tag{6}$$

where $\mathbf{A}_m$, $\mathbf{B}_m$, $\mathbf{C}_m$ are time-varying, periodic, complex coefficient matrices, and $\mathbf{F}_n$ is a complex vector. These coefficients are shown in appendix C. Let us assume the solution of equation (6) as

$$\Delta\mathbf{q} = \sum_{k=-\infty}^{\infty} \hat{\mathbf{q}}_k \exp[i(\omega_G t + k\psi)] \tag{7}$$

where $\hat{\mathbf{q}}_k$ is a complex, constant vector. If equation (7) is substituted into equation (6) and the same harmonic components on either side are equated, we have an infinite number of simultaneous equations involving $\hat{\mathbf{q}}_k$ ($k = -\infty, \ldots, \infty$).

$$\sum_{k=-\infty}^{\infty} \sum_{m=-\infty}^{\infty} [-(\omega_G + k\Omega)^2\mathbf{A}_m + i(\omega_G + k\Omega)\mathbf{B}_m + \mathbf{C}_m]\hat{\mathbf{q}}_k \exp[i(m + k)\psi]\exp(i\omega_G t)$$

$$= \sum_{n=-\infty}^{\infty} \mathbf{F}_n \exp(in\psi)\exp(i\omega_G t) \tag{8}$$

By eliminating $\exp(i\omega_G t)$ from this equation, equation (8) becomes

$$\sum_{k=-\infty}^{\infty} \sum_{m=-\infty}^{\infty} \mathbf{R}_{mk}\hat{\mathbf{q}}_k \exp[i(m + k)\psi] = \sum_{n=-\infty}^{\infty} \mathbf{F}_n \exp(in\psi) \tag{9}$$

Equating $(m + k)$ to be n on the left-hand side of equation (9), and after mathematical manipulation, the following expression results:

$$\sum_{k=n-3}^{n+3} \mathbf{R}_{n-k}\hat{\mathbf{q}}_k = \mathbf{F}_n \qquad (-\infty < n < \infty) \tag{10}$$

where

$$\mathbf{R}_{n-k} = -(\omega_G + k\Omega)^2\mathbf{A}_{n-k} + i(\omega_G + k\Omega)\mathbf{B}_{n-k} + \mathbf{C}_{n-k} \tag{11}$$

For the practical calculations, we assume that

$$\hat{\mathbf{q}}_k = 0 \quad \text{for} \quad |k| > K \tag{12}$$

Then the following equation will be obtained:

$$\Delta \mathbf{q} = \sum_{k=-K}^{K} \hat{\mathbf{q}}_k \exp[i(\omega_G t + k\psi)] \tag{13}$$

$$\begin{bmatrix} R_{-k,-k} & R_{-k,-k+1} & \cdots & R_{-k,-k+3} & & & & & \\ \vdots & & & & & & & 0 & \\ & & & & & & & & \\ R_{-k+3,-k} & & & & & & & & \\ & \ddots & & & & & & & \\ & & \ddots & & & & & & R_{k-3,k} \\ & & & \ddots & & & & & \vdots \\ & 0 & & & \ddots & & & & \\ & & & & & \ddots & & & \\ & & & & & & R_{k,k-3} & \cdots R_{k,k-1} & R_{k,k} \end{bmatrix} \begin{Bmatrix} \hat{q}_{-k} \\ \vdots \\ \hat{q}_o \\ \vdots \\ \hat{q}_k \end{Bmatrix} = \begin{Bmatrix} F_{-N'} \\ \vdots \\ F_o \\ \vdots \\ F_{N'} \end{Bmatrix} \tag{14}$$

where n is truncated at $n = N'$. By solving equation (14), constant amplitudes of $(2k + 1)$ generalized coordinates, $\hat{\mathbf{q}}_k$, can be determined, and the blade perturbation motion can be approximated by equation (13).

Hub Forces and Moments

In the previous section, the blade equation of motion and its solution using the harmonic method are discussed for a sinusoidal vertical gust with frequency ω_G. In this section, hub forces and moments of a rotor responding to a gust are derived. Therefore, we can refer to these responses as "rotor impedance" in the general sense. In this study, airloads are obtained by integrating section loading from two-dimensional quasi-steady thin airfoil theory. The lift deficiency function C' is assumed to be unity.

The solution of the generalized coordinate $\Delta \mathbf{q}$ is expressed by equations (13) and (14), and perturbations of blade deflections from a trim position are given by subtracting an equilibrium value from each expression in equation (1). Let vectors $\Delta \mathbf{F}_\ell$ and $\Delta \mathbf{M}_\ell$ denote the variations in hub forces and moments, respectively, owing to the ℓth blade. The augmented vector $[\Delta \mathbf{F}_\ell^T, \Delta \mathbf{M}_\ell^T]^T$ can be expressed in the following form in the rotating hub frame:

$$\begin{Bmatrix} \Delta \mathbf{F}_\ell \\ \Delta \mathbf{M}_\ell \end{Bmatrix}_H = \sum_{n=-\infty}^{\infty} \{\mathbf{Z}_1\} \exp[i(\omega_G t + n\psi_\ell)] + \{\mathbf{Z}_2\} \Delta \ddot{\mathbf{q}} + \{\mathbf{Z}_3\} \Delta \dot{\mathbf{q}} + \{\mathbf{Z}_4\} \Delta \mathbf{q} \tag{15}$$

where $\{\mathbf{Z}_1\}$ is a complex vector which gives the loads of a completely rigid blade, and $\{\mathbf{Z}_2\}$, $\{\mathbf{Z}_3\}$, and $\{\mathbf{Z}_4\}$ denote complex matrices that account for the effects of the elastic blade displacement. The terms $\{\mathbf{Z}_1\}$ through $\{\mathbf{Z}_4\}$ are all functions of the azimuthal angle of the ℓth blade, ψ_ℓ, and each of them has harmonics in ψ_ℓ up to the third harmonic as follows:

$$\left.\begin{aligned}
\{\mathbf{Z}_1\} &= \sum_{m=-3}^{3} Z_{1m} \exp(im\psi_\ell) \\
\{\mathbf{Z}_2\} &= \sum_{m=-3}^{3} Z_{2m} \exp(im\psi_\ell) \\
\{\mathbf{Z}_3\} &= \sum_{m=-3}^{3} Z_{3m} \exp(im\psi_\ell) \\
\{\mathbf{Z}_4\} &= \sum_{m=-3}^{3} Z_{4m} \exp(im\psi_\ell)
\end{aligned}\right\} \tag{16}$$

Substituting equations (7) and (16) into equation (15) results in the following form:

$$\begin{aligned}
\begin{Bmatrix} \Delta\mathbf{F}_\ell \\ \Delta\mathbf{M}_\ell \end{Bmatrix}_H &= \sum_{m=-3}^{3} \left\{ \sum_{n=-\infty}^{\infty} Z_{1m} \exp[i(\omega_G t + n\psi_\ell + m\psi_\ell)] \right. \\
&\quad \left. + \sum_{k=-\infty}^{\infty} [-(\omega_G + k\Omega)^2 Z_{2m} + i(\omega_G + k\Omega) Z_{3m} + Z_{4m}] \hat{\mathbf{q}}_k \exp[i(\omega_G t + k\psi_\ell + m\psi_\ell)] \right\} \\
&= \sum_{m=-3}^{3} \left\{ \sum_{n=-\infty}^{\infty} Z_{1m} \exp\{i[\omega_G t + (n + m)\psi_\ell]\} \right. \\
&\quad \left. + \sum_{k=-\infty}^{\infty} Z_{5m} \hat{\mathbf{q}}_k \exp\{i[\omega_G t + (k + m)\psi_\ell]\} \right\}
\end{aligned} \tag{17}$$

where

$$Z_{5m} = -(\omega_G + k\Omega)^2 Z_{2m} + i(\omega_G + k\Omega) Z_{3m} + Z_{4m} \tag{18}$$

Here Z_{1m} and Z_{5m} denote a constant vector and a constant matrix, respectively.

The hub loads in the rotating hub frame can be transformed to the rotor frame as follows:

$$\begin{Bmatrix} \Delta\mathbf{F}_\ell \\ \Delta\mathbf{M}_\ell \end{Bmatrix}_R = \begin{bmatrix} \mathbf{T}_{HR} & \cdots & 0 \\ \vdots & \ddots & \vdots \\ 0 & \cdots & \mathbf{T}_{HR} \end{bmatrix} \begin{Bmatrix} \Delta\mathbf{F}_\ell \\ \Delta\mathbf{M}_\ell \end{Bmatrix}_H \tag{19}$$

where $\mathbf{T}_{HR}$ is denoted by equation (A6) in appendix A. Introducing

$$\begin{bmatrix} \mathbf{T}_{HR} & \cdots & 0 \\ \vdots & \ddots & \vdots \\ 0 & \cdots & \mathbf{T}_{HR} \end{bmatrix} = \sum_{p=-1}^{1} K_p \exp(ip\psi_\ell) \tag{20}$$

gives the following form:

$$\begin{Bmatrix}\Delta F_\ell \\ \Delta M_\ell\end{Bmatrix}_R = \sum_{p=-1}^{1}\sum_{m=-3}^{3}\left\{\sum_{n=-\infty}^{\infty} K_p Z_{1m}\exp\{i[\omega_G t + (n+m+p)\psi_\ell]\}\right.$$

$$\left. + \sum_{k=-\infty}^{\infty} K_p Z_{5m}\hat{q}_k \exp\{i[\omega_G t + (k+m+p)\psi_\ell]\}\right\}$$

$$= \sum_{p=-1}^{1}\sum_{\nu=(n+p)-3}^{(n+p)+3}\sum_{n=-\infty}^{\infty} K_p Z_{1,\nu-(n+p)}\exp[i(\omega_G t + \nu\psi_\ell)] \quad : \quad \nu = n+m+p$$

$$+ \sum_{p=-1}^{1}\sum_{\nu=(k+p)-3}^{(k+p)+3}\sum_{k=-\infty}^{\infty} K_p Z_{5,\nu-(k+p)}\hat{q}_k \exp[i(\omega_G t + \nu\psi_\ell)] \quad : \quad \nu = k+m+p \tag{21}$$

where K_p is a complete matrix.

For a practical calculation, the limits of n and k are taken as N' and K, respectively. From equation (21), the following equation can be obtained:

$$\begin{Bmatrix}\Delta F_\ell \\ \Delta M_\ell\end{Bmatrix}_R = \left\{\sum_{\nu=-N'-4}^{N'+4}\sum_{n=-N'}^{N'} T_{\nu n} + \sum_{\nu=-K-4}^{K+4}\sum_{k=-K}^{K} S_{\nu k}\hat{q}_k\right\}\exp[i(\omega_G t + \nu\psi_\ell)]$$

$$= \sum_{\nu=-M-4}^{M+4} Z_\nu \exp[i(\omega_G t + \nu\psi_\ell)] \tag{22}$$

where

$$\left.\begin{aligned} T_{\nu n} &= \sum_{p=-1}^{1} K_p Z_{1,\nu-(n+p)} \\ S_{\nu k} &= \sum_{p=-1}^{1} K_p Z_{5,\nu-(k+p)} \\ M &= \begin{cases} N' & (N' > K) \\ K & (K > N') \end{cases} \end{aligned}\right\} \tag{23}$$

where Z_ν is a vector and denotes the νth harmonic component of the hub loads in the rotor frame. Since the Fourier coefficients have been truncated at the N'th or Kth harmonic in the blade motion, the hub loads should also be truncated at the N'th or Kth harmonic. The total hub loads can be obtained by summing up equation (22) for all blades. Using the multiblade summation formula

$$\sum_{\ell=1}^{N} \exp(i\nu\psi_\ell) = \begin{cases} N \exp(i\nu\psi^*) & : \quad \nu/N = \text{integer} \\ 0 & : \quad \text{otherwise} \end{cases} \tag{24}$$

the following final expression can be obtained:

$$\sum_{\ell=1}^{N} \begin{Bmatrix} \Delta F_\ell \\ \Delta M_\ell \end{Bmatrix}_R = N \cdot \sum_{|q| \leq M/N} Z_{qN} \exp[i(\omega_G t + qN\psi^*)] \tag{25}$$

where N denotes the number of blades, q is an integer, and ψ^* is the azimuthal angle of the reference blade.

Individual Blade Pitch Control and Stability Analysis

The feedback control system which can control blade pitch individually is discussed in this section. Let us consider the following feedback system:

$$\begin{aligned} \Delta\theta &= (K_w \Delta w + K_{\dot{w}} \Delta\dot{w} + K_{\ddot{w}} \Delta\ddot{w}) + (K_v \Delta v + K_{\dot{v}} \Delta\dot{v} + K_{\ddot{v}} \Delta\ddot{v}) + (K_\phi \Delta\phi + K_{\dot{\phi}} \Delta\dot{\phi} + K_{\ddot{\phi}} \Delta\ddot{\phi}) \\ &= \mathbf{K}_w^T \Delta\mathbf{w}(r) + \mathbf{K}_v^T \Delta\mathbf{v}(r) + \mathbf{K}_\phi^T \Delta\boldsymbol{\phi}(r) \end{aligned} \tag{26}$$

where

$$\begin{aligned} \mathbf{K}_w &= (K_w, K_{\dot{w}}, K_{\ddot{w}})^T \\ \mathbf{K}_v &= (K_v, K_{\dot{v}}, K_{\ddot{v}})^T \\ \mathbf{K}_\phi &= (K_\phi, K_{\dot{\phi}}, K_{\ddot{\phi}})^T \\ \Delta\mathbf{w}(r) &= [\Delta w(r), \Delta\dot{w}(r), \Delta\ddot{w}(r)]^T \\ \Delta\mathbf{v}(r) &= [\Delta v(r), \Delta\dot{v}(r), \Delta\ddot{v}(r)]^T \\ \Delta\boldsymbol{\phi}(r) &= [\Delta\phi(r), \Delta\dot{\phi}(r), \Delta\ddot{\phi}(r)]^T \end{aligned}$$

$\mathbf{K}_w$, $\mathbf{K}_v$, and $\mathbf{K}_\phi$ are feedback gains and $\Delta\mathbf{w}(r)$, $\Delta\mathbf{v}(r)$, and $\Delta\boldsymbol{\phi}(r)$ are flap, lead-lag, and torsion blade deflections from trim position at r, respectively. By using equations (1) and (5), $\Delta\mathbf{w}$, $\Delta\mathbf{v}$, and $\Delta\boldsymbol{\phi}$ are given as follows:

$$\left.\begin{aligned} \Delta\mathbf{w} &= \sum_{j=1}^{\infty} (\bar{w}_j \Delta q_j, \bar{w}_j \Delta\dot{q}_j, \bar{w}_j \Delta\ddot{q}_j)^T \\ \Delta\mathbf{v} &= \sum_{j=1}^{\infty} (\bar{v}_j \Delta q_j, \bar{v}_j \Delta\dot{q}_j, \bar{v}_j \Delta\ddot{q}_j)^T \\ \Delta\boldsymbol{\phi} &= \sum_{j=1}^{\infty} (\bar{\phi}_j \Delta q_j, \bar{\phi}_j \Delta\dot{q}_j, \bar{\phi}_j \Delta\ddot{q}_j)^T \end{aligned}\right\} \tag{27}$$

For simplicity, let us consider only the flap deflection of a blade; that is,

$$\mathbf{K}_v = \mathbf{K}_\phi = 0$$

Then $\Delta\theta$ becomes

$$\Delta\theta = K_w \Delta w + K_{\dot{w}} \Delta\dot{w} + K_{\ddot{w}} \Delta\ddot{w} \tag{28}$$

and $\Delta\mathbf{q}$ is

$$\Delta\mathbf{q} = (\Delta q_1, \Delta q_2, \ldots, \Delta q_L)^T = \sum_{k=-K}^{K} \hat{q}_k \exp[i(\omega_G + k\Omega)t]$$

From these equations, the following expressions are obtained:

$$\left.\begin{aligned}
\Delta w &= \sum_{k=-K}^{K} (\bar{w}_1 q_{1k} + \bar{w}_2 q_{2k} + \ldots + \bar{w}_L q_{Lk}) \exp[i(\omega_G + k\Omega)t] \\
\Delta\dot{w} &= i \sum_{k=-K}^{K} (\omega_G + k\Omega)(\bar{w}_1 q_{1k} + \ldots + \bar{w}_L q_{Lk}) \exp[i(\omega_G + k\Omega)t] \\
\Delta\ddot{w} &= -\sum_{k=-K}^{K} (\omega_G + k\Omega)^2 (\bar{w}_1 q_{1k} + \ldots + \bar{w}_L q_{Lk}) \exp[i(\omega_G + k\Omega)t]
\end{aligned}\right\} \tag{29}$$

Substituting equation (29) into equation (20) results in the following form:

$$\begin{aligned}
\Delta\theta &= K_w \Delta w + K_{\dot{w}} \Delta\dot{w} + K_{\ddot{w}} \Delta\ddot{w} \\
&= \sum_{k=-K}^{K} \Delta\theta_k \exp[i(\omega_G + k\Omega)t] \\
&= \Delta\theta_0 \exp(i\omega_G t) + \Delta\theta_{-1} \exp[i(\omega_G - \Omega)t] + \Delta\theta_1 \exp[i(\omega_G + \Omega)t] + \ldots
\end{aligned} \tag{30}$$

In equation (30), $\Delta\theta_k$ ($k = -K, \ldots, K$) are considered as control inputs. Therefore, appropriate combinations of $\Delta\theta_k$ may enable us to alleviate the oscillatory gust response of a helicopter rotor. The extension of this idea to an optimal blade control algorithm will be discussed in the next section.

By substituting equations (26) and (27) into equation (C5) (appendix C), the following equation can be obtained:

$$\sum_i (A'_{ij} \Delta\ddot{q}_i + B'_{ij} \Delta\dot{q}_i + C'_{ij} \Delta q_i) = F'_j \tag{31}$$

where

$$
\left.
\begin{aligned}
A'_{ij} &= A_{ij} - D_j(K_{\ddot{w}}\,\Delta\ddot{w} + K_{\ddot{v}}\,\Delta\ddot{v} + K_{\ddot{\phi}}\,\Delta\ddot{\phi}) \\
B'_{ij} &= B_{ij} - D_j(K_{\dot{w}}\,\Delta\dot{w} + K_{\dot{v}}\,\Delta\dot{v} + K_{\dot{\phi}}\,\Delta\dot{\phi}) \\
C'_{ij} &= C_{ij} - D_j(K_{w}\,\Delta w + K_{v}\,\Delta v + K_{\phi}\,\Delta\phi) \\
F'_j &= F_j - D_j\,\Delta\theta \\
D_j &= \int_o^R \{(\bar{w}_j + ab\bar{\phi}_j)c_2\dot{U}_T + [\bar{w}_j + (1/2 + a)b\bar{\phi}_j]c_1U_T^2 + c_1U_TU_p\bar{v}_j \\
&\quad - m(k^2 + e_oe)\Omega^2\bar{\phi}_j + me\Omega^2\bar{w}_j + me\ddot{\theta}\bar{v}_j\}dr
\end{aligned}
\right\} \tag{32}
$$

In this feedback system, each sensor (that detects blade deflection) is assumed to be located at radial position r along the blade span. Signals from each sensor have trim values subtracted in order to get perturbation quantities such as Δw, Δv, $\Delta\phi$. By multiplying these perturbation values by feedback gains, this system generates inputs to be fed back to the blade pitch control. In this process, any time lags of the sensor/actuator are not considered.

Now let us consider the stability of the blade equation of motion expressed by equation (31). In this equation, each coefficient, A'_{ij}, B'_{ij}, and C'_{ij}, is time-variant with the fundamental period $T = 2\pi$. In this study, Floquet theory (refs. 97-101) is used in order to analyze the stability of a blade. Define a new variable set as

$$
\mathbf{X} = \begin{bmatrix} \Delta\dot{\mathbf{q}} \\ \Delta\mathbf{q} \end{bmatrix} \tag{33}
$$

By this transformation, equation (31) becomes a first-order differential equation with zero external force, as shown by the following:

$$
[\dot{\mathbf{X}}] = -[\mathbf{E}_{ij}(t)][\mathbf{X}] \tag{34}
$$

where

$$
[\mathbf{E}_{ij}(t)] = \begin{bmatrix} [A'_{ij}][B'_{ij}] & [A'_{ij}][C'_{ij}] \\ -I & 0 \end{bmatrix} \tag{35}
$$

and I is a unit matrix. According to the Floquet-Liapunov theory, we can assume the following solution:

$$
[\mathbf{X}(t)] = [\mathbf{G}(t)][\alpha_k \exp(\eta_k t)] \tag{36}
$$

The $G(t)$ is a periodic function with period T, and the η_k are complex characteristic numbers. The α_k are constants derived from initial conditions, that is:

$$\{\alpha_k\} = [\mathbf{G}(0)]^{-1}[\mathbf{X}(0)] \tag{37}$$

The Floquet transition matrix [Q] of this system is defined by

$$[\mathbf{X}(T)] = [Q][\mathbf{X}(0)] \tag{38}$$

The stability of the system, therefore, can be completely determined from the values of η_k. Inserting the relation for $\{\alpha_k\}$ of equation (37) into equation (36), one obtains:

$$[\mathbf{X}(t)] = [\mathbf{G}(t)][-\exp(\eta_k t)][\mathbf{G}(0)]^{-1}[\mathbf{X}(0)] \tag{39}$$

Introducing the state transition matrix $[\phi(t)]$ defined by

$$\left.\begin{aligned}[\mathbf{X}(t)] &= [\phi(t)][\mathbf{X}(0)] \\ [\phi(0)] &= [I]\end{aligned}\right\} \tag{40}$$

one obtains by comparison of equations (39) and (40)

$$[\phi(t)] = [\mathbf{G}(t)][-\exp(\eta_k t)][\mathbf{G}(0)]^{-1} \tag{41}$$

or

$$[\mathbf{G}(t)] = [\phi(t)][\mathbf{G}(0)][-\exp(-\eta_k t)] \tag{42}$$

Setting t to be T and considering [G(T)] = [G(0)] gives

$$[\mathbf{G}(0)]^{-1}[\phi(T)][\mathbf{G}(0)] = [-\exp(-\eta_k T)] \tag{43}$$

Thus

$$[\phi(T)] = [Q] \qquad (t = T) \tag{44}$$

Substituting equation (40) into equation (34) gives the following equation:

$$d[\phi(t)]/dt + [\mathbf{E}_{ij}(t)][\phi(t)] = [0] \tag{45}$$

Equation (45) is solved by numerically integrating from t = 0 to t = T, with initial conditions given by equation (40). Eigenvalues Λ_k are given, by using equations (43) and (44), as

$$\left.\begin{aligned}[-\Lambda_k] &= [-\exp(-\eta_k T)] = [\mathbf{G}(0)]^{-1}[Q][\mathbf{G}(0)] \\ [Q] &= [\phi(T)]\end{aligned}\right\} \tag{46}$$

Numerical Calculations

In this section, numerical calculations are conducted to determine the capability of the individual blade pitch control system. The properties of the blade used in this study (an H-34 rotor blade) are given in table 1. The blade structural characteristics and rotor operating conditions are given in tables 2 and 3, respectively.

Gust shape and sensor locations on a blade are schematically depicted in figure 1. The hub forces (F_x, F_y, F_z) and the hub moments (M_x, M_y, M_z) in the rotor frame are shown in figure 2. Blade natural frequencies and mode shapes were calculated using the Holzer-Myklestad method (ref. 9). Figure 3 shows the natural frequencies and mode shapes for the rotor blade.

All quantities used in this calculation are expressed as complex numbers, for example, $w_G = w_{Go} \exp(i\omega_G t)$. The undeformed elastic axis is assumed to lie in the $X_H Z_H$ plane and to coincide with the aerodynamic center axis ($e_o = 0.0$, $a = -1/2$). Eight coupled modes ($\ell = 8$) were used (see fig. 2). In figure 3, the flapwise bending modes (Nos. 2, 3, 5, and 7) and the lead-lagwise bending modes (Nos. 1, 4, and 8) correspond to those of a blade with collective pitch angle of 8°; the sixth mode is a torsional mode. The highest harmonic numbers are assumed to be truncated at 5 for the gust expression ($n = 5$) and for the solution of the generalized coordinate ($k = 5$). Correspondingly, $|q| \leq M/N$ reduces to $q = 0, \pm 1$ in equation (25). Under the operating conditions, the equilibrium positions (in this case, the time-independent rigid body portion) of the blade deflection are as follows: the flap deflection (w_o') is 0.11 rad, the lead-lag deflection (v_o') is -0.017 rad, and the torsional deflection (ϕ_o) is -0.0004 rad. These values were used in the calculation in order to evaluate the effects of the in-plane Coriolis force. The flowchart of the computer code for the harmonic method is given in appendix D.

Figures 4(a) to 4(g) show the rotor response to a sinusoidal gust. The rotor impedance is defined as the amplitude ratio between the additional responses of the rotor from the steady responses and those owing to sinusoidal gusts with unity amplitude ($w_{Go} = 1.0$ m/sec). Phase shift to a vertical sinusoidal gust is also shown in figure 4. The horizontal axis denotes nondimensional gust frequencies divided by the rotor rotational speed, which varies from 0.0 to 1.0. Each figure (figs. 4(a)-4(g)) includes the responses at frequency (ω_G) and ($\omega_G \pm 4\Omega$). The response at frequency (ω_G) is hereinafter called the major response (shown by solid lines in the figures). The responses with frequency ($\omega_G - 4\Omega$) and ($\omega_G + 4\Omega$) are called the subharmonic response and the superharmonic response, respectively. In the case of the horizontal force F_x (fig. 4(a)), each response increases gradually as nondimensional frequency (ω_G/Ω) increases. The major response has a peak at about 0.7 and has a minimum around 0.9. This phenomenon comes from the effect of the lag dampers. Without any lag dampers for an articulated blade, the responses will diverge at lag frequency ($\omega_L - \Omega$). The lag dampers suppress this extremely large response. The symbols ($\overset{L}{\blacktriangledown}$) on the horizontal frequency axis denote the location of (ω_L/Ω) and ($\omega_L - \Omega)/\Omega$. The subharmonic response is slightly greater than the superharmonic response in the nondimensional frequency range of 0.2 to 0.8. In the case of the side force F_y (fig. 4(b)), the tendency of each response is similar to that in the case of the horizontal force. There is a sharper reduction in response at (ω_G/Ω) = 0.9 for the major response. For both figures 4(a) and 4(b), the major response is dominant up to 0.8. The subharmonic response is again greater than the superharmonic response in the nondimensional frequency range of 0.2 to 0.8. For the vertical force F_z (fig. 4(c)), a significant difference can be seen relative to the other impedances (F_x, F_y). The major response decreases gradually as the gust frequency increases. The subharmonic response is almost the same as the superharmonic response. The amplitude of the major response of F_z is greater than that of F_x or F_y. Qualitatively, the major response of the vertical force is from 2 to 100 times larger than the other responses below the nondimensional frequency 0.5. As the frequency approaches 1.0, the three response amplitudes become similar.

Concerning the phase angle characteristics of the hub forces, the phase shift of the subharmonic response is relatively insensitive to the gust excitation compared with the other responses. From these calculations, the angles are about +90° for the horizontal force, about -150° for the side force, and about -90° for the vertical force. On the other hand, the phase shift characteristics of the major response depends on the gust exciting frequency. Those angles vary from -180° to +180° over the frequency range for the horizontal force. However, in the case of the vertical force, it seems to be insensitive to the vertical gust. It is almost constant at about -10° to 20° below the nondimensional frequency 0.5. These results agree with experimental results (ref. 9). For the case of the side force, those shift angles vary from +90° to -120°.

For the hub moment responses (figs. 4(d) to 4(f)), the trend of the impedance is similar to that of the vertical force. Below the nondimensional frequency 0.5, the major response dominates the other responses. As with the case of the horizontal force and side force, a minimum around the nondimensional frequency 0.9 can be seen in the major response of the rolling moment M_x. In the phase angle characteristics of the hub moments, the angles depend on the gust exciting frequency.

In figures 5(a) to 5(c), root loci of the blade characteristic equation with feedback (the individual feedback gain is fed back independently) are shown. Floquet theory is used in this stability analysis to solve the characteristic equation with time-variant, periodic coefficients. The feedback gain is assumed to be a real number. Figure 5(a) shows the case in which only the flap deflection (Δw) is fed back to the individual blade pitch angle. The feedback gain (K_w) varies from 0.0 to 0.15 rad/m. The limit of the feedback gain is about 0.111, above which the feedback system becomes unstable. Figure 5(b) shows the case in which only the velocity of the flap deflection ($\Delta \dot{w}$) is fed back. The feedback gain ($K_{\dot{w}}$) varies from 0.0 to 0.005 rad/m/sec. The point at which the system becomes unstable is about 0.00515 rad/m/sec. In figure 5(c), root loci for the case of the acceleration feedback ($\Delta \ddot{w}$) is depicted. The feedback gain ($K_{\ddot{w}}$) varies from 0.0 to 5×10^{-3} rad/m/sec^2. In this region, the system is stable; for ($K_{\ddot{w}}$) > 5×10^{-3} the system is unstable.

Figure 6 shows the sensitivity of the phase angle of the feedback gain to the vertical hub force response at gust frequency 0.5 Hz ($\omega_G/\Omega = 0.265$) and amplitude 1.8 m/sec. The vertical axis denotes the amplitude of the oscillatory vertical force or the nondimensional vertical force (thrust coefficient). The horizontal axis is the phase angle of the feedback gain, ϕ, which varies from 0° to 360°. In this calculation, the amplitude of the feedback gain is assumed to be constant. The dashed line in figure 6 shows the vertical force response without any feedback system (base line). The feedback system used here generates the control input to be fed back to the blade pitch according to equation (26). Each sensor is assumed to be located at the blade tip and measures blade deflection independently. Each measured deflection (Δw, Δv, $\Delta\phi$) is assumed to be fed back to the blade pitch. The amplitude of the vertical force depends on the phase angle, and it has a minimum point at the appropriate combination of the amplitude and the phase angle of the feedback gain, that is, (K_w, ϕ), (K_v, ϕ), etc. From these calculations, the minimum point may be realized at ϕ = 30° for Δw feedback, ϕ = 30° for Δv feedback, and ϕ = 210° for $\Delta\phi$ feedback. For $\Delta\phi$ feedback, $|K_\phi|$ = 5.0 was used because the torsional deflection of the blade is very small compared with the other deflections.

Figures 7(a) to 7(c) show the sensitivity of the amplitude of the feedback gain to the vibratory vertical force response at the same operating condition. In figure 7(a), the phase angle ϕ is assumed to be zero; K_w varies from 0.0 to

-1.6 rad/m. The amplitude of the vertical force at first rapidly decreases, then slowly decreases as K_w further decreases. In this figure, the symbol $\otimes$ denotes the calculation results by the local momentum theory (LMT). In the case of Δv feedback (fig. 7(b)), the phase angle ϕ is assumed to be 30°, and K_v varies from 0.0 to -0.1 rad/m. The amplitude of the oscillatory vertical force linearly decreases and reaches a minimum at about $K_v = -0.04$; then, it increases linearly as K_v further decreases. For the $\Delta\phi$ feedback (fig. 7(c)), the general trend is similar to that in the case of Δw feedback. However, K_ϕ is several orders of magnitude greater from that shown in figure 7(a). This difference is due to the magnitude of the blade deflection; that is, usually the torsional deflection is very small compared with the flap deflection. From these three figures, it is found that the vertical force response is not as sensitive to the variation of K_w or K_ϕ for Δw or $\Delta\phi$ feedback as a variation in K_v for Δv feedback. It follows that it is desirable to select the Δw or $\Delta\phi$ deflection as the measuring signal in order to alleviate the vertical hub force response to vertical gusts.

Figures 8(a) to 8(c) show the effect of the sensor position on the hub response to the specified combination of (K_w, ϕ), (K_v, ϕ), and (K_ϕ, ϕ). Four sensor positions are investigated: r = (1/4)R, r = (1/2)R, r = (3/4)R, and r = R. In these figures, the base line is depicted by a dashed line. An effect of sensor position is shown in the vertical force and the yawing moment responses. Positions of the sensor farther outboard are more effective in the gust alleviation system. It should be noted that there is an increase in some responses because of the individual blade pitch control. However, this increase is small compared with the vertical force and the yawing moment reduction.

Figures 9 to 14 show the hub gust response calculated by the LMT. Each figure includes the three hub forces (F_x, F_y, F_z), the three moments (M_x, M_y, M_z), and also the pitch angle input of a reference blade. The same operating conditions used in the harmonic method are used in this calculation. Gust shapes assumed here are sinusoidal (figs. 9-12) and step (figs. 13 and 14). These gusts are applied to the calculation after the thrust level has reached a steady-state trim value (usually requiring six rotor revolutions for the LMT). The gust amplitude is 1.8 m/sec, which is almost half the mean induced velocity of the rotor. The time history of the gust shown in each figure is measured at the rotor head. The hub responses are measured from when the reference blade is located at zero azimuthal angle. The control pitch angle is fed back to the individual blade pitch actuator. Any time lag of the actuator or other mechanism is not considered. The physical limitation of the pitch actuator should be considered for the purpose of implementation. However, in this calculation, physical limits were set at the very large values because the emphasis of this investigation is on the feasibility of this kind of controller.

Figure 9 shows the hub gust responses for a vertical sinusoidal gust without any controller; gust frequency is 0.5 Hz. Among these responses, the vertical force (thrust), the rolling moment, and the yawing moment (torque) respond noticeably to the vertical gust compared with the others. In the case of the thrust response (fig. 9(a)), the amplitude of the fluctuation is about 10% of the steady state response. It should be noted that the phase difference between the vertical force and the rolling and yawing moments is about 180°. The vertical force responds quickly to the vertical gust.

In figure 10, the hub gust response with the individual blade pitch control is shown for the same vertical sinusoidal gust. Feedback gain K_w is -0.5 rad/m. Flap deflection (Δw) at the blade tip is selected as a measuring signal. The reduction of the oscillatory thrust response is about 60% of that calculated for the uncontrolled

case (fig. 9(a)). From figure 7(a), it is expected that the reduction of the thrust response should be about 65%. This result implies that the theoretical calculation using the harmonic method can reasonably predict the reduction of the thrust response. In the case of the rolling moment (fig. 10(d)), a significant reduction of the oscillatory response can be obtained. However, from figure 10(f), it should be noted that the yawing moment response increases about 20% because of the individual blade pitch control. Figure 10(g) shows that the pitch angle of the reference blade varies sinusoidally with a phase difference of 180° relative to the gust. From this result, the change of the pitch angle may be expressed as follows:

$$\left.\begin{aligned} \theta_\ell(t) &= [\theta_0 + \Delta\theta_0(t)] + [\theta_{1c} + \Delta\theta_{1c}(t)]\cos\psi + [\theta_{1s} + \Delta\theta_{1s}(t)]\sin\psi \\ \Delta\theta_0(t) &= \Delta\theta_{0c}\cos(\omega_G t) + \Delta\theta_{0s}\sin(\omega_G t) \\ \Delta\theta_{1c}(t),\ \Delta\theta_{1s}(t) &\cong 0.0 \end{aligned}\right\} \tag{47}$$

where $\Delta\theta_0(t)$, $\Delta\theta_{1c}(t)$, and $\Delta\theta_{1s}(t)$ are control inputs generated by the controller, and all of them are time-variant. The $\Delta\theta_{0c}$ and $\Delta\theta_{0s}$ terms are constant values, which are automatically decided once the feedback gain is selected.

Figures 11(a) to 11(g) show the hub gust response for the vertical sinusoidal gust without control. The gust frequency of 2.0 Hz is used. The operating condition is the same as in the case shown in figure 9. Compared with figure 9, the amplitude of the uncontrolled oscillatory thrust response has decreased noticeably (about 60%). This decrease is in agreement with the result calculated by the harmonic method (about a 63% decrease; fig. 4(c)). Yet the hub forces and moments still respond noticeably to the sinusoidal gust.

Figures 12(a) to 12(g) show the hub gust responses for this vertical sinusoidal gust with the individual blade pitch control. The feedback gain is -0.5 rad/m. In this case, there is a noticeable reduction in the thrust, side force, and yawing moment responses. However, in the rolling and pitching moment response, increases can be seen. Contrary to the case of a 0.5 Hz gust frequency, a slight reduction of the yawing moment response can be seen in the case of the 2.0 Hz gust frequency.

Shown in figures 13(a) to 13(g) are the hub gust responses for a step gust. The gust amplitude is 1.8 m/sec. The change in the thrust and in the yawing moment responses is significant. The thrust response increases gradually to the new steady state without any overshoot. The yawing moment response, however, shows an overshoot and then reaches a steady state value. Other responses do not show any significant changes. Figures 14(a) to 14(g) show the hub gust responses with the individual blade pitch control for this step gust. The feedback gain K_w used in this calculation is -0.5 rad/m and the phase angle is assumed to be zero. The general tendencies of the response are similar to those of the case shown in figure 13. For the thrust response, a reduction of about 70% is achieved. The difference between the steady state value and the trim value for yawing moment (fig. 14(f)) is roughly twice that shown in figure 13(f). A collective pitch angle change of about 0.6° is input to maintain the trimmed condition of the rotor.

3. ADAPTIVE BLADE PITCH CONTROL

In this section, an adaptive blade pitch control designed to alleviate gust-induced vibration is analytically investigated for a helicopter with four articulated blades. Multicyclic control (MCC) and higher harmonic control (HHC) have previously been applied to the reduction of inherent responses of a helicopter, such as N-per-revolution vibratory responses. In these controllers, pitch inputs at harmonics of the rotor rotational speed are used as control inputs. For the gust response of a helicopter, additional vibratory responses, such as gust harmonic (ω_G), subharmonic ($\omega_G - \Omega$), and superharmonic ($\omega_G + \Omega$), appear in the response. Gust harmonic response is the most dominant in the comparatively low gust frequency range (refs. 5 and 9). In this study, this dominant response is selected as the response to be reduced.

An adaptive blade pitch control system is based on digital optimal control theory. This system is composed of a set of measurements (oscillatory hub forces), a control system based on the optimization of the quadratic performance function, and a simulation system of the helicopter rotor. In the following subsection, the details will be explained.

Helicopter Model

In this study, the helicopter is represented by a linear, quasi-static frequency domain model relating the output z to the input θ. Here, z is a vector of the harmonic of the gust-induced vibration in the rotor frame. The input θ is at the frequency corresponding to the gust frequency. It is assumed that the gust is sinusoidal, and that the gust frequency is known a priori. When a rotor penetrates into the gust, the response at the hub position can be considered to be composed of gust and control inputs, such as

$$\{z\} = \{z_G\} + \{z_C\} \tag{48}$$

Equation (48) can be rewritten by using the expression of the rotor impedance $[T_G]$ and rotor transfer function $[T_C]$ as follows:

$$\{z_G\} = [T_G]\{g\}$$

$$\{z_C\} = [T_C]\{\theta\}$$

That is, equation (48) becomes

$$\{z\} = [T_G]\{g\} + [T_C]\{\theta\} \tag{49}$$

where

$$\left.\begin{aligned} \{z\} &= (m \times 1) \quad \text{vector} \\ [T_G] &= (m \times 3) \quad \text{matrix} \\ \{g\} &= (3 \times 1) \quad \text{vector} \\ [T_C] &= (m \times n) \quad \text{matrix} \\ \{\theta\} &= (n \times 1) \quad \text{vector} \end{aligned}\right\} \tag{50}$$

Once the characteristics of a gust are determined, $[T_G]$ becomes a constant matrix. Therefore, we may denote the first term of equation (49) as $\{z_0\}$. Then equation (49) is

$$\{z\} = \{z_0\} + [T_C]\{\theta\} \tag{51}$$

This form resembles the global model formulation of helicopter vibration (ref. 70). The following "local model" can be also taken into account:

$$\{\Delta z\} = [T_C]\{\Delta\theta\} \tag{52}$$

where Δz means $z_n - z_{n-1}$, and $\Delta\theta$ means $\theta_n - \theta_{n-1}$.

From theoretical calculations using the harmonic method, the hub response to a vertical gust in the rotor frame (X_R, Y_R, Z_R) can be expressed as follows:

$$Z = Z_0(t) + Z_1 \cos(\omega_G t) + Z_2 \sin(\omega_G t) + Z_3 \cos(\omega_G - 4\Omega)t + Z_4 \sin(\omega_G - 4\Omega)t$$
$$+ Z_5 \cos(\omega_G + 4\Omega)t + Z_6 \sin(\omega_G + 4\Omega)t + \text{H.O.T.} \tag{53}$$

where $Z_0(t)$ are the inherent responses of a helicopter rotor represented by

$$Z_0(t) = \bar{Z}_0 + Z_C \cos(N\Omega t) + Z_S \sin(N\Omega t) + \text{H.O.T.} \tag{54}$$

In these responses, gust harmonic responses $(Z_1, Z_2)^T$ are the most dominant in the gust response. Oscillatory hub forces and moments at the gust frequency in the rotor frame are chosen here as measurements z:

$$\{z\} = (T_C, T_S, H_C, H_S, M_{YC}, M_{YS}, Y_C, Y_S, M_{XC}, M_{XS}, M_{ZC}, M_{ZS})^T \tag{55}$$

where

$$\left.\begin{aligned}
\Delta T_G &= T_C \cos(\omega_G t) + T_S \sin(\omega_G t) \\
\Delta H_G &= H_C \cos(\omega_G t) + H_S \sin(\omega_G t) \\
\Delta M_{YG} &= M_{YC} \cos(\omega_G t) + M_{YS} \sin(\omega_G t) \\
\Delta Y_G &= Y_C \cos(\omega_G t) + Y_S \sin(\omega_G t) \\
\Delta M_{XG} &= M_{XC} \cos(\omega_G t) + M_{XS} \sin(\omega_G t) \\
\Delta M_{ZG} &= M_{ZC} \cos(\omega_G t) + M_{ZS} \sin(\omega_G t)
\end{aligned}\right\} \tag{56}$$

Control inputs are selected at the gust frequency ω_G, subharmonic frequency $(\omega_G - \Omega)$, and superharmonic frequency $(\omega_G + \Omega)$ in the rotor frame as follows:

$$\Delta\theta = \theta_1 \cos(\omega_G t) + \theta_2 \sin(\omega_G t) + \theta_3 \cos(\omega_G - \Omega)t + \theta_4 \sin(\omega_G - \Omega)t$$
$$+ \theta_5 \cos(\omega_G + \Omega)t + \theta_6 \sin(\omega_G + \Omega)t \tag{57}$$

Hence the control vector θ has six components:

$$\{\theta\} = (\theta_1, \theta_2, \theta_3, \theta_4, \theta_5, \theta_6)^T \tag{58}$$

These control inputs are superimposed on the blade trim pitch input.

Identification

Three cases are distinguished for the helicopter model, depending on the identification approach:

1. Identify $\{z_0\}$ only
2. Identify $[T_C]$ only
3. Identify $\{z_0\}$ and $[T_C]$

For the gust response, the uncontrolled response $\{z_0\}$ is generally time-variant; the matrix $[T_C]$ depends on the operating flight conditions. Hence, it is necessary that the transfer function $[T_C]$ be identified simultaneously with an uncontrolled response $\{z_0\}$. Case 3 is taken into consideration in this investigation. For the local model, it is necessary that the $[T_C]$ matrix be identified for each time-cycle. The Kalman filtering technique (refs. 102 and 103) is applied to identify them. For the global model, equation (51) can be rearranged as follows:

$$\begin{aligned} z_n &= z_0 + T_C\theta_n = [T_C, z_0](\theta_n, 1)^T \\ &= \mathbf{T}\theta_n \end{aligned} \tag{59}$$

where

$$\mathbf{T} = m \times (n + 1) \quad \text{matrix}$$

$$\theta_n = (n + 1) \times 1 \quad \text{vector}$$

and the subscript n denotes the time-step at $t = n\,\Delta t$. For this study, it is assumed that there is no noise in the measurement of θ_n. The identification algorithm can be derived by considering the jth measurement as

$$z_{jn} = \theta_n^T t_{jn} + v_{jn} \tag{60}$$

where t_{jn} is the jth row of $\mathbf{T}$, and v_{jn} is measurement noise, which has zero mean,

$$E(v_n) = 0 \tag{61}$$

and variance

$$E(v_n v_m) = r_n \delta_{nm} \tag{62}$$

and a Gaussian probability distribution. Here δ_{nm} is the Kronecker delta function, and the subscript j will be omitted to simplify the notation. The variation of the parameters will be modeled as a random process:

$$t_{n+1} = t_n + u_n \tag{63}$$

where u_n is a random variable, which has zero mean

$$E(u_n) = 0 \tag{64}$$

and variance

$$E(u_n u_m) = Q_n \delta_{nm} \tag{65}$$

and a Gaussian probability distribution. The minimum error-variance estimate of t_n is then obtained from the Kalman filter (ref. 103),

$$\hat{t}_n = \hat{t}_{n-1} + k_n(z_n - \theta_n^T \hat{t}_{n-1}) \tag{63}$$

where

$$M_n = P_{n-1} + Q_{n-1} \tag{67a}$$

$$P_n = M_n - M_n \theta_n \theta_n^T M_n / (r_n + \theta_n^T M_n \theta_n) \tag{67b}$$

$$k_n = M_n \theta_n / (r_n + \theta_n^T M_n \theta_n) \tag{67c}$$

Here M_n is the variance of the error in the estimate of t_n before the measurement and P_n is the variance after the measurement; k_n is the Kalman gain vector. To simplify the calculation, it will be assumed that Q_n and r_n have the same time variation for all measurements, and that Q_n, r_n, and P_o are proportional to the same function f_j:

$$r_{jn} = f_j r_n \tag{68a}$$

$$Q_{jn} = f_j Q_n \tag{68b}$$

$$P_{jo} = f_j P_o \tag{68c}$$

Then it follows that $P_{jn} = f_j P_n$ and $M_{jn} = f_j M_n$; and that the gain k_n is also then the same for all measurements. With the same gains, the rows can be combined to form

$$\hat{T}_n = \hat{T}_{n-1} + (z_n - \hat{T}_{n-1}\theta_n)k_n^T \tag{69}$$

For the local model, equation (69) becomes the following:

$$\hat{T}_n = \hat{T}_{n-1} + [(z_n - z_{n-1}) - \hat{T}_{n-1}(\theta_n - \theta_{n-1})]k_n^T \tag{70}$$

where

$$M_n = P_{n-1} + Q_{n-1} \tag{71a}$$

$$P_n = M_n - M_n \Delta\theta_n \Delta\theta_n^T M_n / (r_n + \Delta\theta_n^T M_n \Delta\theta_n) \tag{71b}$$

$$k_n = M_n \Delta\theta_n / (r_n + \Delta\theta_n^T M_n \Delta\theta_n) \tag{71c}$$

$$\Delta\theta_n = \theta_n - \theta_{n-1} \tag{71d}$$

Controller

The control algorithm is based on the minimization of a performance index J that is a quadratic function of the input and output variables. The quadratic performance function to be used here is

$$J = z_n^T W_z z_n + \theta_n^T W_\theta \theta_n + \Delta\theta_n^T W_{\Delta\theta} \Delta\theta_n \tag{72}$$

where W_z, W_θ, and $W_{\Delta\theta}$ are weighting matrices, which are assumed to be diagonal and the same value for all harmonics of a particular quantity. Then J is a weighted sum of the mean squares of the gust response and control. The matrix W_θ constrains the amplitude of the control, and $W_{\Delta\theta}$ constrains the rate of change of the control.

For the deterministic controller, the control required to alleviate the helicopter vibration is given by substituting for z_n in the performance function J, using the helicopter model, and then solving for θ_n that minimizes J. For the global model (eq. (51)), the solution can be obtained as follows:

$$\theta_n = Cz_o + C_{\Delta\theta}\theta_{n-1} \tag{73}$$

where

$$C = -DT_C^T W_z \tag{74a}$$

$$C_{\Delta\theta} = DW_{\Delta\theta} \tag{74b}$$

$$D = (T_C^T W_z T_C + W_\theta + W_{\Delta\theta})^{-1} \tag{74c}$$

for the local model (eq. (52)), the solution can be obtained as follows:

$$\theta_n = Cz_{n-1} + (C_{\Delta\theta} - CT_C)\theta_{n-1} \tag{75}$$

In this derivation, the response z is assumed to be deterministic; therefore, it is referred to as the deterministic controller. When the parameter uncertainties are taken into account, the cautious controller can be obtained by using the expected value of the performance function:

$$J = E(z_n^T W_z z_n) + \theta_n^T W_\theta \theta_n + \Delta\theta_n^T W_{\Delta\theta} \Delta\theta_n$$

$$= E\left[\sum_j w_{zj} z_{jn}^2\right] + \theta_n^T W_\theta \theta_n + \Delta\theta_n^T W_{\Delta\theta} \Delta\theta_n \tag{76}$$

where it is assumed that W_z is diagonal, and θ_n remains deterministic. For the case of the open-loop control (z_o feedback), there follows

$$E\left[\sum_j w_{zj} z_{jn}^2\right] = E \sum_j [w_{zj}(z_{jo} + \theta_n^T t_{jn})^2]$$

$$= \sum_j w_{zj}(\hat{z}_{jo} + \theta_n^T t_{jn})^2 + \sum_j w_{zj}(M_{zz} + 2\theta_n^T M_{tz} + \theta_n^T M_{tt} \theta_n) \tag{77}$$

where

$$M = \begin{bmatrix} M_{tt} & M_{tz} \\ M_{zt} & M_{zz} \end{bmatrix} \tag{78}$$

$M_{tt} = (n \times m)$ matrix

$M_{tz} = M_{zt}^T = (n \times 1)$ vector

$M_{zz} =$ scalar

So the performance function becomes

$$J = z_n^T W_z z_n + \theta_n^T W_\theta \theta_n + (\theta_n^T, 1)\left(\sum_j w_{zj} M_{jn}\right)\begin{pmatrix} \theta_n \\ 1 \end{pmatrix} + \Delta\theta_n^T W_{\Delta\theta} \Delta\theta_n \tag{79}$$

The solution for the control that minimizes J is then

$$\theta_n = C z_o + C_{\Delta\theta} \theta_{n-i} + C_o \tag{80}$$

where the gain matrices C and $C_{\Delta\theta}$ are the same as for the deterministic controller, using the identified values of the parameters and with W_θ replaced by

$$W_\theta + \left[\sum_j w_{zj} (M_{tt})_{jn}\right] \tag{81}$$

The new constant term is

$$C_o = -D\left[\sum_j w_{zj} (M_{tz})_{jn}\right] \tag{82}$$

Similarly, for the case of the closed-loop control (z_{n-1} feedback), the performance function is

$$J = z_n^T W_z z_n + \theta_n^T W_\theta \theta_n + \Delta\theta_n^T \left(W_{\Delta\theta} + \sum_j w_{zj} M_{jn} \right) \Delta\theta_n \tag{83}$$

The solution is identical to that for the deterministic controller, using the identified values of the parameters, and with $W_{\Delta\theta}$ replaced by

$$W_{\Delta\theta} + \sum_j w_{zj} M_{jn} \tag{84}$$

Regulators

A controller combining recursive parameter estimation and linear feedback is called a self-tuning regulator. There are two fundamental options for the identification: the use of either an invariable algorithm or an adaptive algorithm. There are also two fundamental options for the controller: open-loop or closed-loop. Hence, there are four possible regulator configurations (fig. 15). For the adaptive algorithm, the parameters are recursively identified on-line, using a Kalman filter. For the open-loop algorithm, the control is based on the uncontrolled vibration level z_o (identified either on-line or off-line). For the closed-loop algorithm, the control is based on the feedback of the measured vibration, z_{n-1}. These four regulator options are reviewed in reference 70.

In this study, two regulators are investigated for a gust alleviation system. Figure 16(a) shows an adaptive open-loop regulator algorithm, in which both $\{z_0\}$ and $[T_C]$ are identified by a Kalman filter. Figure 16(b) shows an adaptive closed-loop regulator algorithm. In this regulator, only $[T_C]$ is updated by a Kalman filter and the output vector z_n is contaminated by measurement noise, v_n. In both regulators, the uncertainty of parameters can be taken into consideration by using the variance of the error in the estimate of t_n before the measurement, M_{n+1} (see eq. (81) or (84)). These regulators consist of on-line identification of the parameters and calculation of the gain matrix, with feedback of the control based on the measured responses. It should be noted that the Kalman filter gains can be calculated in the time interval between application of θ_n to the helicopter and the measurement of the resulting z_n.

Gust Model

In the past, studies that have dealt with gust suppression systems have used gust models, such as the von Kármán model, Dryden model, step model, sinusoidal model, and sine-squares model. These models have some advantages as well as some disadvantages. The von Kármán and the Dryden models are expressions derived from statistical techniques in the frequency domain. These expressions are close to the natural turbulent flows in the sense of the statistics. However, they are not able to show the individual flow pattern of turbulence in the time domain. Therefore, these models are not suitable for timewise numerical calculation. On the other hand, the step and sinusoidal gust models, etc., are very simple yet different from actual gust shapes. These expressions are easy to handle in numerical calculations. By using these

gust models, it is possible to obtain the basic characteristics of the plant model for the gust response. In this study, the following gust representation is assumed:

$$\{g\} = \begin{Bmatrix} u_G \\ v_G \\ w_G \end{Bmatrix} = (u_{Go}, v_{Go}, w_{Go})^T \exp(i\omega_G t) \tag{85}$$

where u_{Go}, v_{Go}, and w_{Go} are horizontal, lateral, and vertical gust amplitudes, respectively; and ω_G is the gust angular velocity. For the step gust, $\omega_G = 0$. The positive direction for the gust velocity is defined in the rotor frame. Most results are for a vertical gust only. For this study, the rotor is assumed to have the blades at 0°, 90°, 180°, and 270° when the sinusoidal gust is initially encountered by the rotor (the gust velocity field is convected past the rotor by the helicopter forward speed). As in reference 20, the ratio of the magnitudes of the gust components is assumed to be

$$u_{Go} : v_{Go} : w_{Go} = 3.0 : 2.0 : 1.8 \tag{86}$$

The helicopter is represented mathematically by a simple linear quasi-static frequency domain model, relating z_n and θ_n. Therefore, a simple sinusoidal gust shape is selected in order to investigate the feasibility of the gust alleviation algorithm.

Numerical Calculations

Numerical calculations have been performed to determine the feasibility of the adaptive blade control algorithm. This adaptive blade pitch control algorithm consists of a set of measurements (oscillatory hub forces and moments), an identification system using a Kalman filter, a control system based on the minimization of the quadratic performance function, and a simulation system of the helicopter rotor. The operating conditions of the rotor are the same as the case of the individual blade pitch control (table 3). The initial estimate of the transfer function $[T_C]$ is obtained by using the harmonic method program. The detailed derivation of $[T_C]$ is given in appendix E. Tables 4 and 5 show the transfer function of the rotor for $f_G = 2.0$ Hz and $f_G = 0.0$ Hz (step gust), respectively. In the case of the step gust, gust frequency is assumed to be zero and the control inputs $\Delta\theta$ and the outputs z are assumed as follows:

$$\begin{aligned} \Delta\theta &= \theta_1 + \theta_2 \cos\psi + \theta_3 \sin\psi \\ \{z\} &= (\Delta T_0,\ \Delta H_0,\ \Delta M_{Y0},\ \Delta Y_0,\ \Delta M_{X0},\ \Delta M_{Z0})^T \end{aligned} \tag{87}$$

where the subscript 0 denotes the mean value. The $[T_C]$ obtained by the harmonic method is regarded as the initial estimate in the adaptive blade pitch control. In the controller, the $[T_C]$ is updated by the Kalman filter at every time-cycle. In this calculation, it is assumed that there is no noise in the measurement of $\Delta\theta$. However, measurements z are usually contaminated by noise. Measurement noise is generated by a random noise generator. Several sets of noise-to-signal ratios were studied before these calculations were made. A noise-to-signal ratio of about 0.05 was used in this study. After trial and error, the initial values of P_o, Q_o in

equation (67) were estimated as follows: $P_o = [9.8\times10^4]$N (or N-m), $Q_o = [9.8\times10^2]$N (or N-m). The variance of the measurement noise, r, is assumed to be 9.8N (or N-m). To keep the noise-to-signal ratio approximately constant, the following relationship is taken into account (see ref. 28):

$$r_{n+1} = r_n(J_{n+1}/J_n)$$
$$r_{min} \leq r_n \leq r_{max} \tag{88}$$

where J_n is the quadratic performance function at the nth time-cycle. The weighting matrices of the quadratic performance function are taken as

$$W_z = [1.0\times10^{-4}]$$
$$W_\theta = [0.0] \tag{89}$$
$$W_{\Delta\theta} = [1.0\times10^4]$$

Since the dimensional values of the measurements z are used, the elements of the weighting matrix W_z become small. The pitch control θ_n are unconstrained; the pitch control rates $\Delta\theta_n$ are constrained. The values given by equation (89) were selected for good algorithm convergence characteristics.

In this gust alleviation system, the gust frequency f_G is specified. Therefore, each time-cycle that updates the parameters must vary depending on the gust frequency. In most calculations, a 2.0 Hz gust frequency is used. This frequency is more than half of the rotor rotational speed, and somewhat larger than the typical mean atmospheric turbulence (usually below 1.0 Hz). An updated parameter estimate is performed every four rotor revolutions. During that time, the measurements z are discretely sampled by the measuring system. Since the measurements z are data in the time domain, it is required that they be converted from the time domain to the frequency domain using the fast Fourier transform (FFT) (ref. 104). In the FFT, the solution of the data in the frequency domain depends on the sampling time Δt (Shannon's theorem); in this calculation, $\Omega\Delta t = 10°$. Therefore, when the gust frequency f_G falls between two points (that is, $n\Delta f < f_G < (n + 1)\Delta f$, n = integer, Δf = frequency step), it is impossible to calculate the correct values by the FFT. In this analysis, correct values are approximated from known gust frequency f_G and by using a cubic spline interpolation method. Furthermore, it is necessary to consider the calculation time of the optimal control, which determines the optimal control for the next time-cycle using the output data from the FFT. One time-cycle is 8π rad (fig. 17). The sampling interval is $(128/144)(8\pi)$ rad. Data are sampled at every 10° (144 samples in four revolutions); 128 samples are used in FFT since powers of 2 are typically computationally more efficient ($2^7 = 128$). Consequently the required calculation time is assumed to be $(16/144)(8\pi)$ rad. As a result, there is a phase shift ($\phi_I + \phi_{II}$) in the measured response at the beginning of the next time-cycle relative to the phase at the end of the previous sampling interval. In the program code, this phase shift is accounted for in implementing the control as follows:

$$
\left.
\begin{aligned}
(Z_1)_n &= (Z_1)_{n-1} \cos[(\omega_G/\Omega)\phi_{II}] + (Z_2)_{n-1} \sin[(\omega_G/\Omega)\phi_{II}] \\
(Z_2)_n &= (Z_2)_{n-1} \cos[(\omega_G/\Omega)\phi_{II}] - (Z_1)_{n-1} \sin[(\omega_G/\Omega)\phi_{II}] \\
Z_{n-1} &= (Z_0)_{n-1} + (Z_1)_{n-1} \cos(\omega_G t) + (Z_2)_{n-1} \sin(\omega_G t) + \ldots \\
Z_n &= (Z_0)_n + (Z_1)_n \cos(\omega_G t) + (Z_2)_n \sin(\omega_G t) + \ldots
\end{aligned}
\right\} \qquad (90)
$$

where Z_1, Z_2 are coefficients of the cosine and sine term of the response, respectively. The subscripts n denote the nth time-cycle. If this phase shift is not considered, $(Z_1)_n$ and $(Z_2)_n$ coincide with $(Z_1)_{n-1}$ and $(Z_2)_{n-1}$. By using the above equations, the optimal control inputs for the next time-cycle can be determined. A global helicopter model is used. For the open-loop controller, both z_0 and $[T_C]$ are updated by the Kalman filter. Only $[T_C]$ is updated for the closed-loop controller.

In figures 18(a) to 18(g) and figures 19(a) to 19(g), the hub gust responses without control are shown separately for the horizontal and the lateral components of the gust. The amplitude of the horizontal gust is 3.0 m/sec, and that of the lateral gust is 2.0 m/sec. The gust frequency of 2.0 Hz is used. Figures 18 and 19 show little influence on the thrust response. In the horizontal and side forces and yawing moment responses, the effect of these types of gusts on the hub response can be seen. Figures 20(a) to 20(g) show the hub responses without control for the three dimensional gust. The amplitude of the three gust components are $u_{Go} = 3.0$ m/sec; $v_{Go} = 2.0$ m/sec; and $w_{Go} = 1.8$ m/sec. The three components of the gust have the same frequency ($f_G = 2.0$ Hz). The increase of the horizontal force, the side force, and the yawing moment responses can be seen by comparing figure 20 with figure 11. From these results, a vertical component of the gust is the most influential on the rotor gust response (specifically in the thrust response).

Figures 21(a) to 21(g) show the hub gust responses with the adaptive blade pitch control for a vertical gust component only ($f_G = 2.0$ Hz). The controller is deterministic, and the global helicopter model was used. Two inputs (θ_1 and θ_2) and two outputs (cosine and sine elements of the thrust response) are considered. Therefore, the dimension of $[T_C]$ becomes (2 × 2). The thrust response (fig. 21(a)) gradually decreases, but the yawing moment response (fig. 21(f)) responds dramatically (see fig. 11(f)). The other responses (F_x, F_y, M_x, M_y) are similar to that shown in figure 11. In this case, the aim of the controller is to reduce the thrust fluctuation owing to the gust, and no attempt is made to reduce the other responses.

In figures 22(a) to 22(g), the hub gust responses are shown with adaptive blade pitch control, again for the vertical gust component only. In this case, the dimension of $[T_C]$ is (6 × 12). As control inputs, six elements (θ_1 to θ_6) are used to alleviate the responses. Measurements z involve the hub forces (F_x, F_y, F_z) and the hub moments (M_x, M_y, M_z). Compared with figure 21, the reduction of the thrust response is significant (about 50% to 80%). From this figure, it is observed that the fluctuation of the thrust does not reduce uniformly; in other words, it sometimes diverges and converges. This phenomenon is explained as follows. The control inputs generated by the controller depend on the measurements. When the hub responses are decreased by means of the controller, the optimal control inputs necessarily become small. However, the gust itself is unchangeable. Therefore, the effect of the controller on the reduction of the responses becomes weak. At the same time, the uncertainty of the identified parameters may increase, even if the noise to signal ratio

is kept constant by equation (88). In the yawing moment response (fig. 22(f)), the characteristics of the response are improved (see fig. 21(f)), and the amplitude of the fluctuation is a little less than that of the case shown in figure 11. Similar to the thrust response, the response sometimes diverges and converges. This is due to the change of the induced drag which is directly related to the thrust. Contrary to expectations, the responses (F_x, F_y, M_x, M_y) show a slight increase in magnitude. In the pitch angle change of the reference blade (fig. 22(g)), the sinusoidal change with the gust frequency can be observed, similar to that shown in figure 21(g).

Figure 23 shows the time histories of the mean square thrust response. In this figure, the solid line denotes uncontrolled response. The dashed line corresponds to figure 21 (two inputs and two outputs) and the broken line corresponds to figure 22 (six inputs and 12 outputs). As explained before, the parameters are updated at every four revolutions. During one time-cycle, the control inputs are kept constant. The response for the case of thrust control only is at first constant, and then gradually decreases. The response is reduced by almost 50% after 20 revolutions with the controller engaged (five time-cycles). The response for the case of complete hub response control decreases to a much lower value, although not continuously. A 50% to 80% reduction of the thrust response is attained for the case of complete hub response control. From these results, it is found that the measurements z should include not only the thrust response but also other hub responses.

Shown in figures 24(a) to 24(g) are the hub responses for the vertical step gust. Operating conditions are the same as in the case shown in figure 13. The adaptive closed-loop controller is used. The measurements z involve only the longitudinal response of the rotor; that is, the horizontal force F_x, the thrust F_z, and the pitching moment M_y. The control inputs have three elements (θ_1, θ_2, θ_3) according to equation (87). All parameters (z_0 and $[T_C]$) are updated at every rotor revolution by the Kalman filter. Significant reduction in the thrust response (fig. 24(a)) is achieved by the controller (almost 100%). However, compared with figure 14, the horizontal and side force responses transfer to a new steady state condition. The rolling and pitching moment responses (figs. 24(d) and 24(e)) transfer to new steady state conditions. In the yawing moment response (fig. 24(f)), there is a significant change in the steady state condition. This phenomenon is a result of the strong effect of the controller on the gust alleviation system. The controller generates the optimal control inputs in order to reduce the change from the steady value. If these control inputs are large values, a new trim condition could result. Referring to figure 24(g), the maximum change of the pitch angle is about 2°. The cyclic pitch angles for the trim condition itself are of the order of several degrees. Therefore, the pitch angle change by the controller has an effect on the rotor trim condition. In this case, the ratio between the control angles $\Delta\theta$ and the trim pitch angle θ becomes more than 10%. The flight trim condition consequently changes and transfers to the new steady state condition.

In figures 25(a) to 25(g), the hub responses for the vertical step gust are shown. The adaptive closed-loop controller is used, and the operating conditions are the same as those shown in figure 24. To investigate the sensitivity of the transfer function to the controller performance, arbitrary small initial values of the transfer function are used in this calculation. Compared with figure 24, the thrust fluctuation (fig. 25(a)) decreases very slowly. For the other responses except yawing moments the trim condition remains the same. In the case of the yawing moment (fig. 25(f)), the transfer to the steady state can be seen after showing an overshoot. This phenomenon is due to the induced drag, as mentioned before. From these results, it can be concluded that the performance of the controller

depends on the initial estimate of the rotor transfer function. If a more correct transfer function is used, convergence of the responses can be obtained more quickly. As shown previously, the transfer function derived by the harmonic method gives a reasonable initial estimate.

Figures 26(a) to 26(g) show the hub responses, again for the vertical step gust. In this case, the adaptive open-loop controller is used. The measurements z involve six responses of the rotor; that is, three hub forces (F_x, F_y, F_z) and three hub moments (M_x, M_y, M_z). Similar to the case shown in figure 24, all elements of $[T_C]$ are updated at every rotor revolution. The magnitude of the controller inputs is constrained by a prescribed maximum value ($\Delta\theta_{max} = 2.0°$). Three components ($\theta_1$, θ_2, θ_3) of the control inputs (eq. (87)) are used in this calculation. In this thrust response (fig. 26(a)), the deviation from the steady value of the thrust gradually decreases after responding to the step gust. Compared with the case of figure 24, the pitch angle change is very slow and small. The other hub forces, together with the rolling and pitching moments, remain steady. The yawing response deviates slowly from the steady value because of the thrust response. In the case of the open-loop controller, the optimal control inputs depend on the uncontrolled response z_0. If the z_0 are small, then the optimal control inputs may be small. For this case, the optimal control inputs at the beginning stage of controller operation are less than 0.5°.

In figure 27, the time histories of the quadratic performance function J are shown. The solid line denotes the function J without control. The J's with control are shown for both the adaptive closed-loop control (corresponding to fig. 24) and the adaptive open-loop control (corresponding to fig. 26). For the adaptive closed-loop controller, the J decreases rapidly after showing a sharp increase. The J for the adaptive open-loop controller decreases moderately after showing the same increase. Both control schemes show the effect the controller has on the reduction of the hub gust responses.

Since deterministic controllers have been considered in this analysis, the uncertainty of the parameter identification has not been considered in the calculation of the optimal control inputs. These cautious properties can play an important role for inherent helicopter vibration reduction schemes (ref. 68). In figures 28(a) to 28(g), the hub gust responses with the cautious controller are shown for the vertical gust ($f_G = 2.0$ Hz). Referring to figure 22, there is no significant difference between these figures. The cautious controller involves the variance of the error in the estimate of the transfer function $[T_C]$ before the measurement. The more uncertain the parameter estimates, the larger the variance of the error. In this calculation, the term concerned with the cautious properties

$$\left[\sum_j w_{zj}(M_{tt})_{jn}\right]$$

in equation (81) was about 1% of the term $T_C^T W_z T_C$ in equation (74c). Therefore, these calculated results show that the cautious properties have little effect on the controller performance in this study.

Results from applying adaptive blade pitch control for the three dimensional gust are shown in figures 29(a) to 29(g). Operating conditions are the same as those in the case of figure 20. The large reduction in the thrust response can be observed by comparing figure 28 with figure 20. The yawing moment response shows the same

characteristics as for a vertical gust only (fig. 22). In general, all the hub responses are similar to those of the case shown in figure 22. In this calculation, the cautious properties have not been considered because of their minimal effect on controller performance.

4. CONCLUSIONS

Control systems to reduce the gust-induced vibration of helicopter rotors have been studied by two means. One is an individual blade pitch control scheme, and the other is an adaptive blade pitch control scheme. Among three gust components, the horizontal and lateral components of gust have little influence on the hub gust response. However, the vertical component of the gust has a great influence on the rotor hub response. In studying the gust response of the rotor, the thrust response shows the most significant change compared with the other responses. Hence, reducing the thrust response should be the aim of the gust alleviation system. Both control schemes show significant effects of the controllers on the reduction of the gust-induced vibration of the helicopter rotor. From these theoretical analyses, the following conclusions are drawn.

For the individual blade pitch control scheme:

1. A computer code that calculates the gust response of a rotor has been developed by using the harmonic method. This code is applicable to the rotor impedance calculation for gust response or the transfer function calculation of the rotor.

2. Outboard measurement sensors are more effective in reducing the gust-induced vibration than are inboard radial station locations.

3. The gust-induced thrust response determined by the harmonic method is about 10% to 20% larger than that given by the LMT. However, the results by the harmonic method can qualitatively predict the characteristics of the gust response.

4. Individual blade pitch control can significantly reduce gust-induced vibration. For example, reductions of the thrust response for the sinusoidal gust by almost 60% and for the step gust by almost 70% can be obtained for a specified feedback gain K_w.

5. For the gust models used, an increase in the yawing moment fluctuation is observed. A control scheme to include the reduction of the transient yawing response should be incorporated.

6. The magnitude of the control inputs is less than 1.0°. For these pitch angles, there is little effect on the trim condition of the rotor.

7. Because the flapwise blade deflection is most sensitive to the gust (compared with the lead-lag and torsion deflections), it is a good measurement of the gust-induced rotor response for an articulated rotor.

For the adaptive blade pitch control scheme:

1. The major, the subharmonic, and the superharmonic inputs are considered in the controller. As the gust frequency increases, higher frequency terms of the gust

response become large. To alleviate these high frequency terms in the vibratory response, the number of terms included in the control inputs increases, making the controller more complex.

2. The performance of the controller depends on the initial estimate of the rotor transfer function. When the exact transfer function is used, the convergence of the hub responses can be achieved quickly. The transfer function derived by the harmonic method gives a good estimate.

3. In using the FFT to convert measurements from the time domain to the frequency domain, some approximations must be made because of the arbitrary gust frequency. This may increase the uncertainty of the measurement. A more accurate frequency domain determination method is required.

4. For the case of a sinusoidal gust, the adaptive open-loop regulator is best suited for the gust alleviation system. Results show that a 50% to 80% reduction in the thrust response can be obtained. The regulator studied in this report is shown to be applicable to a three dimensional gust.

5. For the step gust, the adaptive closed-loop regulator performs better than the adaptive open-loop regulator. The closed-loop regulator yields a rapid reduction of the gust-induced thrust response (almost 100%), even though it violates the trim condition. The open-loop regulator shows that convergence of the thrust response is slow.

6. The uncertainty of the parameter identification has little influence on the improvement of the regulator in this investigation.

7. In this adaptive control scheme, the gust frequency is prescribed at the initial stage of the calculations. Therefore, this type of regulator does not apply to random gust responses.

APPENDIX A

COORDINATE SYSTEMS

Five Cartesian frames are used in this study to describe the blade and hub motions. The definition of these frames is briefly reviewed in this appendix.

Inertial frame (X_I, Y_I, Z_I)— This frame is inertially fixed and coincides with the body frame under the steady flight condition.

Body frame (X_B, Y_B, Z_B)— This frame is fixed to the fuselage with its origin at the center of gravity; X_B is oriented to the direction of the steady flight, Y_B is taken to be positive in the right-hand direction, Z_B is positive downward. The relationship between the inertial frame and the body frame is as shown:

$$\begin{Bmatrix} X_I \\ Y_I \\ Z_I \end{Bmatrix} = [T_{BI}] \begin{Bmatrix} X_B \\ Y_B \\ Z_B \end{Bmatrix} + \begin{Bmatrix} X_{Bo} \\ Y_{Bo} \\ Z_{Bo} \end{Bmatrix} \tag{A1}$$

$$[T_{BI}] = \begin{vmatrix} \cos\Psi, & -\sin\Psi, & 0 \\ \sin\Psi, & \cos\Psi, & 0 \\ 0, & 0, & 1 \end{vmatrix} \begin{vmatrix} \cos\Theta, & 0, & \sin\Theta \\ 0, & 1, & 0 \\ -\sin\Theta, & 0, & \cos\Theta \end{vmatrix} \begin{vmatrix} 1, & 0, & 0 \\ 0, & \cos\Phi, & -\sin\Phi \\ 0, & \sin\Phi, & \cos\Phi \end{vmatrix} \tag{A2}$$

where (Φ, Θ, Ψ) are Euler angles of the body, and (X_{Bo}, Y_{Bo}, Z_{Bo}) is the position of the origin of the body frame in the inertial frame.

Rotor frame (X_R, Y_R, Z_R)— This frame is fixed to the fuselage with its origin at hub center; Z_R coincides with the rotor shaft and X_R is positive rearward. This frame is related to the body frame by the following transformation:

$$\begin{Bmatrix} X_B \\ Y_B \\ Z_B \end{Bmatrix} = [T_{RB}] \begin{Bmatrix} X_R \\ Y_R \\ Z_R \end{Bmatrix} + \begin{Bmatrix} X_{Ro} \\ Y_{Ro} \\ Z_{Ro} \end{Bmatrix} \tag{A3}$$

$$[T_{RB}] = \begin{vmatrix} -\cos i_S, & 0, & -\sin i_S \\ 0, & 1, & 0 \\ \sin i_S, & 0, & -\cos i_S \end{vmatrix} \tag{A4}$$

where i_S is the shaft inclination angle and (X_{Ro}, Y_{Ro}, Z_{Ro}) is the position of the origin of the rotor frame in the body frame.

Rotating hub frame (X_H, Y_H, Z_H)— This frame is rotated about the Z_R axis by $\psi = \Omega t$. The coordinate transformation between the rotor frame and the hub frame is expressed as

$$\begin{Bmatrix} X_R \\ Y_R \\ Z_R \end{Bmatrix} = [\mathbf{T}_{HR}] \begin{Bmatrix} X_H \\ Y_H \\ Z_H \end{Bmatrix} \tag{A5}$$

$$[\mathbf{T}_{HR}] = \begin{vmatrix} \cos\psi, & -\sin\psi, & 0 \\ \sin\psi, & \cos\psi, & 0 \\ 0, & 0, & 1 \end{vmatrix} \tag{A6}$$

Blade frame (X_b, Y_b, Z_b)— This is a local frame fixed to each blade section considered. The blade section itself is assumed to be rigid; Z_b is directed outward along the local elastic axis, and Y_b is directed toward the zero-lift angle of the blade section. The displacements of the elastic axis are denoted by (u, v, w) in the hub frame. Angular changes related to the hub frame are given by the Euler angles ($\theta + \phi$, $-w'$, v') where $(\,)'$ denotes $d(\,)/dX_H$. The transformation between the hub frame and the blade frame is given as

$$\begin{Bmatrix} X_H \\ Y_H \\ Z_H \end{Bmatrix} = [\mathbf{T}_{bH}] \begin{Bmatrix} X_b \\ Y_b \\ Z_b \end{Bmatrix} + \begin{Bmatrix} r + u \\ e_o + v \\ w \end{Bmatrix} \tag{A7}$$

$$\begin{aligned} [\mathbf{T}_{bH}] &= \begin{vmatrix} 1, & -v', & 0 \\ v', & 1, & 0 \\ 0, & 0, & 1 \end{vmatrix} \begin{vmatrix} 1, & 0, & -w' \\ 0, & 1, & 0 \\ w', & 0, & 1 \end{vmatrix} \begin{vmatrix} 1, & 0, & 0 \\ 0, & \cos(\theta+\phi), & -\sin(\theta+\phi) \\ 0, & \sin(\theta+\phi), & \cos(\theta+\phi) \end{vmatrix} \\ &\cong \begin{vmatrix} 1, & -v' - \theta w', & -w' + \theta v' \\ v', & 1 - \theta^2/2 - \theta\phi, & -(\theta+\phi) \\ w', & (\theta+\phi), & 1 - \theta^2/2 - \theta\phi \end{vmatrix} \end{aligned} \tag{A8}$$

In figures 30(a) and 30(b), four coordinate systems (except the inertial frame) are shown schematically.

Since motion of a fuselage is not considered ($\Phi = \Theta = \Psi = 0$), and shaft inclination angle is zero ($i_S = 0$), three coordinate systems, (X_R, Y_R, Z_R), (X_H, Y_H, Z_H), and (X_b, Y_b, Z_b) are used in this study.

APPENDIX B

BLADE SECTION LOADS

In this appendix, total loads on the blade section are defined (fig. 31).

Inertial loads— The inertial forces {P} and moments {Q} acting on a unit span of the blade are given as follows:

$$\{P\} = \begin{Bmatrix} p_x \\ p_y \\ p_z \end{Bmatrix} \tag{B1}$$

$$\begin{Bmatrix} p_x \\ p_y \\ p_z \end{Bmatrix} = -m \begin{Bmatrix} \ddot{u} - e(\ddot{v}' + \theta\ddot{w}') + 2\Omega[-\dot{v} + e\theta(\dot{\theta} + \dot{\phi})] - \Omega^2[r + u - e(v' + \theta w')] \\ \ddot{v} - e\theta(\ddot{\theta} + \ddot{\phi}) + 2\Omega[\dot{u} - e(\dot{v}' + \theta\dot{w}')] - \Omega^2[e_o + e + v - e\theta\phi] \\ \ddot{w} + e(\ddot{\theta} + \ddot{\phi}) \end{Bmatrix} \tag{B2}$$

$$\{Q\} = \begin{Bmatrix} q_x \\ q_y \\ q_z \end{Bmatrix} \tag{B3}$$

$$\begin{Bmatrix} q_x \\ q_y \\ q_z \end{Bmatrix} = -mk^2 \begin{Bmatrix} \ddot{\theta} + \ddot{\phi} + \Omega^2(\theta + \phi) + 2\Omega\theta v' \\ -\theta\ddot{v}' + \Omega^2\theta v' \\ \ddot{v}' + \theta\ddot{w}' - 2\Omega\theta(\dot{\theta} + \dot{\phi}) \end{Bmatrix} - me \begin{Bmatrix} \ddot{w} - \theta[\ddot{v} + 2\Omega\dot{u} - \Omega^2(e_o + v)] + e_o\Omega^2\phi \\ \theta[\ddot{u} - 2\Omega\dot{v} - \Omega^2(r + u)] - r\Omega^2\phi \\ -[\ddot{u} - 2\Omega\dot{v} - \Omega^2(r + u)] - r\Omega^2\theta\phi + e_o\Omega^2(v' + \theta w') \end{Bmatrix} \tag{B4}$$

where

$$m = \int_{\text{chord}} dm \ , \qquad e = \frac{1}{m}\int_{\text{chord}} \eta \, dm \ , \qquad k = \left(\frac{1}{m}\int_{\text{chord}} \eta^2 \, dm\right)^{1/2} \tag{B5}$$

are mass, distance between mass center and elastic axis, and polar radius of gyration of the blade per unit span, respectively. Equations (B2) through (B4) are the inertial loads owing to the blade motion when the hub is not in motion.

Aerodynamic loads— Aerodynamic forces and moments are derived from two-dimensional quasi-steady thin airfoil theory (ref. 96) and assuming airfoil plunging

to be zero (h = 0). Blade lift, pitching moment, and profile drag are given as follows:

$$L = 2\pi\rho b U_a C'[H_a + \alpha U_a + (1/2 - a)b(\dot{\alpha} + Q_o)] + \pi\rho b^2 (d/dt)[H_a + \alpha U_a - ab(\dot{\alpha} + Q_o)] \tag{B6}$$

$$M = (a + 1/2)2\pi\rho b^2 U_a C'[H_a + \alpha U_a + (1/2 - a)b(\dot{\alpha} + Q_o)] - (\pi\rho b^3/2)U_a(\dot{\alpha} + Q_o)$$
$$+ \pi\rho b^3 (d/dt)[a(H_a + \alpha U_a) - b(1/8 + a^2)(\dot{\alpha} + Q)] \tag{B7}$$

$$D = \rho b U_a^2 C_{do} \tag{B8}$$

$$D_i = -L \sin \phi = -LH_a/U_a \tag{B9}$$

where C' is the lift deficiency function and is assumed to be unity in this study. The quantities D_i, ϕ, and C_{do} are induced drag, inflow angle, and drag coefficient, respectively. It is noted that in equations (B6) through (B8) differentiation (d/dt) must be operated on U_a as well as H_a, Q_o, and α. Quantities of U_a, H_a, Q_o, and α are expressed as follows:

$$\left.\begin{aligned} U_a &= r\Omega + \dot{v} + U_o \sin\psi + v'U_o \cos\psi + u_G \sin\psi + v_G \cos\psi \\ H_a &= -v_S - \dot{w} + \dot{w}_G - w'U_o \cos\psi \\ Q_o &= \Omega w' \\ \alpha &= \theta + \phi \end{aligned}\right\} \tag{B10}$$

By using equations (B6) through (B9), aerodynamic forces and moments acting on the blade are

$$\begin{Bmatrix} F_{ax} \\ F_{ay} \\ F_{az} \end{Bmatrix} = [\Delta_A] \begin{vmatrix} 1, & 0 & , & 0 \\ 0, & \cos\phi, & \sin\phi \\ 0, & -\sin\phi, & \cos\phi \end{vmatrix} \begin{vmatrix} 0 \\ -D \\ L \end{vmatrix} \cong \begin{Bmatrix} -w'L \\ -D - D_i \\ L \end{Bmatrix} \tag{B11}$$

$$\begin{Bmatrix} M_{ax} \\ M_{ay} \\ M_{az} \end{Bmatrix} = [\Delta_A] \begin{Bmatrix} M \\ 0 \\ 0 \end{Bmatrix} \cong \begin{Bmatrix} M \\ v'M \\ w'M \end{Bmatrix} \tag{B12}$$

$$[\Delta_A] = \begin{vmatrix} 1 & , & -v', & 0 \\ v', & & 1 & , & 0 \\ 0 & , & 0 & , & 1 \end{vmatrix} \begin{vmatrix} 1 & , & 0, & -w' \\ 0 & , & 1, & 0 \\ w', & & 0, & 1 \end{vmatrix} \cong \begin{vmatrix} 1 & , & -v', & -w' \\ v', & & 1 & , & 0 \\ w', & & 0 & , & 1 \end{vmatrix} \tag{B13}$$

The wing motions in the two-dimensional thin airfoil theory and the lift, drag, and pitching moment acting on the wing section are shown in figures 32 and 33, respectively.

Total loads— Total loads acting on the blade section can be obtained as the sum of inertial, aerodynamic, and gravitational loads as

$$\begin{Bmatrix} P_x \\ P_y \\ P_z \end{Bmatrix} = \begin{Bmatrix} p_x \\ p_y \\ p_z \end{Bmatrix} + \begin{Bmatrix} F_{ax} \\ F_{ay} \\ F_{az} \end{Bmatrix} + \begin{Bmatrix} 0 \\ 0 \\ -mg \end{Bmatrix} \tag{B14}$$

$$\begin{Bmatrix} Q_x \\ Q_y \\ Q_z \end{Bmatrix} = \begin{Bmatrix} q_x \\ q_y \\ q_z \end{Bmatrix} + \begin{Bmatrix} M_{ax} \\ M_{ay} \\ M_{az} \end{Bmatrix} + \begin{Bmatrix} -meg \\ 0 \\ 0 \end{Bmatrix} \tag{B15}$$

where g is the gravitational acceleration.

APPENDIX C

COEFFICIENTS OF EQUATION (6): A_m, B_m, C_m, AND F_n

The equation given from equation (2) is

$$\sum_i \left(A_{ij}\,\Delta\ddot{q}_i + B_{ij}\,\Delta\dot{q}_i + C_{ij}\,\Delta q_i\right) = F_j \tag{C1}$$

where

$$A_{ij} = m_j\delta_{ij} + \int_o^R \bar{\phi}_j\left(\frac{b^2}{8}\,C_2\bar{\phi}_i\right)dr - \int_o^R (\bar{w}_j + ab\bar{\phi}_j)C_2(\theta\bar{v}_i - \bar{w}_i - ab\bar{\phi}_i)dr \tag{C2}$$

$$B_{ij} = \int_o^R 2m\Omega[\bar{\phi}_j(k^2\theta\bar{v}_i' - e\theta\bar{u}_i) + w_o'\bar{w}_j\bar{v}_i + \bar{v}_j\{\bar{u}_i + e(\bar{v}_i' + \theta\bar{w}_i')\}]dr$$

$$+ \int_o^R \bar{\phi}_j\,\frac{b}{2}\,C_2\left\{U_T\bar{\phi}_i + \frac{b}{4}\,\Omega\bar{w}_i'\right\}dr - \int_o^R \left\{\bar{w}_j + \left(a + \frac{1}{2}\right)b\bar{\phi}_j\right\}C_1\left\{(2\theta U_T + U_p)\bar{v}_i - U_T\bar{w}_i\right.$$

$$\left. + \left(\frac{1}{2} - a\right)bU_T\bar{\phi}_i + \left(\frac{1}{2} - a\right)b(\dot{\theta} + \Omega w_o')\bar{v}_i\right\}dr - \int_o^R (\bar{w}_j + ab\bar{\phi}_j)C_2\{U_R(\theta\bar{v}_i' - \bar{w}_i')$$

$$+ U_T\bar{\phi}_i + \dot{\theta}\bar{v}_i - ab\Omega\bar{w}_i'\}dr + \int_o^R \bar{v}_jC_3U_T\bar{v}_i\,dr + \int_o^R \bar{v}_jC_1\left\{(\theta U_T + 2U_p)\bar{w}_i - \theta U_p\bar{v}_i\right.$$

$$\left. - \left(\frac{1}{2} - a\right)bU_p\bar{\phi}_i + \left(\frac{1}{2} - a\right)b(\dot{\theta} + \Omega w_o')\bar{w}_i\right\}dr + C_\zeta\bar{v}_i'(r_\zeta)\bar{v}_j'(r_\zeta) \tag{C3}$$

$$C_{ij} = \omega_j^2m_j\delta_{ij} + \int_o^R \bar{\phi}_j\left(\frac{b}{2}\,C_2\Omega U_T\bar{w}_i'\right)dr - \int_o^R \left\{\bar{w}_j + \left(\frac{1}{2} + a\right)b\bar{\phi}_j\right\}C_1\left[\left\{-U_TU_R + \left(\frac{1}{2} - a\right)b\Omega U_T\right\}\bar{w}_i'\right.$$

$$\left. + (2\theta U_T + U_p)U_R\bar{v}_i' + \left(\frac{1}{2} - a\right)b(\dot{\theta} + \Omega w_o')U_R\bar{v}_i' + U_T^2\bar{\phi}_i\right]dr - \int_o^R (\bar{w}_j + ab\bar{\phi}_j)C_2$$

$$\times\{\theta\dot{U}_R\bar{v}_i' - \dot{U}_R\bar{w}_i' + \dot{\theta}U_R\bar{v}_i' + \dot{U}_T\bar{\phi}_i\}dr + \int_o^R \bar{v}_jC_1\left\{-(\theta U_T + 2U_p)U_R\bar{w}_i' + \left(\frac{1}{2} - a\right)bU_p\Omega\bar{w}_i'\right.$$

$$\left. + U_TU_p\bar{\phi}_i + \theta U_pU_R\bar{v}_i' - \left(\frac{1}{2} - a\right)b(\dot{\theta} + \Omega w_o')U_R\bar{w}_i'\right\}dr + \int_o^R \bar{v}_j(C_3U_TU_R\bar{v}_i')dr \tag{C4}$$

$$F_j = \int_o^R (\bar{w}_j + ab\bar{\phi}_j)C_2[-\dot{w}_G]dr + \int_o^R \left[\left\{\bar{w}_j + \left(\frac{1}{2} - a\right)b\bar{\phi}_j\right\}C_1U_T + \bar{v}_jC_1(\theta U_T + 2U_p)\right.$$

$$+ \bar{v}_jC_1\left(\frac{1}{2} - a\right)b(\dot{\theta} + \Omega w_o')\Big][-w_G]dr + \left[\int_o^R [(\bar{w}_j + ab\bar{\phi}_j)C_2\dot{U}_T + \left\{\bar{w}_j + \left(\frac{1}{2} + a\right)b\bar{\phi}_j\right\}C_1U_T^2\right.$$

$$\left. + C_1U_TU_p\bar{v}_j - m(k^2 + e_oe)\Omega^2\bar{\phi}_j + me\Omega^2\bar{w}_j + me\ddot{\theta}\bar{v}_j]dr\right]\Delta\theta + C_\zeta\bar{v}_j'(r_\zeta)\dot{v}'(r_\zeta) \qquad (C5)$$

and where

$$C_1 = 2\pi\rho bC'$$

$$C_2 = \pi\rho b^2$$

$$C_3 = 2\rho bC_{do}$$

$$b = C/2$$

$$U_R = U_o \cos\psi$$

$$U_T = r\Omega + U_o \sin\psi$$

$$U_p = W_o - v_o$$

$$\theta = \theta_0 + \theta_{1c}\cos\psi + \theta_{1s}\sin\psi$$

Here w_G is a vertical gust and $\Delta\theta$ is the additional control input to be fed back to the actuator. These equations can be expanded, using Euler's formula, to yield

$$\cos\psi = \frac{\exp(i\psi) + \exp(-i\psi)}{2}, \qquad \sin\psi = \frac{\exp(i\psi) - \exp(-i\psi)}{2}$$

where

$$i = \sqrt{-1}$$

When the two-dimensional quasi-steady thin airfoil theory is used, there appear harmonics of ψ up to the third in each coefficient; that is,

$$A_{ij} = A_{-3}\exp(-i3\psi) + A_{-2}\exp(-i2\psi) + A_{-1}\exp(-i\psi) + A_0 + A_1\exp(i\psi)$$

$$+ A_2\exp(i2\psi) + A_3\exp(i3\psi)$$

$$= \sum_{m=-3}^{3} A_m\exp(im\psi) \qquad (C6)$$

$$B_{ij} = \sum_{m=-3}^{3} \mathbf{B}_m \exp(im\psi) \tag{C7}$$

$$C_{ij} = \sum_{m=-3}^{3} \mathbf{C}_m \exp(im\psi) \tag{C8}$$

Each term of these coefficients has the ith and jth mode of the blade deflection; for example:

$$A_{-1} = -2 \int_o^R mea_5 \bar{v}_j \bar{\phi}_j \, dr \cdot \delta_{ij} - \int_o^R (\bar{w}_j + ab\bar{\phi}_j) C_2 a_5 \bar{v}_i \, dr \tag{C9}$$

$$A_0 = \int_o^R m\{(k^2\bar{\phi}_j + e\bar{w}_j - ea_6\bar{v}_j)\bar{\phi}_j + (\bar{w}_j + e\bar{\phi}_j)\bar{w}_j + (\bar{v}_j - ea_6\bar{\phi}_j)\bar{v}_j\} dr \cdot \delta_{ij}$$

$$+ \int_o^R \left(\frac{1}{8} b^2 C_2 \bar{\phi}_i\right)\bar{\phi}_j \, dr - \int_o^R (a_6\bar{v}_i - \bar{w}_i - ab\bar{\phi}_i) C_2 (\bar{w}_j + ab\bar{\phi}_j) dr \tag{C10}$$

$$A_1 = -2 \int_o^R mea_7 \bar{v}_j \bar{\phi}_j \, dr \cdot \delta_{ij} - \int_o^R (\bar{w}_j + ab\bar{\phi}_j) C_2 a_7 \bar{v}_i \, dr \tag{C11}$$

$$A_{-3} = A_{-2} = A_2 = A_3 = 0 \tag{C12}$$

where

$$a_5 = \frac{1}{2} (\theta_{1c} + i\theta_{1s})$$

$$a_6 = \theta_0 + \theta_t(x - 0.75)$$

$$a_7 = \frac{1}{2} (\theta_{1c} - i\theta_{1s})$$

$$x = \frac{r}{R}$$

and δ, θ_t are the Kronecker delta function and pre-twist angle of a blade, respectively. For the practical calculation, both i and j are truncated by L. Then the following equation can be obtained:

$$\sum_{m=-3}^{3} \{[\mathbf{A}_m \exp(im\psi)]\Delta\ddot{\mathbf{q}} + [\mathbf{B}_m \exp(im\psi)]\Delta\dot{\mathbf{q}} + [\mathbf{C}_m \exp(im\psi)]\} = \sum_{n=-\infty}^{\infty} \mathbf{F}_n \exp[i(\omega_G t + n\psi)] \tag{C13}$$

where $\mathbf{A}_m$, $\mathbf{B}_m$, $\mathbf{C}_m$ are (L × L) matrices in which all elements are complex.

Now, consider the expression of a sinusoidal gust in the rotating hub frame at the position of hub center. In the rotor frame, a sinusoidal gust is assumed to be expressed as follows:

$$w_G = w_{Go} \exp(i\omega_G t) \tag{C14}$$

Then, it can be transformed at position (r,ψ) in the rotating hub frame as

$$w_G = w_{Go} \exp(i\omega_G t) \cdot f(x,\psi) \tag{C15}$$

where

$$f(x,\psi) = \exp[-i(\omega_G/\Omega)(x/\mu)\cos\psi]$$

$$= \sum_{n=-\infty}^{\infty} (-i)^n J_n(\omega_G/\Omega \cdot x/\mu)\exp(in\psi) \tag{C16}$$

In this derivation, the following formula is used:

$$\exp(iz \sin\theta) = \sum_{n=-\infty}^{\infty} J_n(z)\exp(in\theta)$$

where J_n is nth order Bessel function. By substituting equation (C16) into (C15), the expression of the coefficient F_n is given by

$$F_n = w_{Go}(-i)^n J_n(\omega_G/\Omega \cdot x/\mu) \tag{C17}$$

APPENDIX D

FLOWCHART OF THE HARMONIC METHOD

The flowchart of the computer code by the harmonic method is shown in figure 34. In this program, the feedback gains are specified in advance and read as data. It is possible to analyze the stability of a blade and also to calculate the rotor transfer function using this code. Approximately 1.0 sec of CPU time was required for one execution of this code on the CDC 7600 computer.

APPENDIX E

TRANSFER FUNCTION OF A ROTOR

In this appendix, the derivation of the transfer function of a rotor is described by using the harmonic method. First, gust amplitude is assumed to be zero in the computer code. Second, the transfer function is assumed to be expressed in the frequency domain as follows:

$$\{z\} = [T_C]\{\theta\} \tag{E1}$$

where $\{z\}$ and $\{\theta\}$ are the response vector and the input vector, respectively; $\{z\}$ and $\{\theta\}$ are given by equations (55) and (58), respectively. Therefore, $[T_C]$ becomes a (12×6) matrix.

In order to calculate the transfer function of a rotor, it is necessary to modify equation (31). Let us consider the following control input $\Delta\theta$:

$$\begin{aligned}\Delta\theta &= (\theta_1 - i\theta_2)\exp(i\omega_G t) + (\theta_3 - i\theta_4)\exp[i(\omega_G - \Omega)t] + (\theta_5 - i\theta_6)\exp[i(\omega_G + \Omega)t] \\ &= \{(\theta_1 \cos \omega_G t + \theta_2 \sin \omega_G t) + i(\theta_1 \sin \omega_G t - \theta_2 \cos \omega_G t)\} \\ &\quad + \{[\theta_3 \cos(\omega_G - \Omega)t + \theta_4 \sin(\omega_G - \Omega)t] + i[\theta_3 \sin(\omega_G - \Omega)t - \theta_4 \cos(\omega_G - \Omega)t]\} \\ &\quad + [\theta_5 \cos(\omega_G + \Omega)t + \theta_6 \sin(\omega_G + \Omega)t] + i[\theta_5 \sin(\omega_G + \Omega)t - \theta_6 \cos(\omega_G + \Omega)t]\}\end{aligned} \tag{E2}$$

The real part of the input $\Delta\theta$ corresponds with equation (57). On the other hand, the response vector $\{z\}$ can be obtained by equation (25). From assumptions used here (i.e., $K = N' = 5$), q becomes zero in equation (25). For simplicity, let us consider only the vertical response:

$$\begin{aligned}\Delta T &= \mathbf{Z}_T \cdot \exp(i\omega_G t) \\ &= [Z_{TC} \cos(\omega_G t) - Z_{TS} \sin(\omega_G t)] + i[Z_{TC} \sin(\omega_G t) + Z_{TS} \cos(\omega_G t)]\end{aligned} \tag{E3}$$

where $\mathbf{Z}_T$ is the complex response vector. The real part of the $\mathbf{Z}_T$ is Z_{TC} and the imaginary part is Z_{TS}. The comparison of the real part of both response and input gives the following relationship:

$$\left.\begin{aligned}Z_{TC} &= t_{11}\theta_1 + t_{12}\theta_2 + t_{13}\theta_3 + t_{14}\theta_4 + t_{15}\theta_5 + t_{16}\theta_6 \\ -Z_{TS} &= t_{21}\theta_1 + t_{22}\theta_2 + t_{23}\theta_3 + t_{24}\theta_4 + t_{25}\theta_5 + t_{26}\theta_6\end{aligned}\right\} \tag{E4}$$

where t_{ij} $(i = 1, \ldots, 12, j = 1, \ldots, 6)$ are elements of the $[T_C]$ matrix. Similar relationships can be given for the other responses.

To determine all the elements of $[T_C]$ matrix, the least-squares method is used. Let us consider the sum of the squares of errors:

$$S = \sum_{n=1}^{N} (z_{jn} - \theta_n^T t_j)^2 = (z_j - \Theta t_j)^T (z_j - \Theta t_j) \tag{E5}$$

where N denotes the number of parameters (the dimension of z_j). The number of parameters to be identified (the dimension of t_j) is assumed to be L. N must be greater than or equal to L. Here, the vector z_j and matrix Θ are defined as

$$z_j = \begin{pmatrix} \vdots \\ z_{jn} \\ \vdots \end{pmatrix}, \quad \Theta = \begin{bmatrix} \vdots \\ \theta_n^T \\ \vdots \end{bmatrix} \tag{E6}$$

The solution that minimizes S is the least-squares estimate:

$$\hat{t}_j = (\Theta^T \Theta)^{-1} \Theta^T z_j \tag{E7a}$$

or

$$\hat{t}_j^T = z_j^T \Theta (\Theta^T \Theta)^{-1} \tag{E7b}$$

Putting the rows together again gives

$$\hat{T} = Z \Theta (\Theta^T \Theta)^{-1} \tag{E8}$$

where

$$Z = \begin{bmatrix} \vdots \\ z_j^T \\ \vdots \end{bmatrix} = [\ \ldots z_n \ldots] \tag{E9}$$

In this study, both N and L have values of 12. Therefore, equation (E8) can be rewritten as follows:

$$\hat{T} = Z(\Theta^T)^{-1} \tag{E10}$$

Elements for the transfer function $[T_C]$, calculated using equation (E10), are shown in tables 4 and 5.

REFERENCES

1. Harvey, K. W.; Blankenship, B. L.; and Drees, J. M.: Analytical Study of Helicopter Gust Response at High Forward Speeds. USAAVLABS, TR 69-1, Sept. 1969.

2. Drees, J. M.; and Harvey, K. W.: Helicopter Gust Response at High Forward Speed. J. Aircraft, vol. 7, no. 3, May-June 1970, pp. 225-230.

3. Bergquist, R. R.: Helicopter Gust Response Including Unsteady Aerodynamic Stall Effects. U.S. Army Air Mobility Research and Development Laboratory, TR 72-68, May 1973.

4. Arcidiacono, D. J.; Bergquist, R. R.; and Alexander, W. I., Jr.: Helicopter Gust Response Characteristics Including Unsteady Aerodynamic Stall Effects. NASA SP-352, Feb. 1974.

5. Yasue, M.: A Study of Gust Response for a Rotor-Propeller in Cruising Flight. NASA CR-137537, Aug. 1974.

6. Judd, M.; and Newman, S. J.: An Analysis of Helicopter Rotor Response due to Gusts and Turbulence. Vertica, vol. 1, no. 3, 1977, pp. 179-188.

7. Mirandy, L.: A Dynamic Loads Scaling Methodology for Helicopter Rotors. J. Aircraft, vol. 15, no. 2, Feb. 1978, pp. 106-113.

8. Dahl, H. J.; and Faulkner, A. J.: Helicopter Simulation in Atmospheric Turbulence. 4th European Rotorcraft and Powered Lift Aircraft Forum, Sept. 13-15, 1978.

9. Azuma, A.; and Saito, S.: Study of Gust Response by Means of the Local Momentum Theory. 5th European Rotorcraft and Powered Lift Aircraft Forum, Sept. 4-7, 1979. Also J. Am. Helicopter Soc., vol. 27, no. 1, Jan. 1982, pp. 58-72.

10. Gaonkar, G. H.; and Hohenemser, K. H.: Flapping Response of Lifting Rotor Blades to Atmospheric Turbulence. J. Aircraft, vol. 6, no. 6, Nov.-Dec. 1969, pp. 496-503.

11. Gaonkar, G. H.; and Hohenemser, K. H.: Stochastic Properties of Turbulence Excited Rotor Blade Vibrations. AIAA J., vol. 9, no. 3, Mar. 1971, pp. 419-424.

12. Gaonkar, G. H.; and Hohenemser, K. W.: An Advanced Stochastic Model for Threshold Crossing Studies of Rotor Blade Vibrations. AIAA J., vol. 10, no. 8, Aug. 1972, pp. 1100-1101.

13. Gaonkar, G. H.; Hohenemser, K. H.; and Yin, S. K.: Random Gust Response Statics for Coupled Torsion-Flapping Rotor Blade Vibrations. J. Aircraft, vol. 9, no. 10, Oct. 1972, pp. 726-729.

14. Gaonkar, G. H.: A Study of Lifting Rotor Flapping Response Peak Distribution in Atmospheric Turbulence. J. Aircraft, vol. 11, no. 2, Feb. 1974, pp. 104-111.

15. Fujimori, Y.: Shear and Moment Response of the Airplane Wing to Nonstationary Turbulence. National Aeronautics Laboratory, Technical Report 404T, Japan, 1975.

16. Fujimori, Y.: Effect of Atmospheric Turbulence on the Stability of a Lifting Rotor Blade. Ph.D. Thesis, U. of Illinois, Urbana, Ill., 1978.

17. Lin, Y. K.; Fujimori, Y.; and Ariaratnam, S. T.: Rotor Blade Stability in Turbulence Flows. Part I. AIAA J., vol. 17, no. 6, June 1979, pp. 545-552.

18. Fujimori, Y.; Lin, Y. K.; and Ariaratnam, S. T.: Rotor Blade Stability in Turbulent Flows. Part II. AIAA J., vol. 17, no. 7, July 1979, pp. 673-678.

19. Briczinski, S. J.; and Cooper, D. E.: Flight Investigation of Rotor/Vehicle State Feedback. NASA CR-132546, Jan. 1975.

20. Briczinski, S. J.: Analytical Investigation of Gust Suppression Techniques for CH-53 Helicopter. NASA CR-145013, 1976.

21. Frick, J. K.; and Johnson, W.: Optimal Control Theory Investigation of Proprotor/Wing Response to Vertical Gust. NASA TM X-62384, Sept. 1974.

22. Johnson, W.: Optimal Control Alleviation of Tilting Proprotor Gust Response. NASA TM X-62494, Oct. 1975.

23. Ham, N. D.; Bauer, P. H.; Lawrence, T. H.; and Yasue, M.: A Study of Gust and Control Response of Model Rotor-Propellers in a Wind Tunnel Airstream. NASA CR-137756, Aug. 1975.

24. Cheng, Y.: Application of Active Control Technology to Gust Alleviation System for Tilt Rotor Aircraft. NASA CR-137958, Nov. 1976.

25. Jenie, S. D.: The Application of Active Control Technology to a Gust Alleviation System for the Tilt-Rotor Aircraft with Hingeless Rotors. NASA CR-152173, Feb. 1978.

26. Yasue, M.; Vohlow, C. A.; and Ham, N. D.: Gust Response and its Alleviation for a Hingeless Helicopter Rotor in Cruising Flight. 4th European Rotorcraft and Powered Lift Aircraft Forum, Sept. 13-15, 1978.

27. Zwicke, P. E.: Helicopter Gust Alleviation: An Optimal Sampled-Data Approach. Proceedings of the 36th Annual National Forum of the American Helicopter Society, May 1980.

28. Taylor, R. B.; Zwicke, P. E.; Gold, P.; and Miao, W.: Analytical Design and Evaluation of an Active Control System for Helicopter Vibration Reduction and Gust Response Alleviation. NASA CR-152377, July 1980.

29. Ham, N. D.; and McKillip, R. M., Jr.: A Simple System for Helicopter Individual-Blade-Control and its Application to Gust Alleviation. Proceedings of the 36th Annual National Forum of the American Helicopter Society, May 1980. Also 6th European Rotorcraft and Powered Lift Aircraft Forum, Sept. 16-19, 1980.

30. Ham, N. D.: A Simple System for Helicopter Individual-Blade-Control using Modal Decomposition. Vertica, vol. 4, no. 1, 1980, pp. 23-28.

31. Rahnema, R. M.: Alleviation of Helicopter Fuselage-Induced Rotor Unsteady Loads through Deterministic Variation of the Individual Blade Pitch. NASA CR-166234, May 1981.

32. Quackenbush, T. R.: Testing and Evaluation of a Stall-Flutter-Suppression System for Helicopter Rotors Using Individual-Blade-Control. NASA CR-166233, Aug. 1981.

33. Ham, N. D.; and Quackenbush, T. R.: A Simple System for Helicopter Individual-Blade-Control and its Application to Stall-Induced Vibration Alleviation. Proceedings of the American Helicopter Society Northeast Region National Specialists' Meeting on Helicopter Vibration Technology for the Jet Smooth Ride, Nov. 1981.

34. Ham, N. D.; Behal, B. L.; and McKillip, R. M., Jr.: A Simple System for Helicopter Individual-Blade-Control and its Application to Lag Damping Augmentation. 8th European Rotorcraft Forum, Aug. 31-Sept. 3, 1982.

35. Ham, N. D.: A Preliminary Note on the Application of Individual-Blade-Control to Vertical Vibration Alleviation. VTOL Technology Laboratory, Massachusetts Institute of Technology, Cambridge, Mass., TR 196-5, Oct. 1962.

36. Ham, N. D.: Helicopter Individual-Blade-Control and its Application. Proceedings of the 39th Annual National Forum of the American Helicopter Society, May 1983.

37. Saito, S.; Azuma, A.; and Nagao, M.: Gust Response of Rotary Wing Aircraft and its Alleviation. 6th European Rotorcraft and Powered Lift Aircraft Forum, Sept. 16-19, 1980. Also, Vertica, vol. 5, no. 2, 1981, pp. 173-184.

38. Kidd, D. L.; Balke, R. W.; Wilson, W. F.; and Wernicke, R. K.: Recent Advances in Helicopter Vibration Control. Proceedings of the 26th Annual National Forum of the American Helicopter Society, June 1970.

39. Simons, I. A.: Advanced Control Systems for Helicopters. Vertica, vol. 1, no. 1, 1976, pp. 17-29.

40. McCloud, J. L., III; and Kretz, M.: Multicyclic Jet-Flap Control for Alleviation of Helicopter Blade Stresses and Fuselage Vibration. NASA SP-352, Feb. 1974.

41. McCloud, J. L., III: An Analytical Study of a Multicyclic Controllable Twist Rotor. Proceedings of the 31st Annual National Forum of the American Helicopter Society, May 1975.

42. Biggers, J. O.; and McCloud, J. L., III: A Note on Multicyclic Control by Swashplate Oscillation. NASA TM-78475, Apr. 1978.

43. McCloud, J. L., III: Multicyclic Control for Helicopters: Research in Progress at Ames Research Center. Proceedings of the AIAA/ASME/ASCE/AHS 21st Structures, Structural Dynamics and Materials Conference, May 1980.

44. Brown, T. J.; and McCloud, J. L., III: Multicyclic Control of a Helicopter Rotor Considering the Influence of Vibration, Loads, Control Motion. Proceedings of the AIAA/ASME/ASCE/AHS 21st Structures, Structural Dynamics and Materials Conference. May 1980.

45. McCloud, J. L., III: The Promise of Multicyclic Control for Helicopter Vibration Reduction. Vertica, vol. 4, no. 1, 1980, pp. 29-41.

46. Chopra, I.; and McCloud, J. L., III: Considerations of Open-Loop, Closed-Loop and Adaptive Multicyclic Control Systems. Proceedings of the AHS Northeast Region National Specialists' Meeting on Helicopter Vibration Technology for the Jet Smooth Ride, Nov. 1981. Also, J. Am. Helicopter Soc., vol. 28, no. 1, Jan. 1983, pp. 63-77.

47. Kretz, M.: Research in Multicyclic and Active Control of Rotary Wings. Vertica, vol. 1, no. 1/2, 1976, pp. 95-105.

48. Kretz, M.; and Larche, M.: Future of Helicopter Rotor Control. Vertica, vol. 4, no. 1, 1980, pp. 13-22.

49. Kretz, M.: Active Elimination of Stall Conditions. Proceedings of the 37th Annual National Forum of the American Helicopter Society, May 1981.

50. Sissingh, G. H.; and Donham, R. E.: Hingeless Rotor Theory and Experiment on Vibration Reduction by Periodic Vibration of Conventional Controls. NASA SP-352, Feb. 1974.

51. Young, M. I.: Optimizing the Cyclic Control Response of Helicopter Rotors. Vertica, vol. 1, no. 1/2, 1976, pp. 107-112.

52. Taylor, R. B.; Farrar, F. A.; and Miao, W.: An Active Control System for Helicopter Vibration Reduction by Higher Harmonic Pitch. Proceedings of the 35th Annual National Forum of the American Helicopter Society, May 1979.

53. Beiner, L.: Optimal Second Harmonic Pitch for Minimum Oscillatory Blade Lift Loads. 5th European Rotorcraft and Powered Lift Aircraft Forum, Sept. 4-7, 1979.

54. Beiner, L.: Optimal Higher Harmonic Blade Pitch Control for Minimum Vibration of a Hinged Rotor. 6th European Rotorcraft and Powered Lift Aircraft Forum, Sept. 16-19, 1980.

55. Jacob, H. G.; and Lehmann, G.: Optimization of Blade Pitch Angle for Higher Harmonic Rotor Control. 7th European Rotorcraft and Powered Lift Aircraft Forum, Sept. 8-11, 1981.

56. Lehmann, G.: A Digital System for Higher Harmonic Control of a Model Rotor. 8th European Rotorcraft Forum, Aug. 31-Sept. 3, 1982.

57. Reichert, G.: Helicopter Vibration Control — A Survey. 6th European Rotorcraft and Powered Lift Aircraft Forum, Sept. 16-19, 1980.

58. Yen, J. G.: Higher Harmonic Control for Helicopters with Two-Bladed and Four-Bladed Rotors. J. Aircraft, vol. 18, no. 12, Dec. 1981, pp. 1064-1069.

59. Abramson, J.; and Rogers, E. O.: Optimization Theory Applied to Higher Harmonic Control of Circulation Controlled Rotors. Proceedings of the 37th Annual National Forum of the American Helicopter Society, May 1981.

60. McHugh, F. J.; and Shaw, J.: Benefits of Higher-Harmonic Blade Pitch: Vibration Reduction, Blade-Load Reduction, and Performance Improvement. Proceedings of the American Helicopter Society Mideast Region Symposium on Rotor Technology, Aug. 1976.

61. Shaw, J.: Higher Harmonic Blade Pitch Control: A System for Helicopter Vibration Reduction. Ph.D. Thesis, Massachusetts Inst. of Tech., Cambridge, Mass., May 1980.

62. Shaw, J.; and Albion, N.: Active Control of the Helicopter Rotor for Vibration Reduction. Proceedings of the 36th Annual National Forum of the American Helicopter Society, May 1980.

63. Shaw, J.; and Albion, N.: Active Control of Rotor Blade Pitch for Vibration Reduction: A Wind Tunnel Demonstration. Vertica, vol. 4, no. 1, 1980, pp. 3-11.

64. Wood, E. R.; Powers, R. W.; and Hammond, C. E.: On Method for Application of Harmonic Control. Vertica, vol. 4, no. 1, 1980, pp. 43-60.

65. Wood, E. R.; and Powers, R. W.: Practical Design Consideration for a Flightworthy Higher Harmonic Control System. Proceedings of the 36th Annual National Forum of the American Helicopter Society, May 1980.

66. Powers, R. W.: Preliminary Design Study of a Higher Harmonic Blade Feathering Control System. NASA CR-159327, June 1980.

67. Hammond, C. E.: Wind Tunnel Results Showing Rotor Vibratory Loads Reduction Using Higher Harmonic Blade Pitch. Proceedings of the 36th Annual National Forum of the American Helicopter Society, May 1980. Also, J. Am. Helicopter Soc., vol. 28, no. 1, Jan. 1983, pp. 10-15.

68. Molusis, J. A.; Hammond, C. E.; and Cline, J. H.: A Unified Approach to the Optimal Design of Adaptive and Gain Scheduled Controllers to Achieve Minimum Helicopter Rotor Vibration. Proceedings of the 37th Annual National Forum of the American Helicopter Society, May 1981.

69. Molusis, J. A.; and Bar-Shalom, Y.: Identification and Stochastic Control of Helicopter Dynamic Modes. NASA CR-166425, Jan. 1983.

70. Johnson, W.: Self-Tuning Regulators for Multicyclic Control of Helicopter Vibration. NASA TP-1996, Mar. 1982.

71. Molusis, J. A.; Mookerjee, P.; and Bar-Shalom, Y.: Evaluation of the Effect of Vibration Nonlinearity on Convergence Behavior of Adaptive Higher Harmonic Controllers. NASA CR-166424, Jan. 1983.

72. Molusis, J. A.: The Importance of Nonlinearity on the Higher Harmonic Control of Helicopter Vibration. Proceedings of the 39th Annual National Helicopter Society, May 1983.

73. White, F.; and Blake, B. B.: Improved Method of Predicting Helicopter Control Response and Gust Sensitivity. Proceedings of the 35th Annual National Forum of the American Helicopter Society, May 1979.

74. Hall, W. E., Jr.; Gupta, N. K.; and Hansen, R. S.: Rotorcraft System Identification Techniques for Handling Qualities and Stability and Control Evaluation. Proceedings of the 34th Annual National Forum of the American Helicopter Society, May 1978.

75. Fuller, J. W.: Rotor State Estimation for Rotorcraft. Proceedings of Northeast Region National Specialists' Meeting on Helicopter Vibration, Nov. 1981.

76. DuVal, R. W.: Use of Multicyclic Sensors for On-Line Rotor Tip-Path Plane Estimation. J. Am. Helicopter Soc., vol. 25, no. 4, Oct. 1980, pp. 13-21.

77. DuVal, R. W.; and Mackie, D. B.: Identification of a Linear Model of Rotor-Fuselage Dynamics from Nonlinear Simulation Data. Vertica, vol. 5, no. 4, 1981, pp. 317-335.

78. DuVal, R. W.; Gregory, C. Z., Jr.; and Gupta, N. K.: Design and Evaluation of a State-Feedback Vibration Controller. Proceedings of the American Helicopter Society Northeast Region National Specialists' Meeting on Helicopter Vibration Technology for the Jet Smooth Ride, Nov. 1981.

79. Done, G. T. S.; and Hughes, A. D.: Reducing Vibration by Structural Modification. Vertica, vol. 1, no. 1/2, 1976, pp. 31-38.

80. Walker, W. R.: Experimental Application of a Vibration Reduction Technique. Vertica, vol. 4, no. 2/4, 1980, pp. 135-146.

81. Taylor, R. B.: Helicopter Vibration Reduction by Blade Model Shaping. Proceedings of the 38th Annual National Forum of the American Helicopter Society, May 1982.

82. Friedmann, P. P.; and Shanthakumaran, P.: Aeroelastic Tailoring of Rotor Blades for Vibration Reduction in Forward Flight. Proceedings of the AIAA/ASME/ASCE/AHS 24th Structures, Structural Dynamics and Materials Conference, May 1983.

83. Friedmann, P. P.; and Shanthakumaran, P.: Optimum Design of Rotor Blades for Vibration Reduction in Forward Flight. Proceedings of the 39th Annual National Forum of the American Helicopter Society, May 1983.

84. Azuma, A.; and Kawachi, K.: Local Momentum Theory and Its Application to the Rotary Wing. J. Aircraft, vol. 16, no. 1, Jan. 1979, pp. 6-14.

85. Azuma, A., Saito, S., Kawachi, K.; and Karasudani, T.: Application of the Local Momentum Theory to the Aerodynamic Characteristics of Multi-Rotor Systems. 4th European Rotorcraft and Powered Lift Aircraft Forum, Sept. 13-15, 1978. Also, Vertica, vol. 3, no. 2, 1979, pp. 131-144.

86. Kawachi, K.: An Extension of the Local Momentum Theory to a Distorted Wake Model of a Hovering Rotor. NASA TM-81258, Feb. 1981.

87. Saito, S.; and Azuma, A.: A Numerical Approach to Co-Axial Rotor Aerodynamics. 7th European Rotorcraft and Powered Lift Aircraft Forum, Sept. 8-11, 1981. Also, Vertica, vol. 6, no. 4, 1983, pp. 253-266.

88. Kato, K.; and Yamane, T.: A Calculation of Rotor Impedance for Hovering Articulated-Rotor Helicopters. J. Aircraft, vol. 16, no. 1, Jan. 1979, pp. 15-22.

89. Kato, K.; and Yamane, T.: Calculation of Rotor Impedance for Articulated-Rotor Helicopters in Forward Flight. J. Aircraft, vol. 16, no. 7, July 1979, pp. 470-476.

90. Kato, K.; and Yamane, T.: Numerical Prediction of Typical Articulated Rotor Impedance. J. Aircraft, vol. 16, no. 7, July 1979, pp. 417-418.

91. Kato, K.; Yamane, T.; et al.: Experimental Substantiation for Hovering Rotor Vertical Impedance Calculations. J. Aircraft, vol. 18, no. 6, June 1981, pp. 445-450.

92. Gessow, A.; and Myers, C. G., Jr.: Aerodynamics of the Helicopter. Frederick Ungar Publishing Co., 1952.

93. Bramwell, A. R. S.: Helicopter Dynamics. Edward Arnold, London, 1976.

94. Johnson, W.: Helicopter Theory. Princeton University Press, Princeton, N.J., 1980.

95. Etkin, B.: Dynamics of Atmospheric Flight. John Wiley & Sons, Inc., New York, 1972.

96. Bisplinghoff, L. R.; Ashley, H.; and Halfman, L. R.: Aeroelasticity. Addison Wesley Publishing Co., San Francisco, 1957.

97. Peters, D. A.; and Hohenemser, K. H.: Application of the Floquet Transition Matrix to Problems of Lifting Rotor Stability. J. Am. Helicopter Soc., vol. 16, no. 2, Apr. 1971, pp. 25-33.

98. Bielawa, R. L.: Dynamic Analysis of Multi-Degree-of-Freedom Systems Using Phasing Matrices. NASA SP-352, Feb. 1974.

99. Biggers, J. C.: Some Applications to the Flapping Stability of Helicopter Rotors. NASA SP-352, Feb. 1974. Also, J. Am. Helicopter Soc., vol. 19, no. 4, Oct. 1974.

100. Hammond, C. E.: An Application of Floquet Theory to Prediction of Mechanical Instability. NASA SP-352, Feb. 1974. Also, J. Am. Helicopter Soc., vol. 19, no. 4, Oct. 1974, pp. 14-23.

101. Gaonkar, G. H.; Simha Prasad, D. S.; and Sastry, D.: On Computing Floquet Transition Matrices of Rotorcraft. J. Am. Helicopter Soc., vol. 26, no. 3, July 1981, pp. 56-61.

102. Franklin, G. F.; and Powell, J. D.: Digital Control of Dynamic Systems. Addison-Wesley Publishing Company, San Francisco, 1981.

103. Bryson, A. E., Jr.; and Ho, Yu.-Chi.: Applied Optimal Control: Optimization, Estimation and Control. Hemisphere Publishing Corporation, Washington, 1975.

104. Otnes, R. K.; and Enochson, L.: Applied Time Series Analysis. Vol. 1. Basic Techniques. John Wiley and Sons, New York, 1978.

TABLE 1.- BLADE CHARACTERISTICS

Rotor radius, R	8.53 m
Blade lift slope, a	5.73
Blade semi-chord, b	0.2185 m
Number of blades, N	4
Rotor rotational speed, Ω	23.67 rad/sec
Blade twist rate, θ_t	-8°
Position of flapping hinge, r_β	0.3 m
Blade cutoff, r_c	0.594 m
C.G. position of blade, r_{CG}	2.74 m
Position of lag damper, r_ζ	0.3 m
Lag damper coefficient, C_ζ	1000.0 N-m-sec/rad
Blade mass, m	106.4 kg
Moment of inertia of blade, I_β	1593.9 kg-m^2
Mass moment of blade, M_β	1659.1 kg-m^2
Lock number, γ	8.84
Wing section	NACA 0012
Gross weight, W	62259.4 N

TABLE 2.- BLADE PROPERTIES

I	Length, m	GJ, N-m^2 $\times10^4$	EI_y, N-m^2 $\times10^4$	EI_z, N-m^2 $\times10^5$	ΔI, kg-m^2 $\times10^{-3}$	Δm, kg $\times10^{-1}$	$\Delta\theta$, deg $\times10^{-1}$	e, m $\times10^{-2}$
1	0.003	34.13	22.37	26.68	94.71	3.063	0.0	0.0
2	.327	34.13	143.4	13.19	87.80	320.7	.0	.0
3	.254	12.97	20.28	6.801	59.35	144.9	.0	.0
4	.508	6.017	4.900	4.929	29.81	24.06	-.28	.4167
5	.610	5.018	4.214	4.567	31.57	38.50	-6.81	↓
6	.280	↓	↓	↓	40.37	24.21	-3.12	↓
7	.787	↓	↓	↓	47.02	62.13	-8.80	↓
8	.457	↓	↓	↓	47.82	39.67	-5.10	↓
9	.737	↓	↓	↓	43.22	58.05	-8.23	↓
10	.406	↓	↓	↓	44.71	35.29	-4.54	↓
11	.711	↓	↓	↓	55.68	53.82	-7.94	↓
12	.762	↓	↓	↓	38.35	57.75	-8.52	↓
13	.254	↓	↓	↓	34.55	22.02	-2.83	↓
14	.610	↓	↓	↓	47.02	48.13	-6.81	↓
15	.635	↓	↓	↓	39.70	60.23	-7.09	↓
16	.356	↓	↓	↓	23.03	29.17	-3.97	↓
17	.254	↓	↓	↓	33.22	30.04	-2.84	↓
18	.280	↓	↓	↓	7.448	22.02	-3.12	↓

TABLE 3.- ROTOR OPERATING CONDITIONS

Advance ratio, μ	0.18
Collective pitch angle, θ_0	8.0°
Longitudinal pitch angle, θ_{1s}	-1.48°
Lateral pitch angle, θ_{1c}	.695°
Inflow ratio, λ	.0179

TABLE 4.- TRANSFER FUNCTION OF ROTOR FOR GUST FREQUENCY OF 2.0 Hz

$$[T_C] = \begin{bmatrix} -25.52 & -576.5 & -192.6 & 22.40 & 81.50 & -11.92 \\ 576.5 & -25.52 & 22.40 & -192.6 & 11.92 & 81.50 \\ 9.831 & -59.62 & -211.6 & -44.92 & 50.86 & 53.35 \\ 66.51 & 15.42 & 3.635 & -179.3 & -88.02 & 59.16 \\ 34.46 & -112.7 & 2397. & -85.89 & 2561. & 91.49 \\ 112.7 & 34.46 & 85.89 & 2397. & -91.49 & 2561. \\ -63.17 & 2.580 & -48.63 & 216.3 & -56.87 & 37.14 \\ -2.580 & -63.17 & -216.3 & -48.63 & -37.15 & -56.87 \\ -1185. & 4.166 & 96.97 & 2508. & 87.10 & -2618. \\ -4.166 & -1185. & -2508. & 96.97 & 2618. & 87.10 \\ 969.5 & 77.35 & -10.06 & -293.7 & 4.302 & 202.5 \\ -77.35 & 969.5 & 293.7 & -10.06 & -202.6 & 4.305 \end{bmatrix} \times 10^2$$

Advance ratio = 0.18

Rotor rotational speed = 23.67 rad/sec

Gust frequency = 2.0 Hz

Gust amplitude: $u_{Go} = v_{Go} = 0.0$, $w_{Go} = 1.0$ m/sec

$\{z\} = [T_C]\{\theta\}$

$\{z\} = (T_C, T_S, H_C, H_S, M_{YC}, M_{YS}, Y_C, Y_S, M_{XC}, M_{XS}, M_{ZC}, M_{ZS})^T$

$\{\theta\} = (\theta_1, \theta_2, \theta_3, \theta_4, \theta_5, \theta_6)^T$

TABLE 5.- TRANSFER FUNCTION OF ROTOR FOR STEP GUST

$$[T_C] = \begin{bmatrix} 0.996 & 8.545 & 2.984 \\ -0.496 & 8.004 & 2.077 \\ 1.849 & 1.872 & 0.635 \\ 68.42 & 252.3 & 95.31 \\ -16.62 & 289.0 & 81.92 \\ 8.599 & 17.79 & 5.652 \end{bmatrix} \times 10^3$$

Advance ratio = 0.18

Rotor rotational speed = 23.67 rad/sec

Gust frequency = 0.0 Hz (step gust)

Gust amplitude: $u_{Go} = v_{Go} = 0.0$, $w_{Go} = 1.0$ m/sec

$\{z\} = [T_C]\{\theta\}$

$\{z\} = (\Delta T_o, \Delta H_o, \Delta M_{Yo}, \Delta Y_o, \Delta M_{Xo}, \Delta M_{Zo})^T$

$\{\theta\} = (\theta_1, \theta_2, \theta_3)^T$

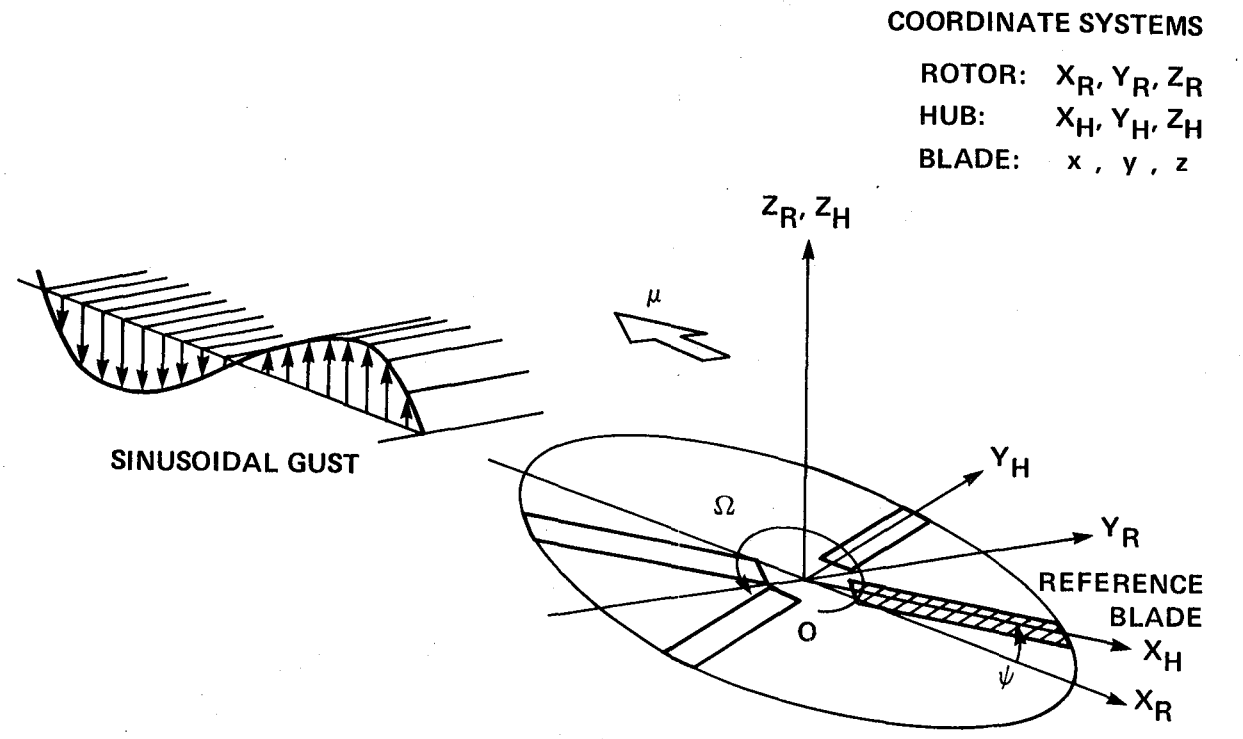

(a) Gust shape and coordinate systems.

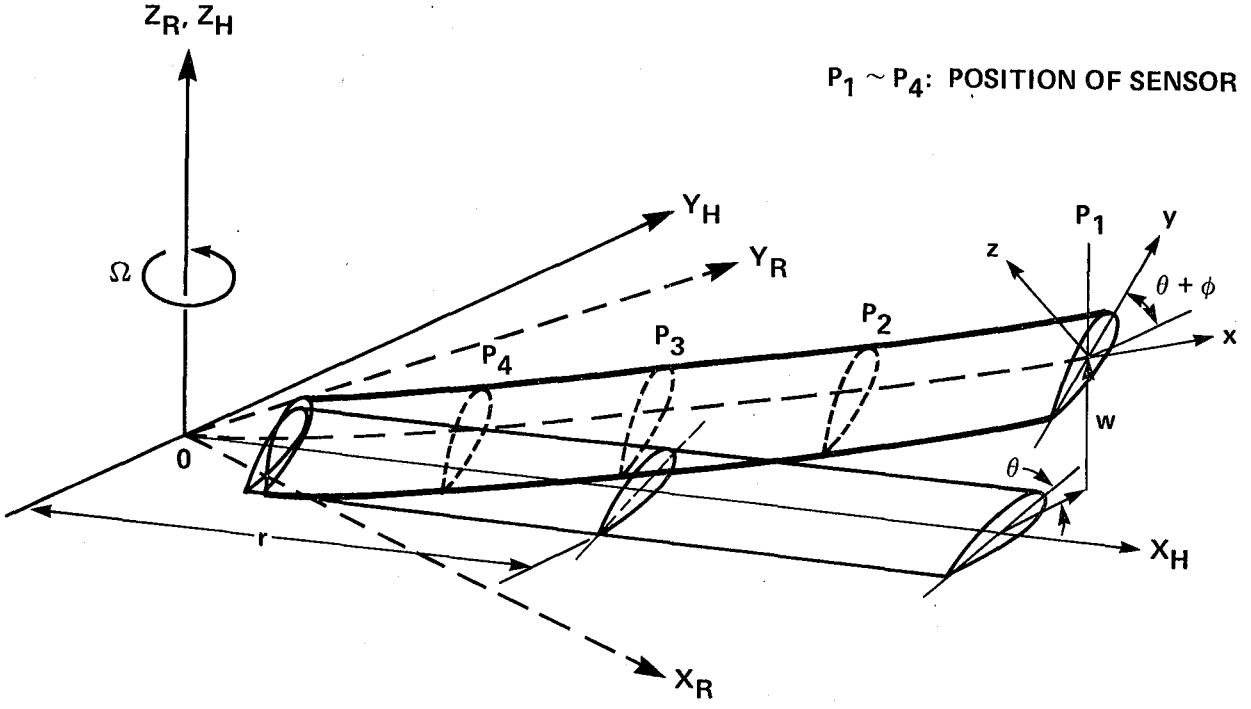

(b) Blade deflection geometry.

Figure 1.- Coordinate systems and blade deflection.

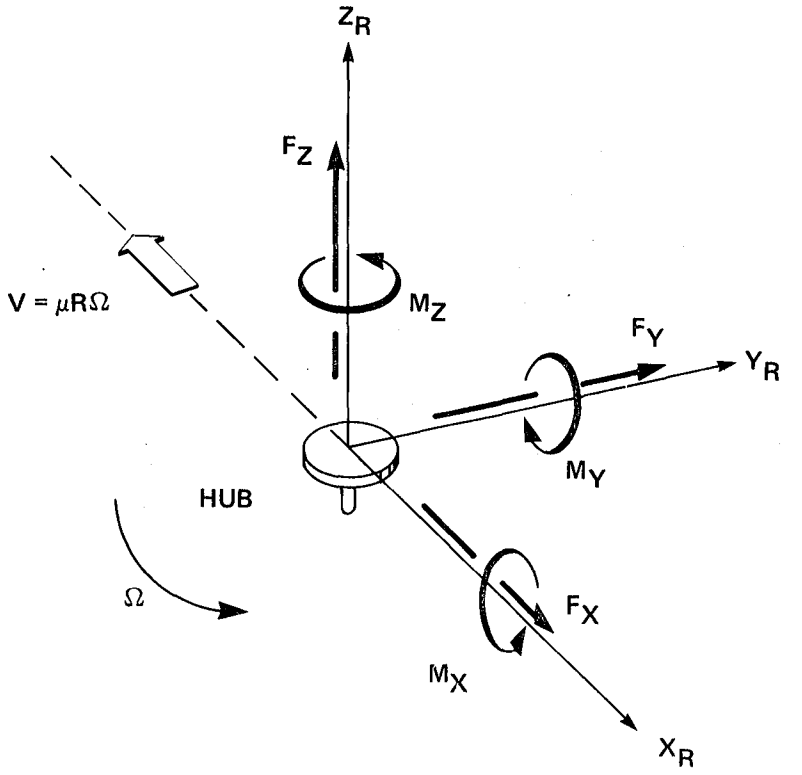

Figure 2.- Mode shapes and mode frequencies of blade: Ω = 226 rpm, $\theta_0 = 8°$, $\theta_t = -8°$.

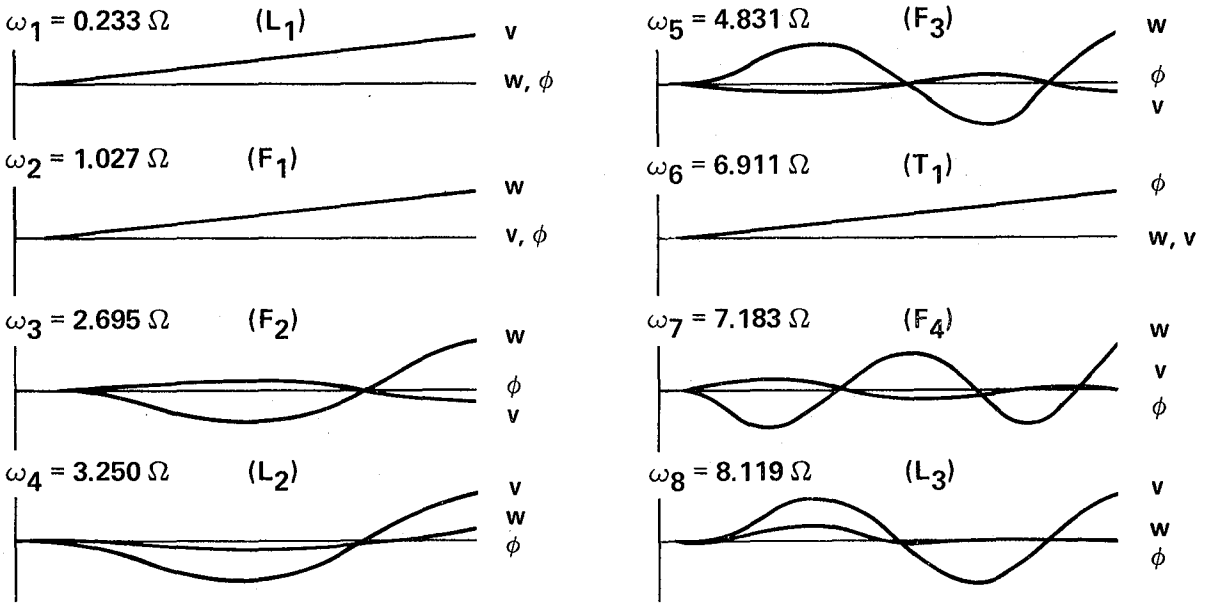

Figure 3.- Hub forces and moments.

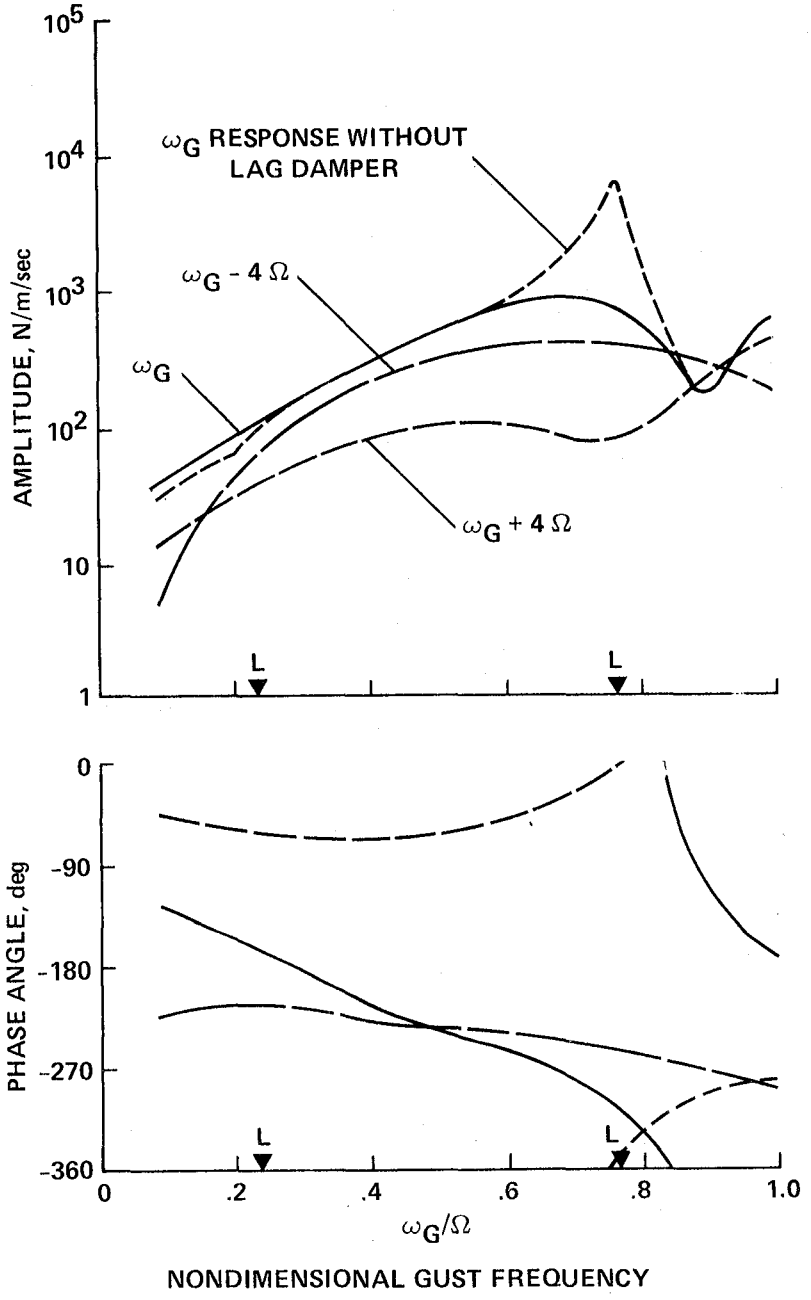

(a) Horizontal force, F_x.

Figure 4.- Rotor impedance to gust excitation without feedback: w_{Go} = 1.0 m/sec, μ = 0.18.

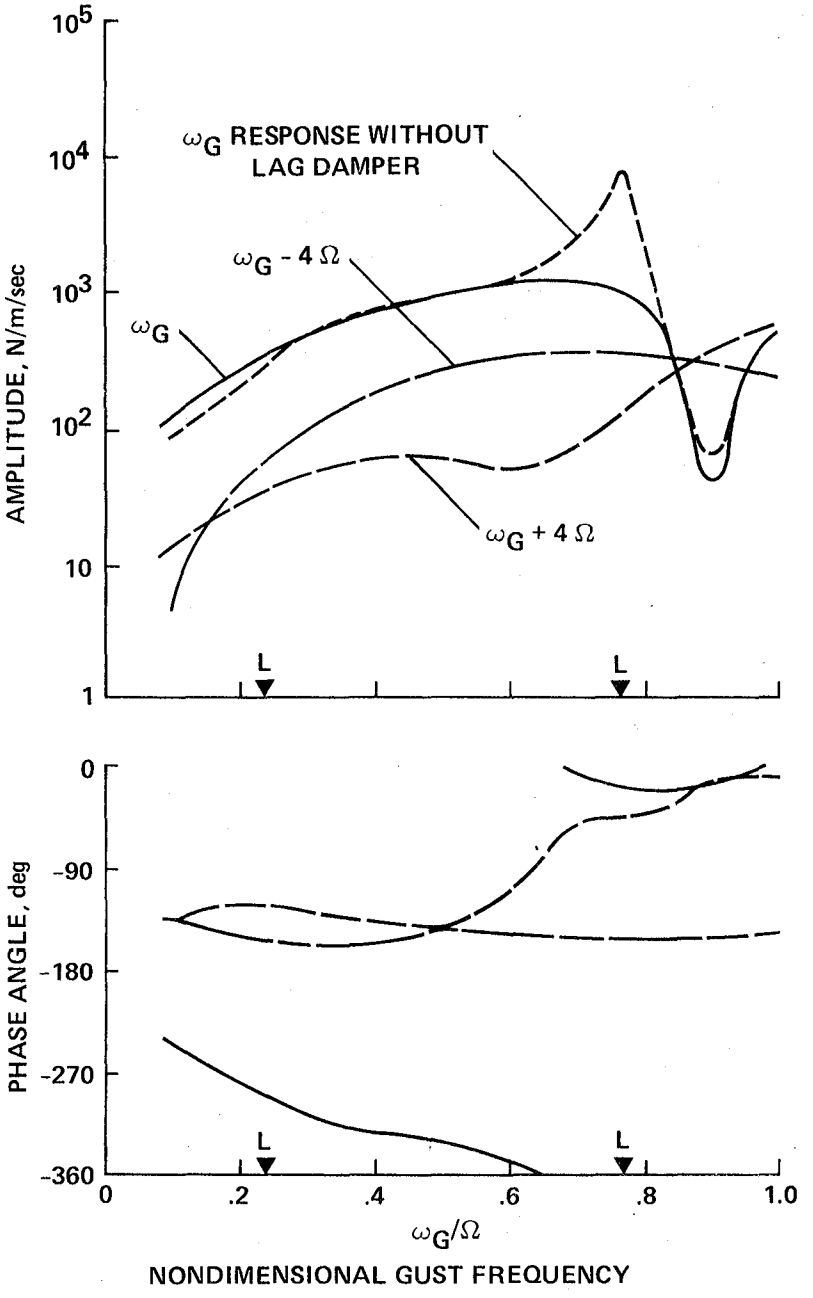

(b) Side force, F_y.

Figure 4.- Continued.

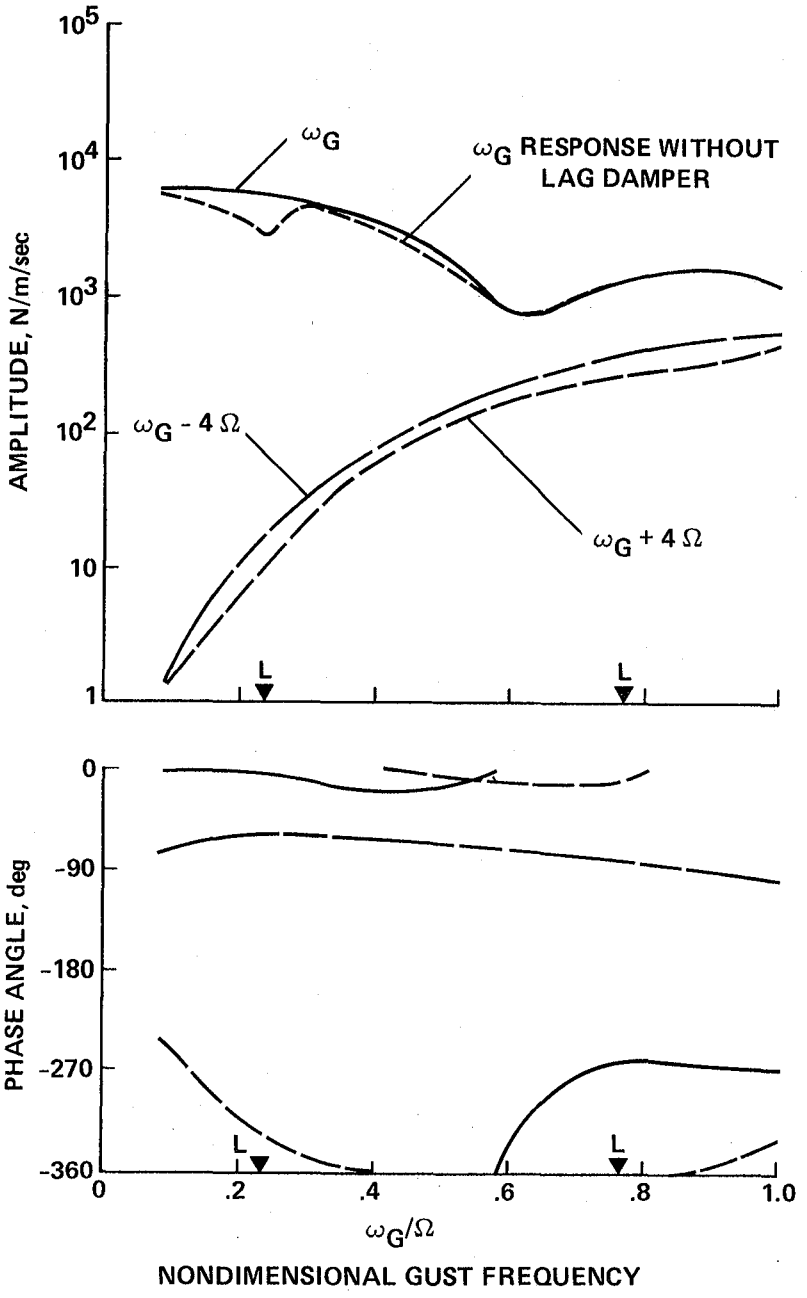

(c) Vertical force, F_z.

Figure 4.- Continued.

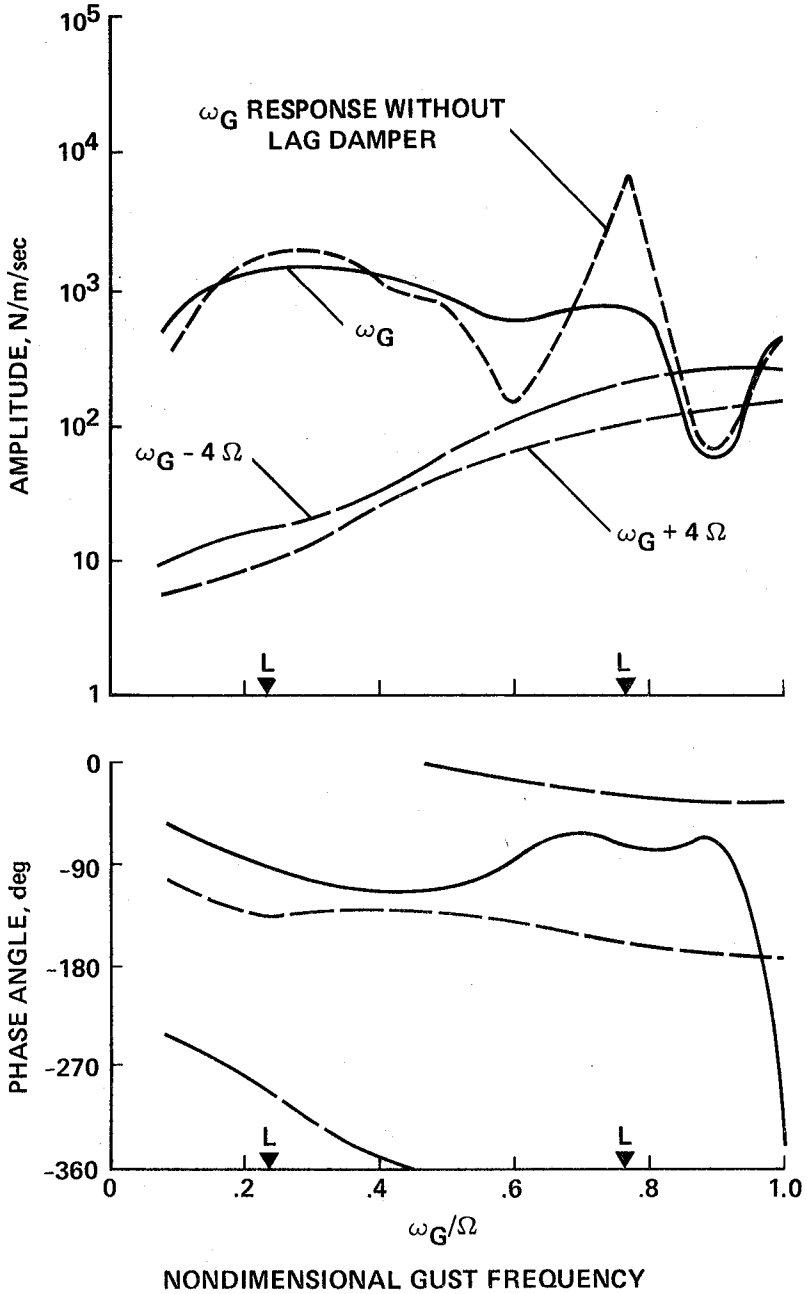

(d) Rolling moment, M_X.

Figure 4.- Continued.

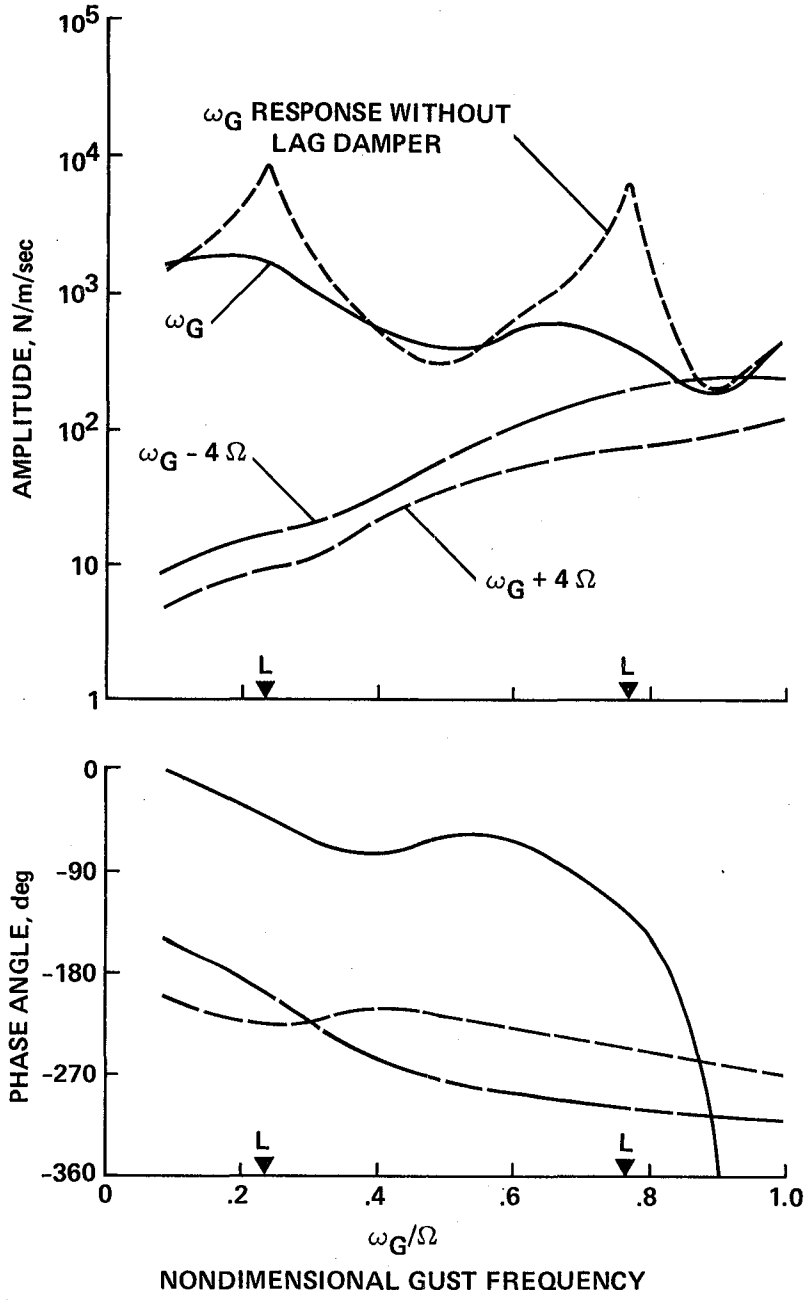

(e) Pitching moment, M_y.

Figure 4.- Continued.

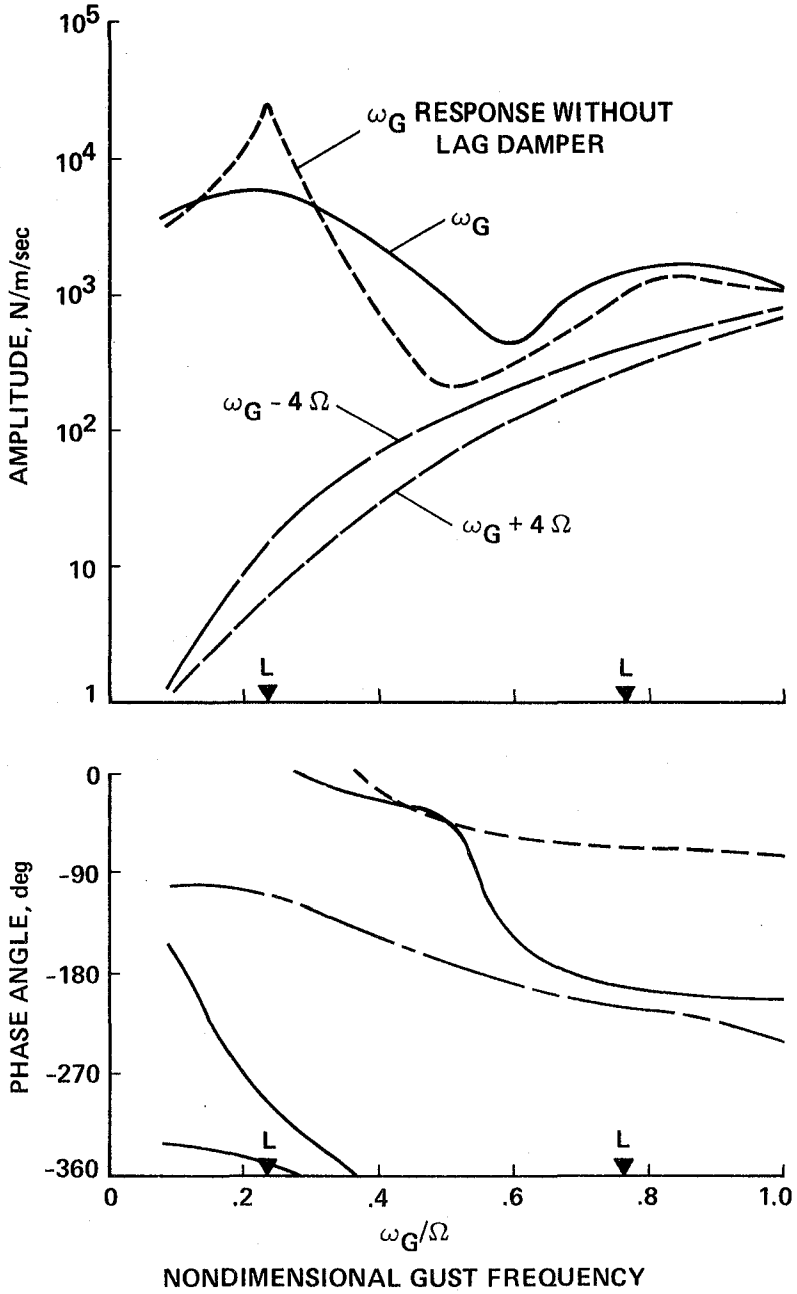

(f) Yawing moment, M_Z.

Figure 4.- Concluded.

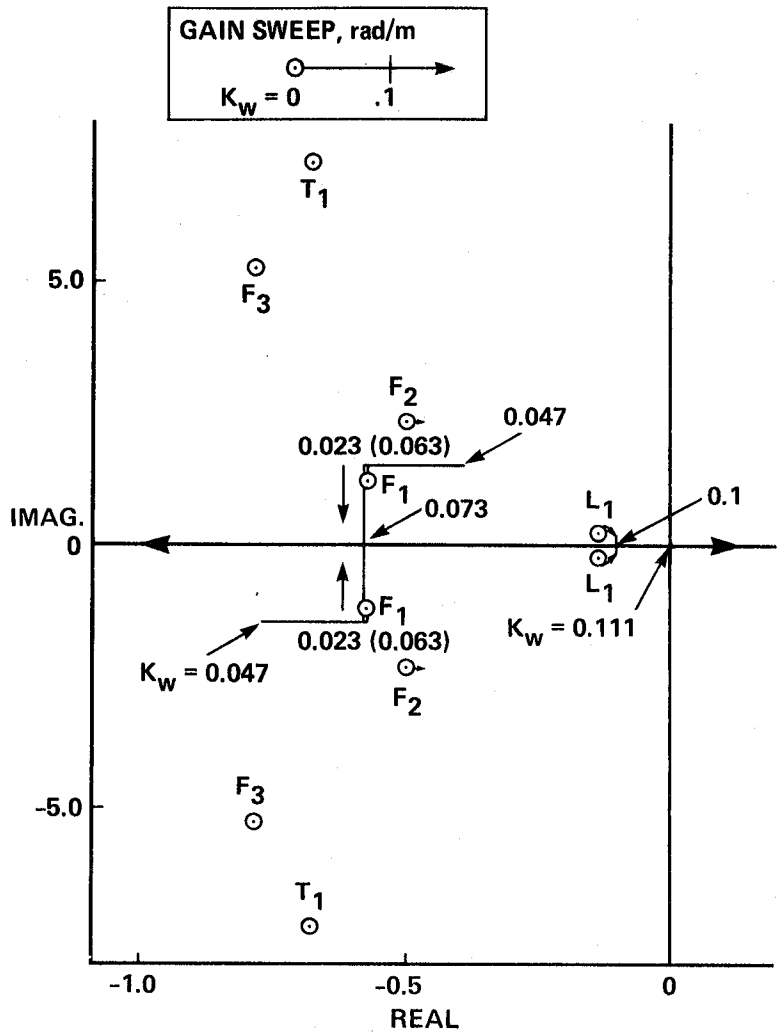

(a) $\Delta\theta = K_w \cdot \Delta w$.

Figure 5.- Stability analysis (root loci): $\mu = 0.18$.

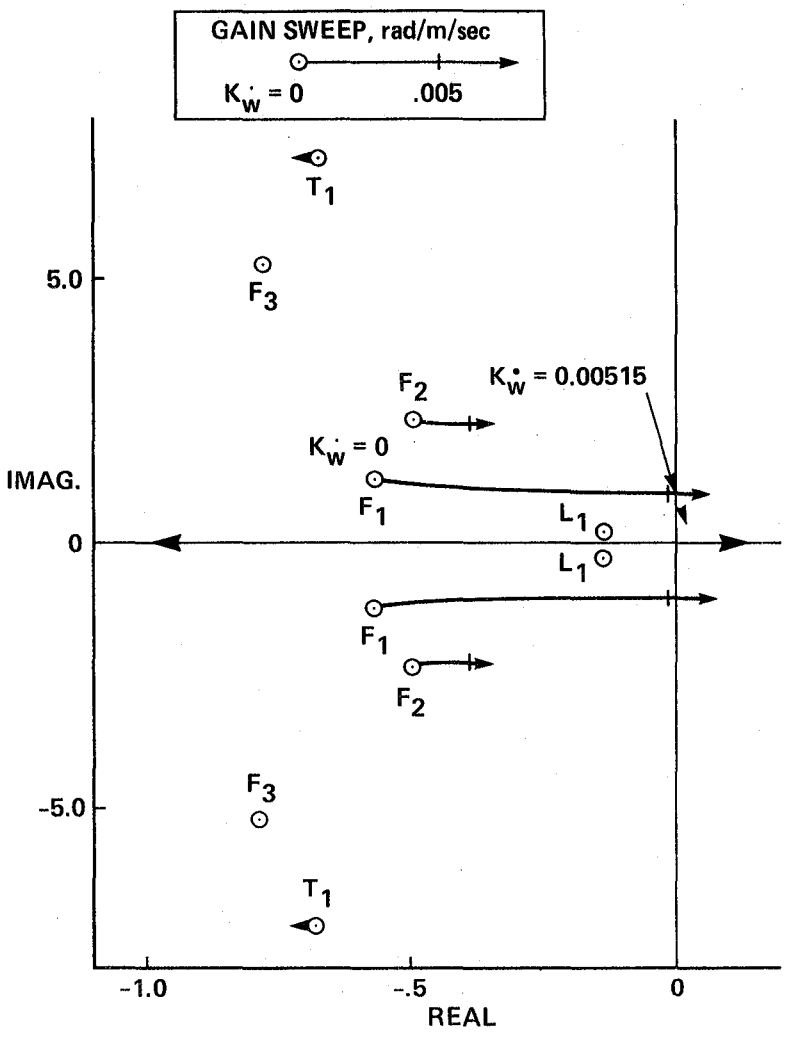

(b) $\Delta\theta = K_{\dot{w}} \cdot \Delta\dot{w}$.

Figure 5.- Continued.

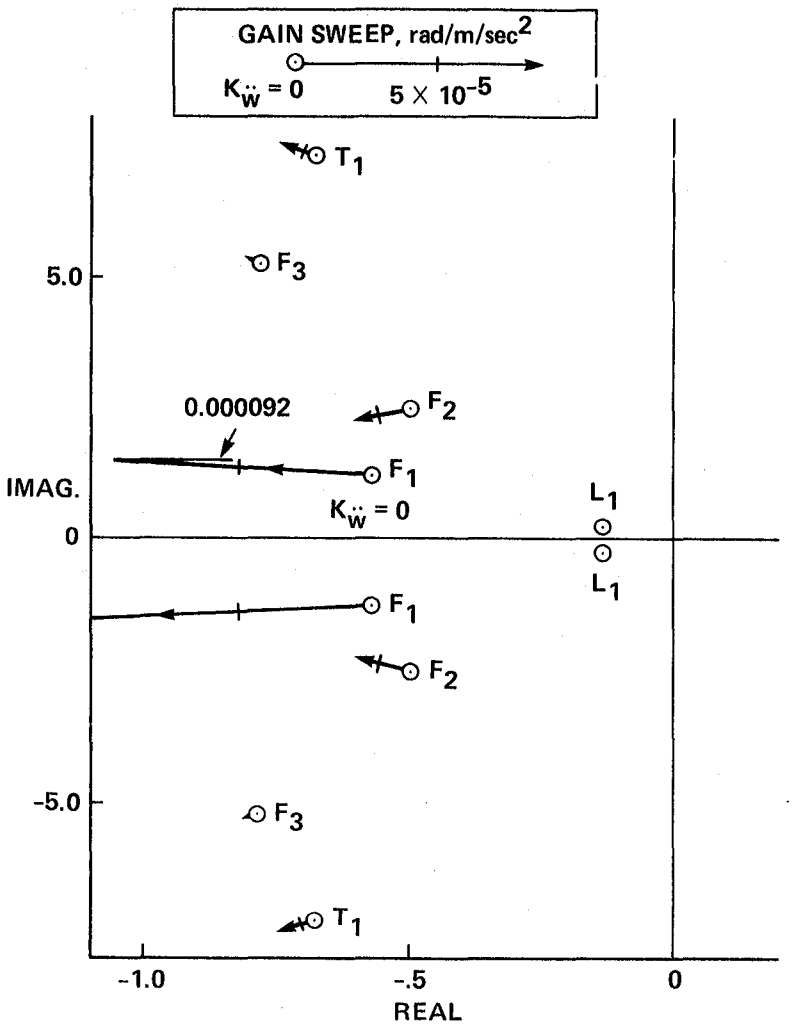

(c) $\Delta\theta = K_{\ddot{w}} \cdot \Delta\ddot{w}$.

Figure 5.- Concluded.

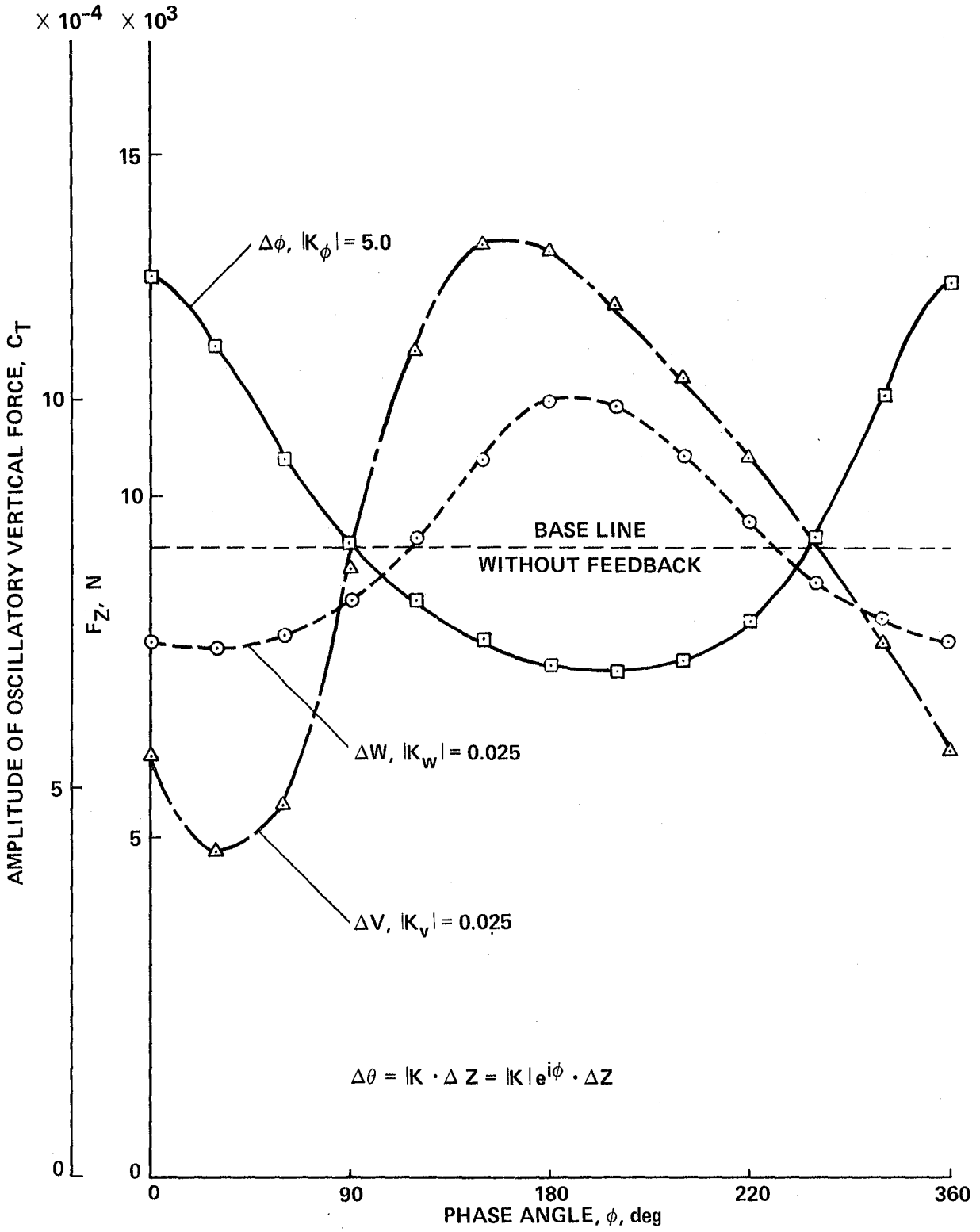

Figure 6.- Sensitivity of the phase angle to the vertical hub force, sensor at blade tip position: w_{Go} = 1.8 m/sec, f_G = 0.5 Hz, μ = 0.18.

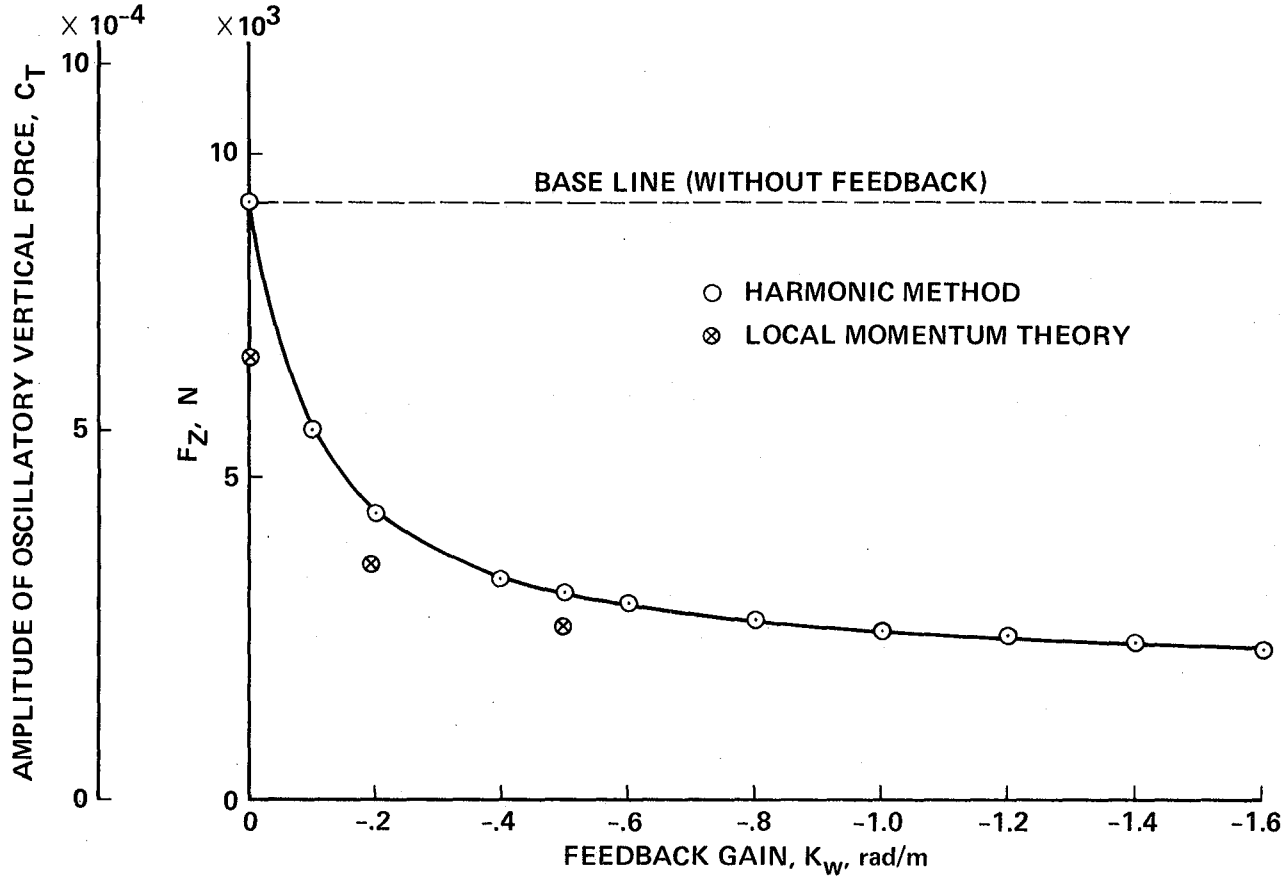

(a) Δw feedback, $\phi = 0°$.

Figure 7.- Sensitivity of the feedback gain to the vertical hub force, sensor at blade tip position: $w_{Go} = 1.8$ m/sec, $f_G = 0.5$ Hz, $\mu = 0.18$.

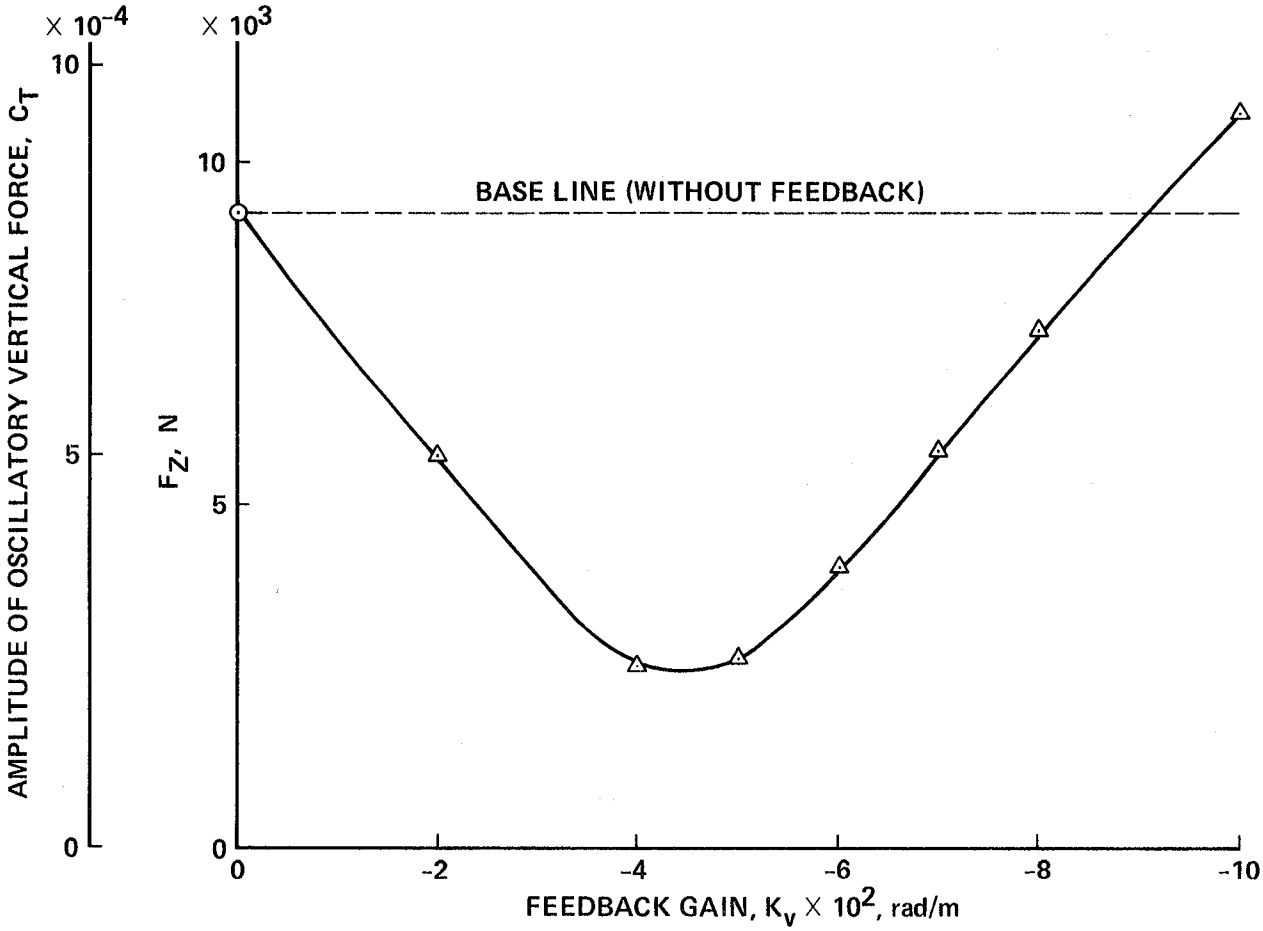

(b) Δv feedback, $\phi = 30°$.

Figure 7.- Continued.

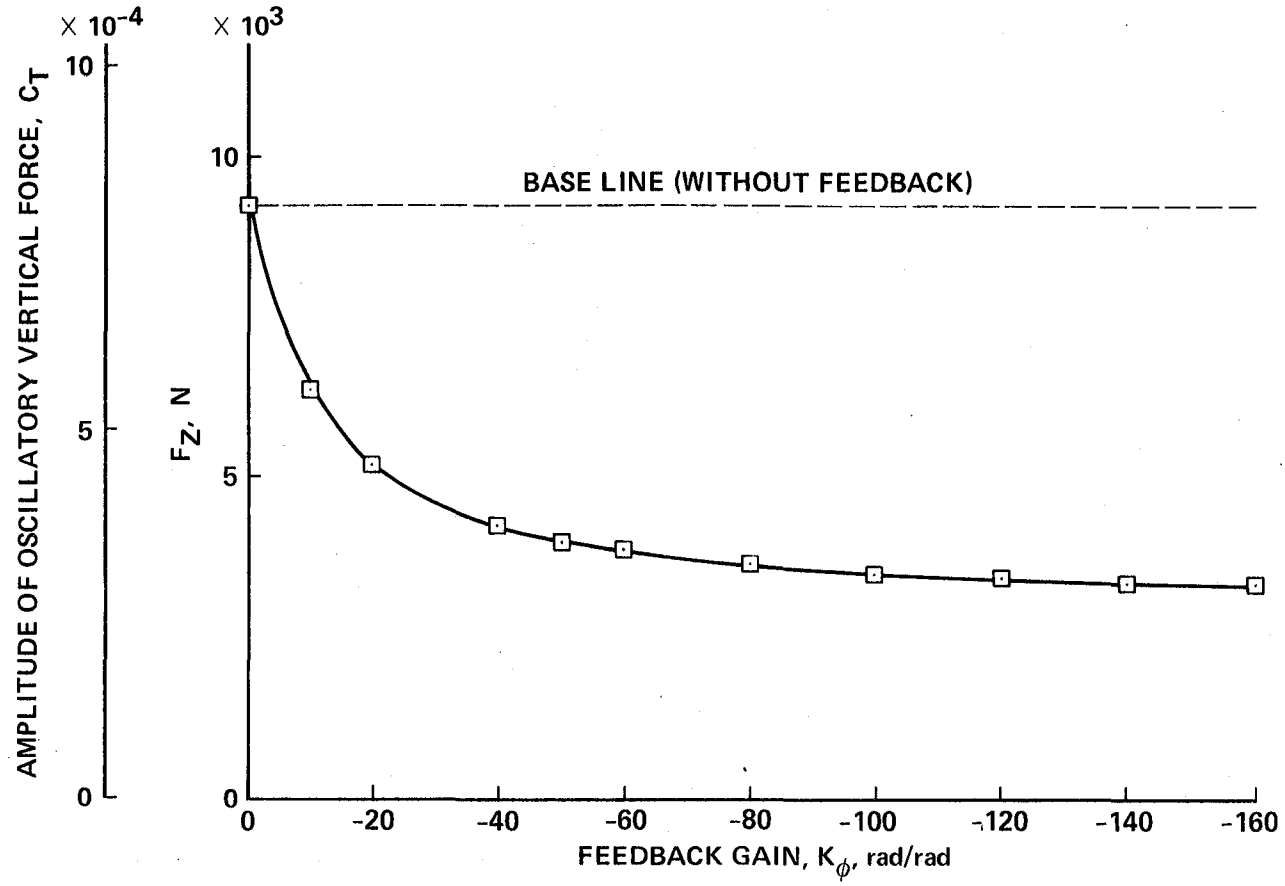

(c) $\Delta\phi$ feedback, ϕ = 270°.

Figure 7.- Concluded.

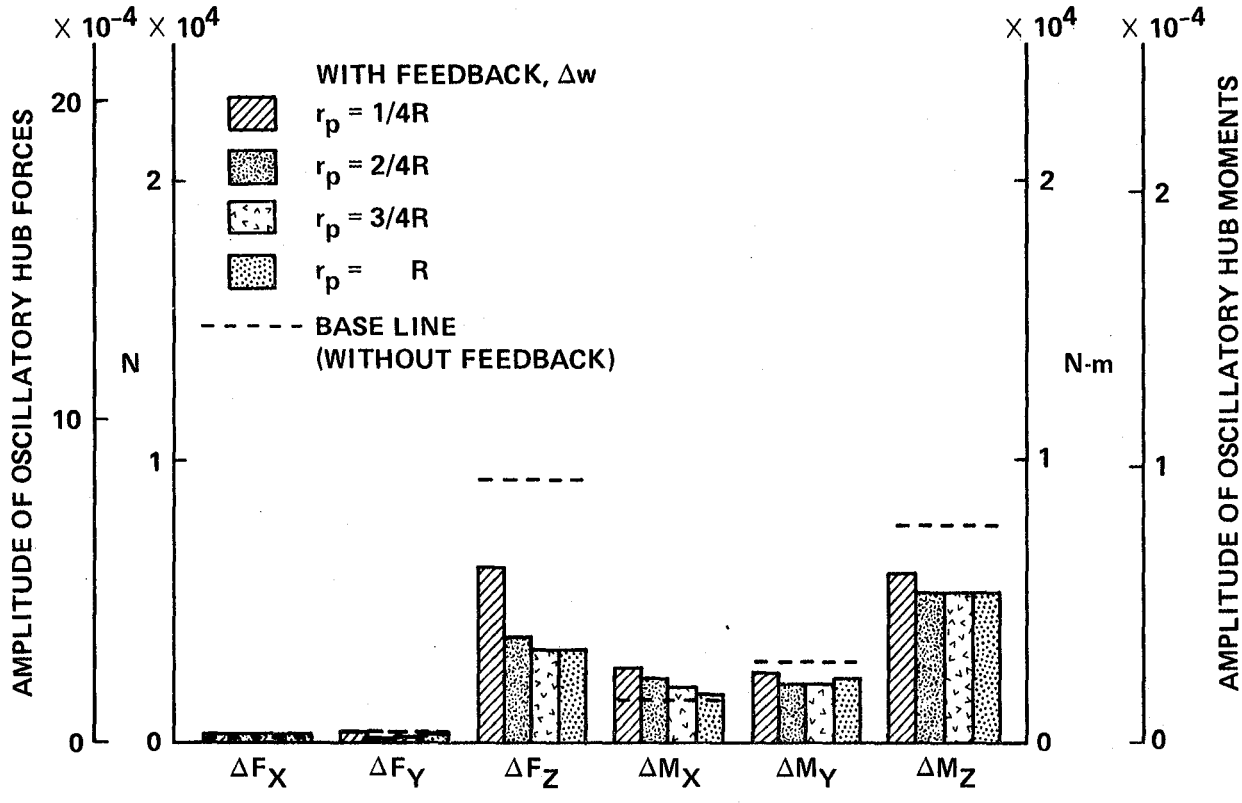

(a) Δw feedback: $\phi = 0°$, $K_w = -0.5$ rad/m.

Figure 8.- Effect of the sensing points on the feedback system: $w_{Go} = 1.8$ m/sec, $f_G = 0.5$ Hz, $\mu = 0.18$.

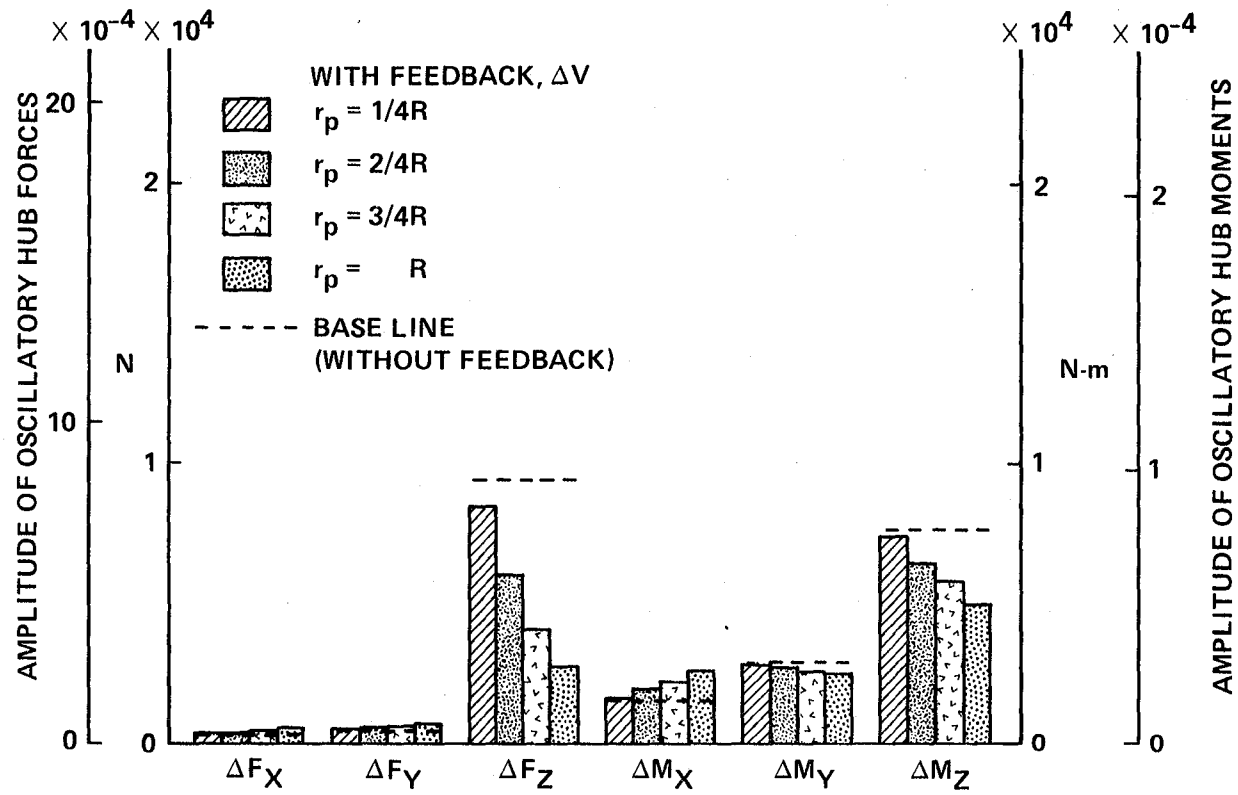

(b) Δv feedback: $\phi = 30°$, $K_v = -0.04$ rad/m.

Figure 8.- Continued.

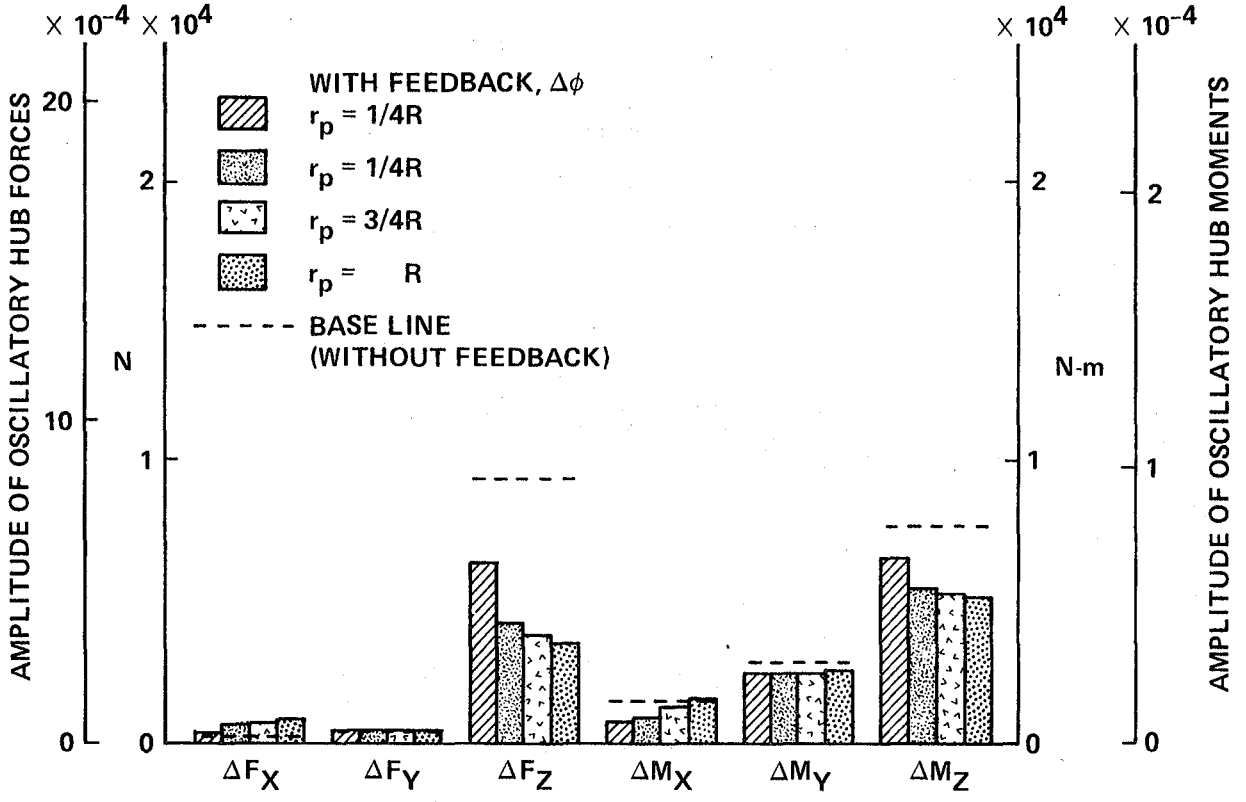

(c) $\Delta\phi$ feedback: $\phi = 210°$, $K_\phi = -100$ rad/rad.

Figure 8.- Concluded.

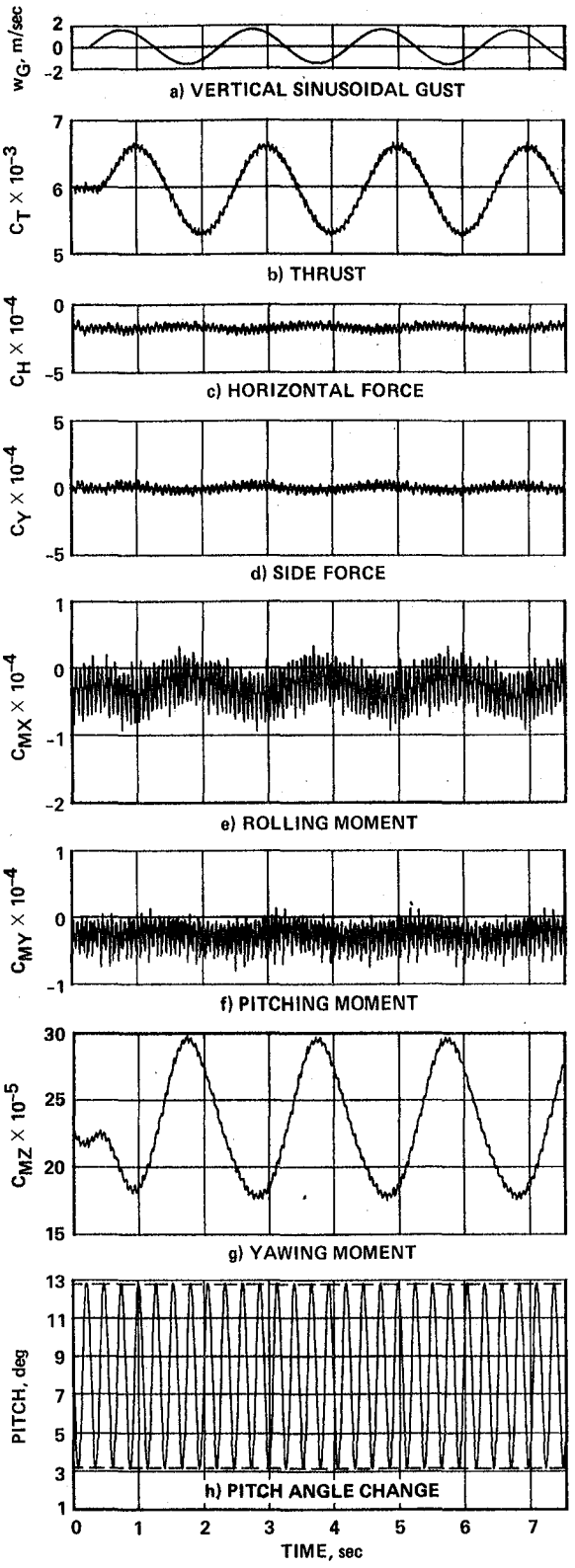

Figure 9.- Time history of hub gust responses without control for a vertical sinusoidal gust: w_{Go} = 1.8 m/sec, f_G = 0.5 Hz, μ = 0.18, Ω = 226 rpm.

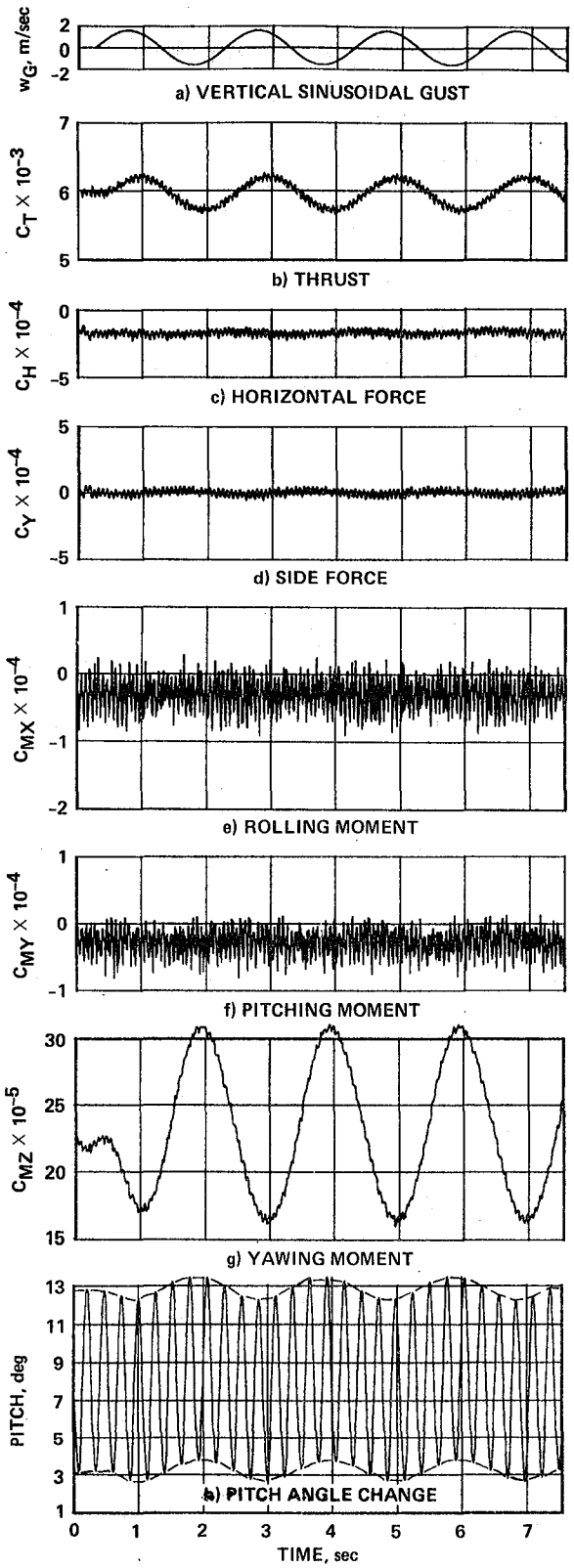

Figure 10.- Time history of hub gust responses with individual blade pitch control for a vertical sinusoidal gust: w_{Go} = 1.8 m/sec, f_G = 0.5 Hz, μ = 0.18, Ω = 226 rpm, K_w = -0.5 rad/m.

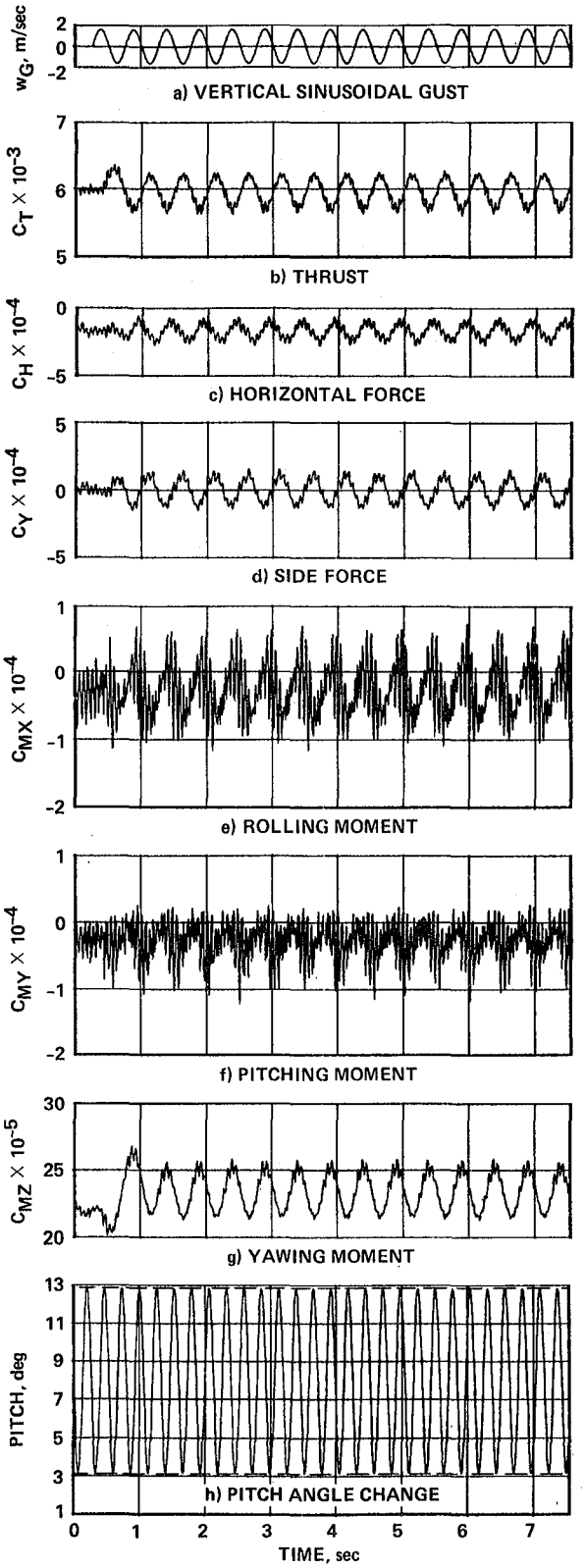

Figure 11.- Time history of hub gust responses without control for a vertical sinusoidal gust: w_{Go} = 1.8 m/sec, f_G = 2.0 Hz, μ = 0.18, Ω = 226 rpm.

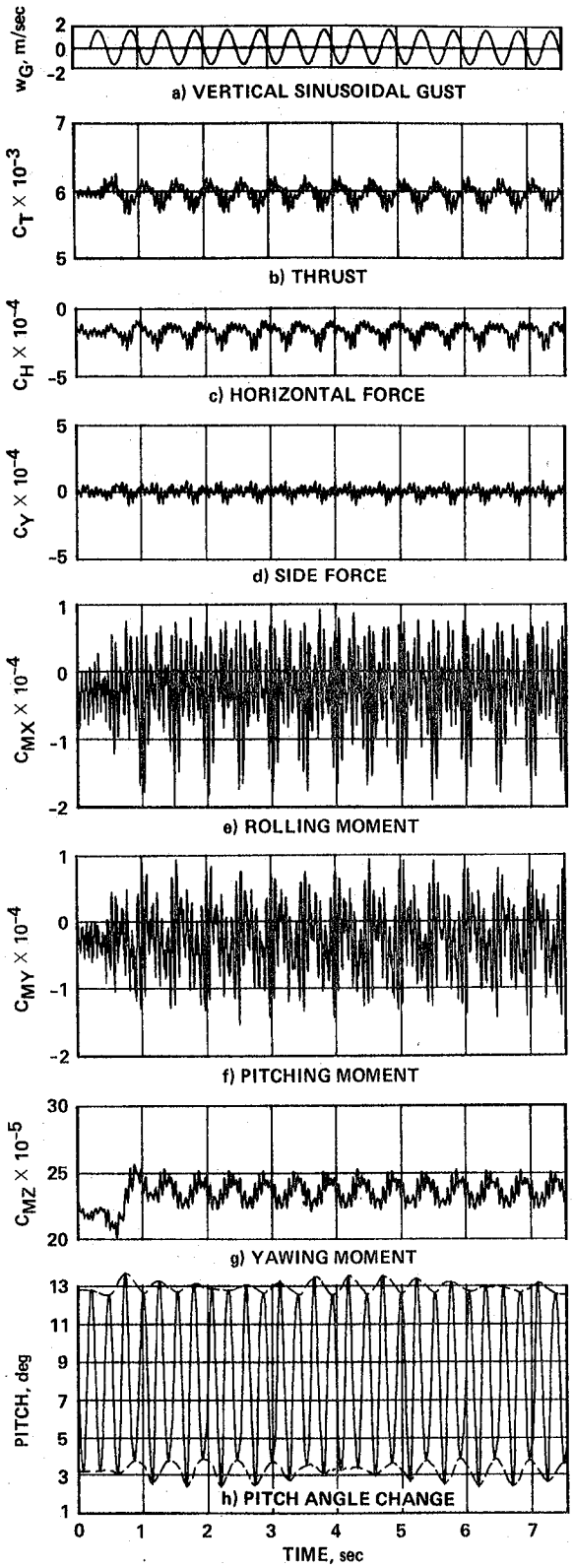

Figure 12.- Time history of hub gust responses with individual blade pitch control for a vertical sinusoidal gust: w_{Go} = 1.8 m/sec, f_G = 0.5 Hz, μ = 0.18, Ω = 226 rpm, K_w = -0.5 rad/m.

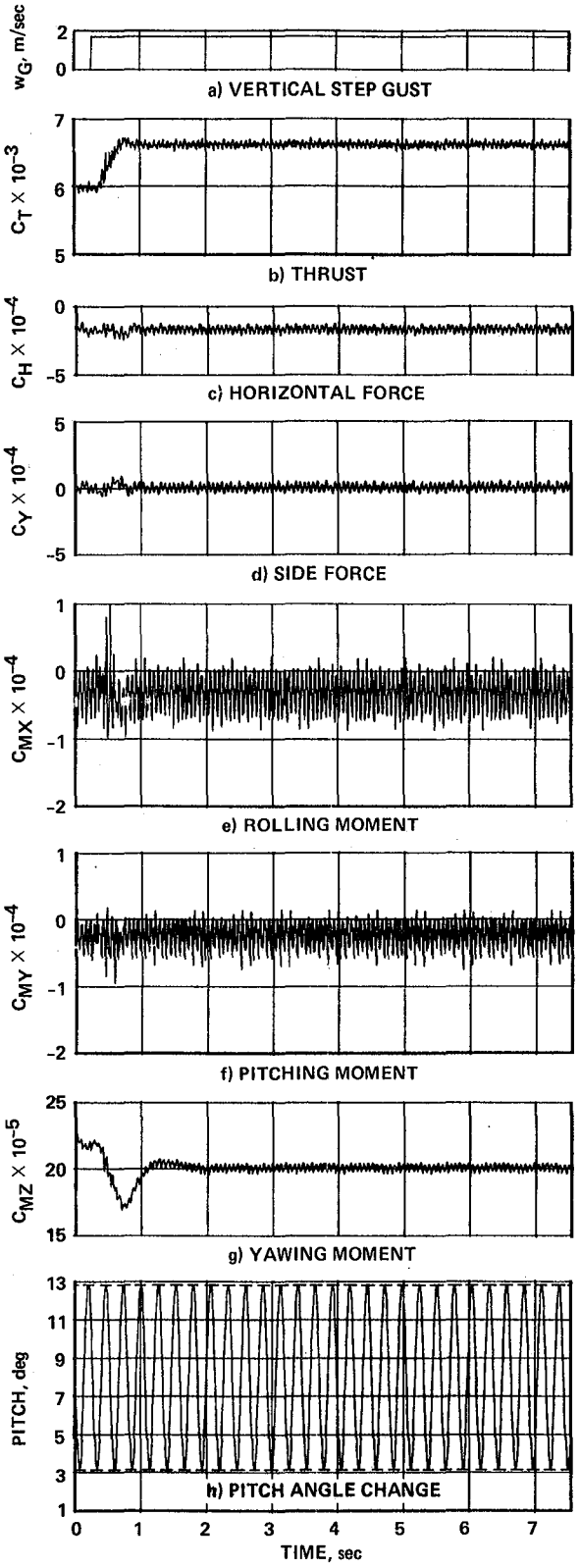

Figure 13.- Time history of hub gust responses without control for a vertical step gust: w_{G_0} = 1.8 m/sec, μ = 0.18, Ω = 226 rpm.

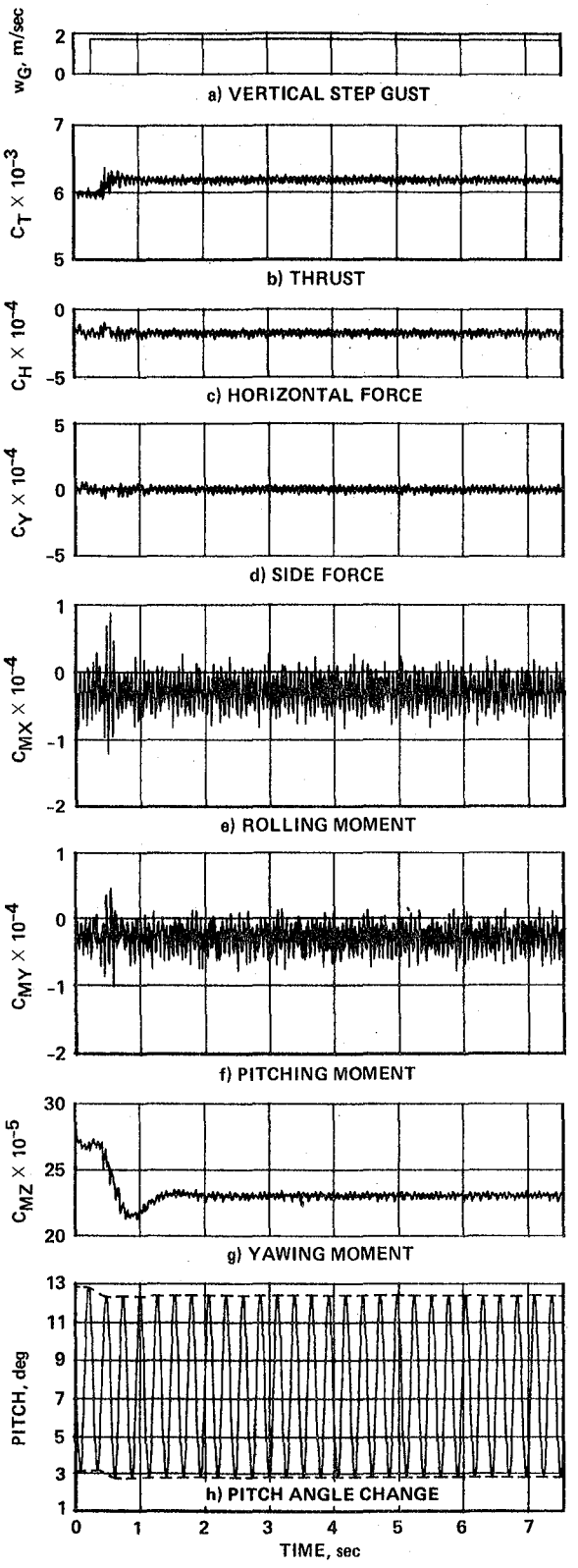

Figure 14.- Time history of hub gust responses with individual blade pitch control for a vertical step gust: w_{Go} = 1.8 m/sec, μ = 0.18, Ω = 226 rpm, K_w = -0.5 rad/m.

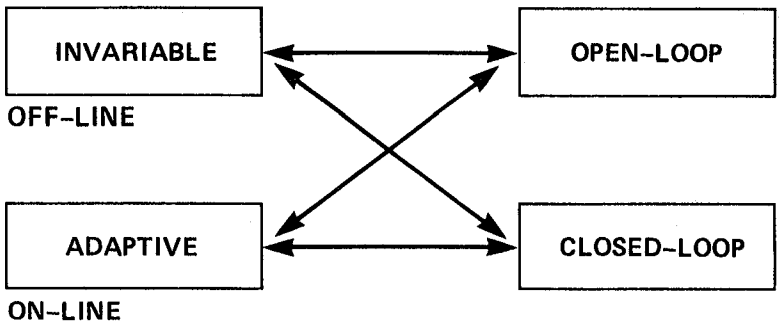

Figure 15.- Four regulator options.

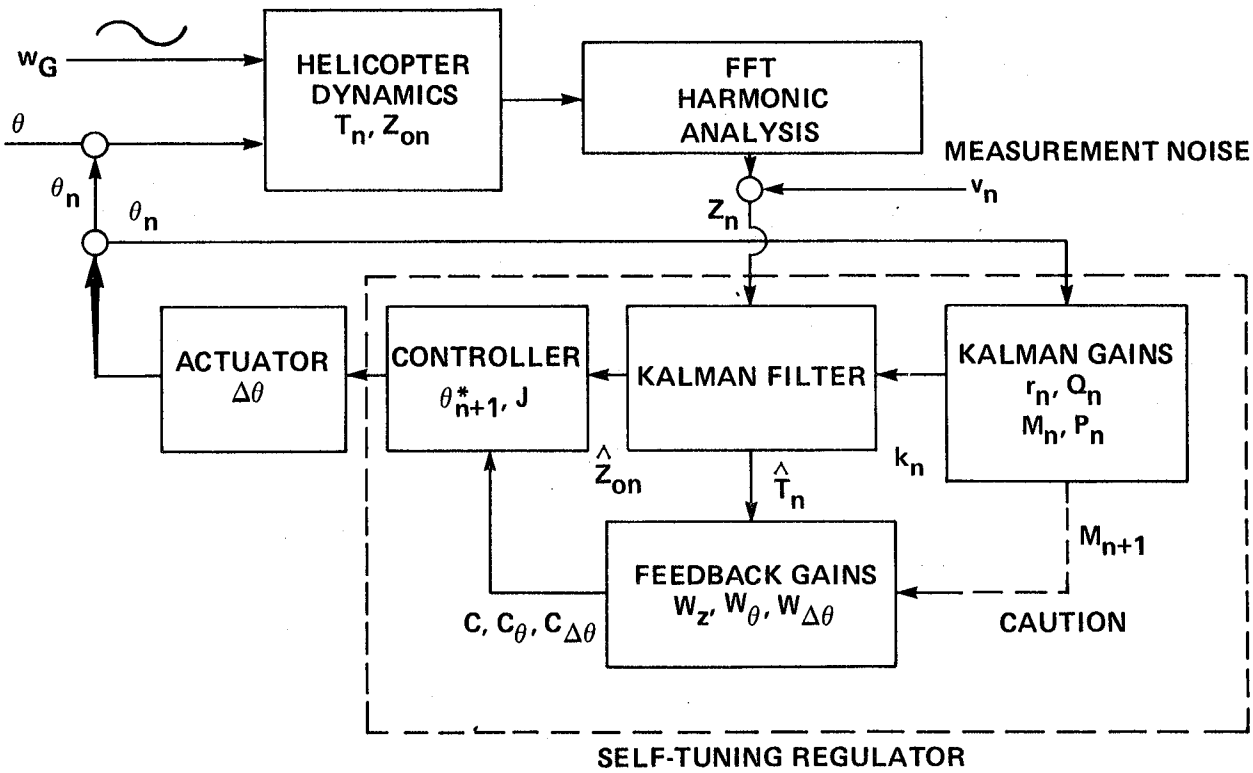

(a) Open-loop regulator.

Figure 16.- Adaptive regulators for gust alleviation.

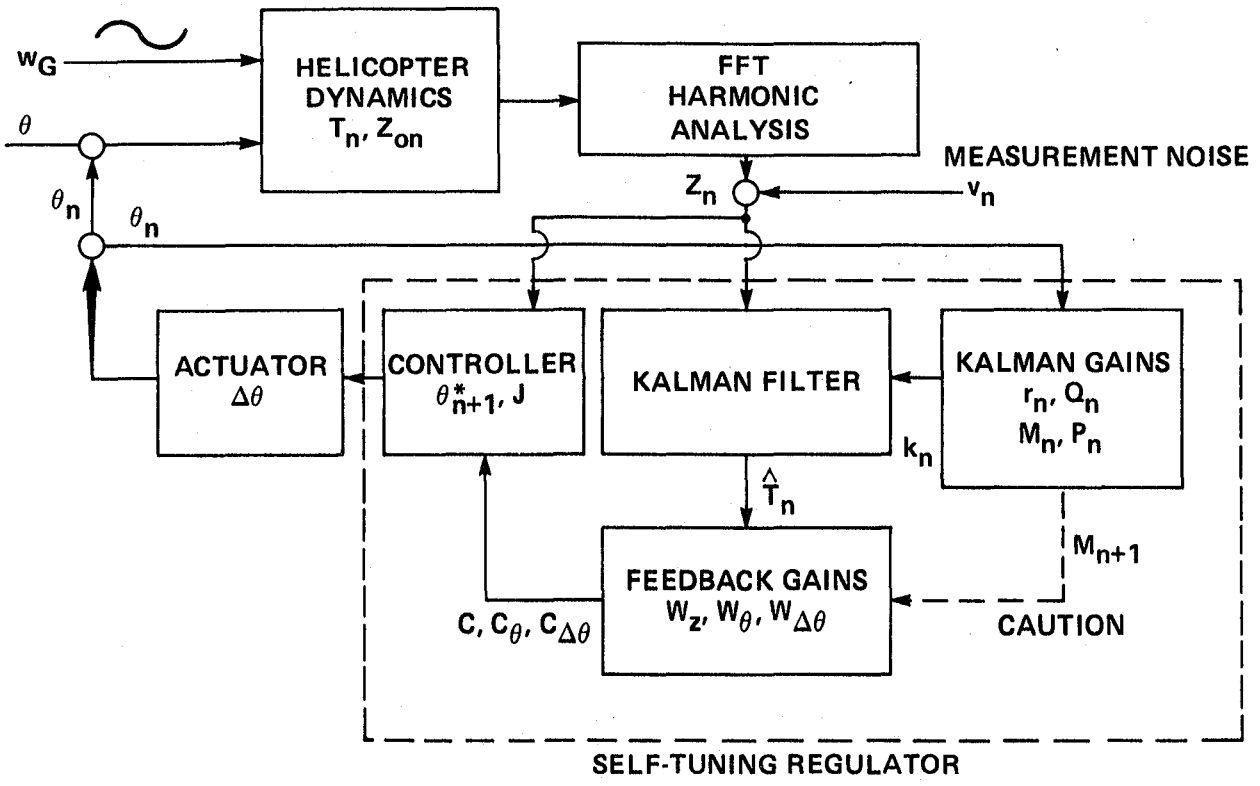

(b) Closed-loop regulator.

Figure 16.- Concluded.

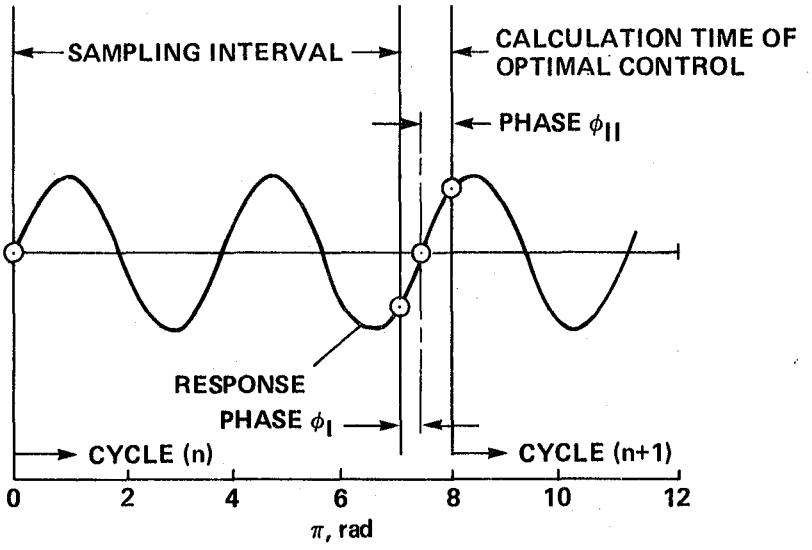

Figure 17.- Sequence of controller implementation.

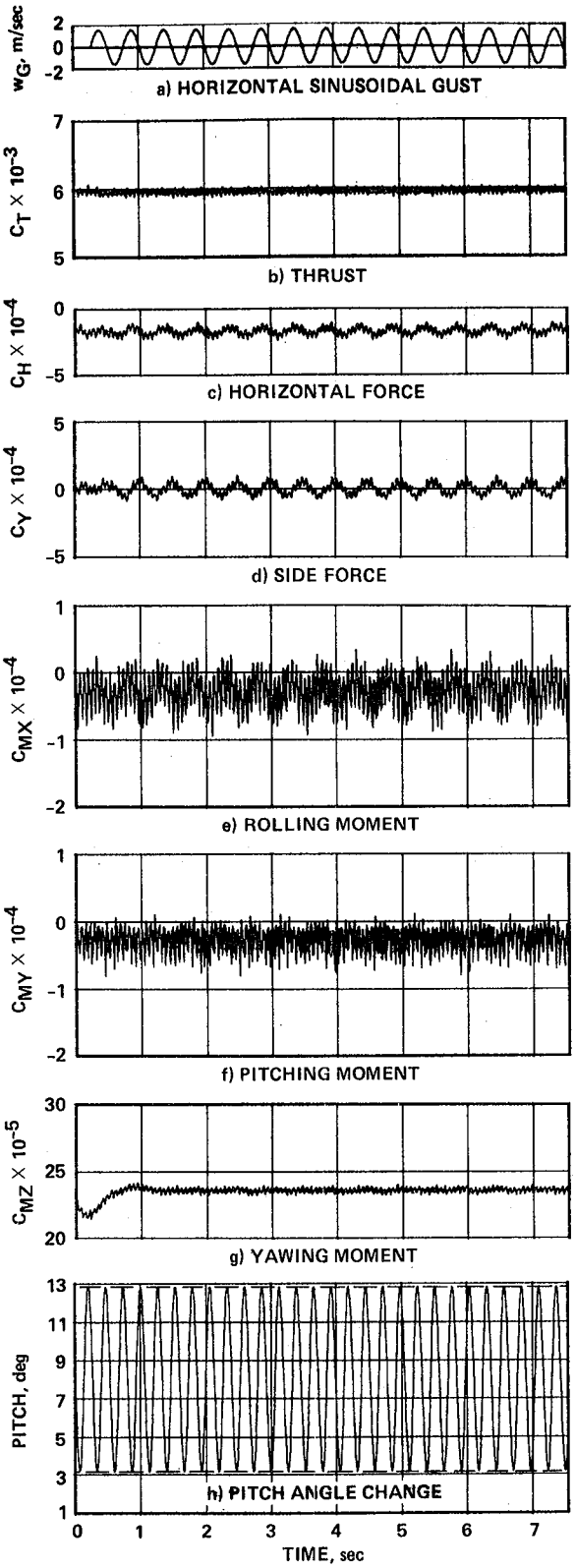

Figure 18.- Time history of hub gust responses without control for a horizontal sinusoidal gust: u_{Go} = 3.0 m/sec, f_G = 2.0 Hz, μ = 0.18, Ω = 226 rpm.

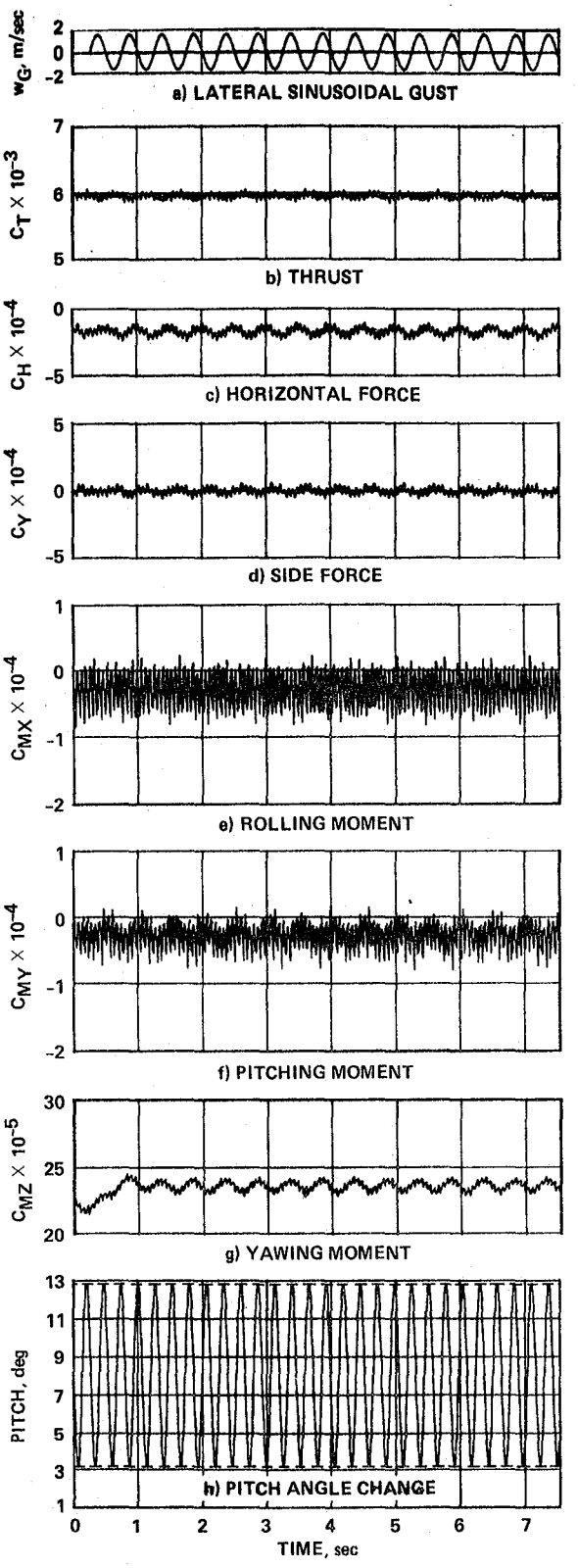

Figure 19.- Time history of hub gust responses without control for a lateral sinusoidal gust: v_{Go} = 2.0 m/sec, f_G = 2.0 Hz, μ = 0.18, Ω = 226 rpm.

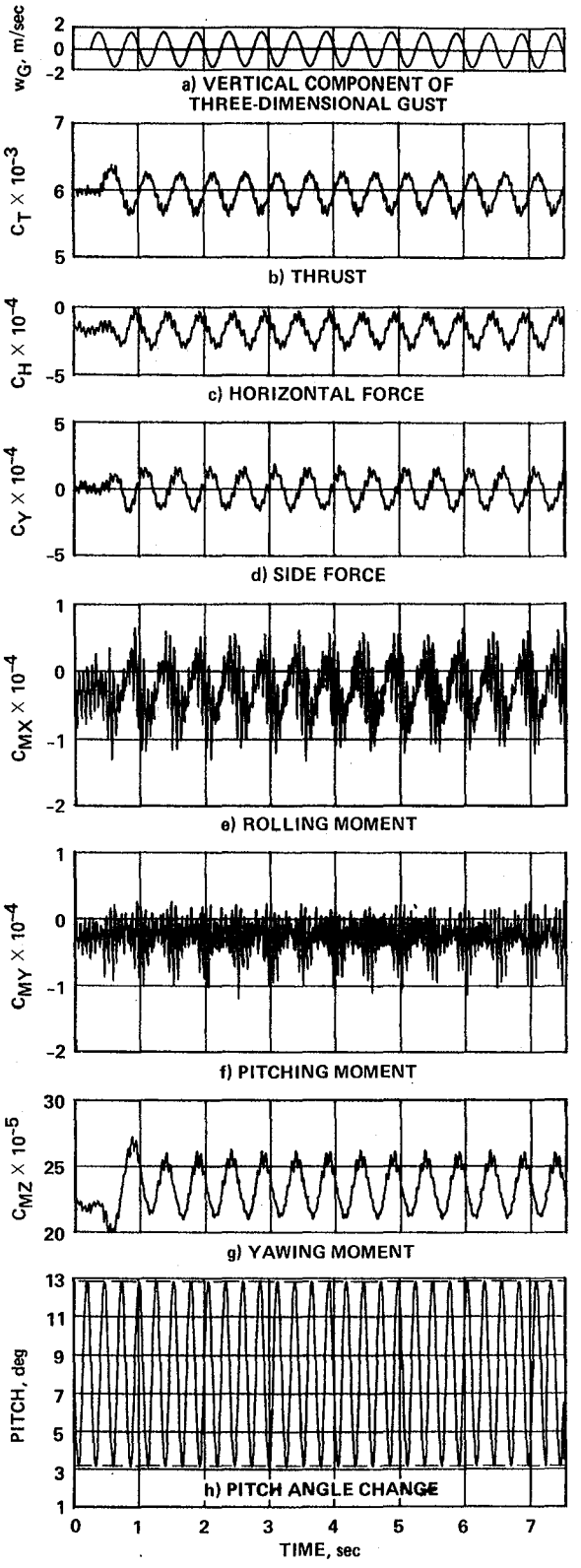

Figure 20.- Time history of hub gust responses without control for three dimensional gust: u_{Go} = 3.0 m/sec, v_{Go} = 2.0 m/sec, w_{Go} = 1.8 m/sec, f_G = 2.0 Hz, μ = 0.18, Ω = 226 rpm.

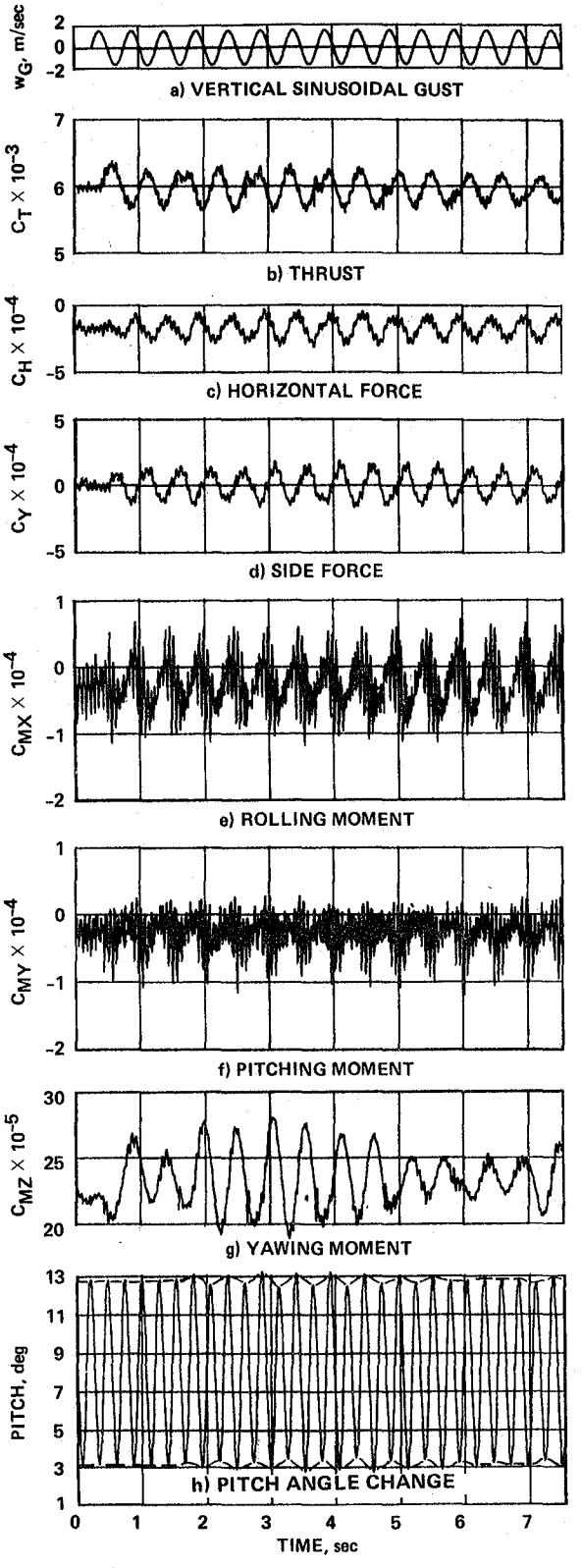

Figure 21.- Time history of hub gust responses with adaptive blade pitch control for a vertical sinusoidal gust. Adaptive open-loop regulator without caution (two inputs, two outputs): w_{Go} = 1.8 m/sec, f_G = 2.0 Hz, μ = 0.18, Ω = 226 rpm.

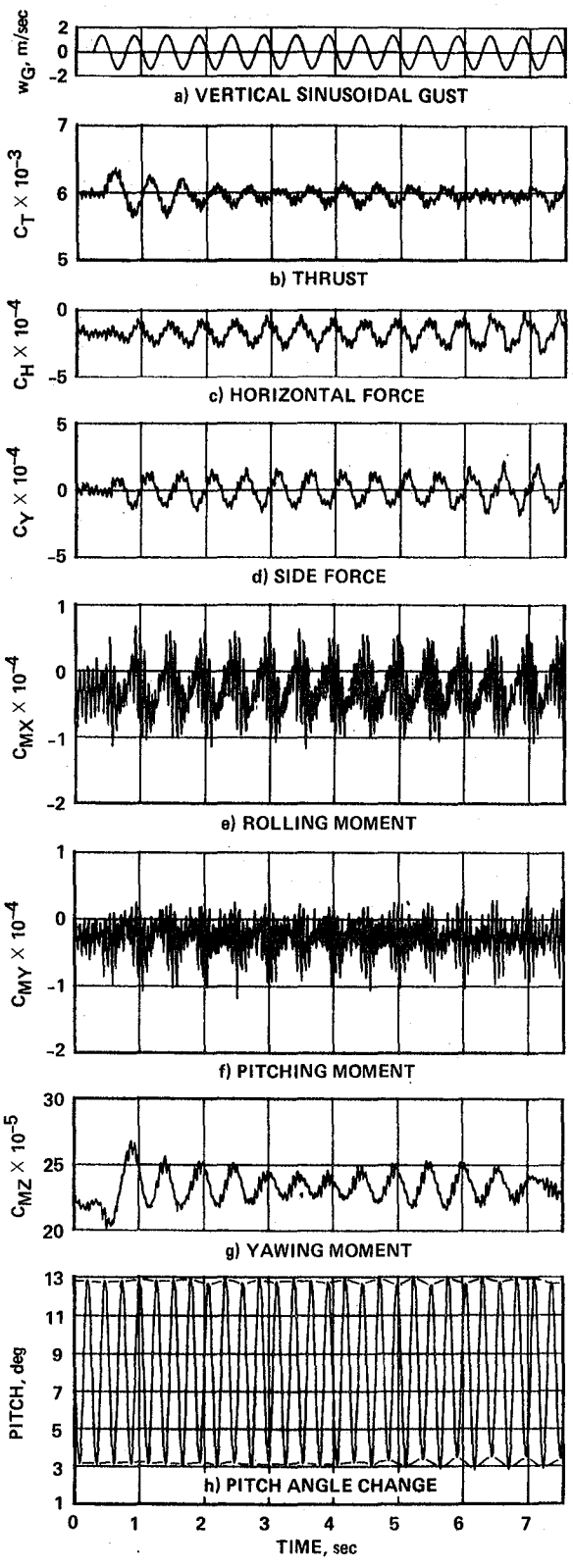

Figure 22.- Time history of hub gust responses with adaptive blade pitch control for a vertical sinusoidal gust. Adaptive open-loop regulator without caution (six inputs, 12 outputs): w_{Go} = 1.8 m/sec, f_G = 2.0 Hz, μ = 0.18, Ω = 226 rpm.

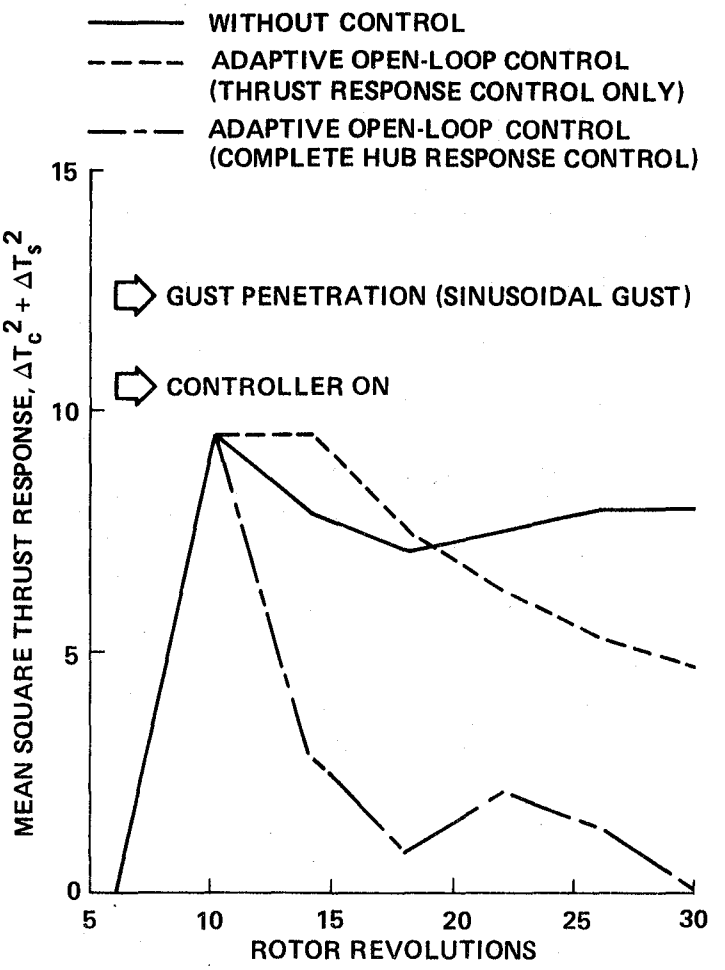

Figure 23.- Time history of the mean square thrust perturbation: f_G = 2.0 Hz, μ = 0.18.

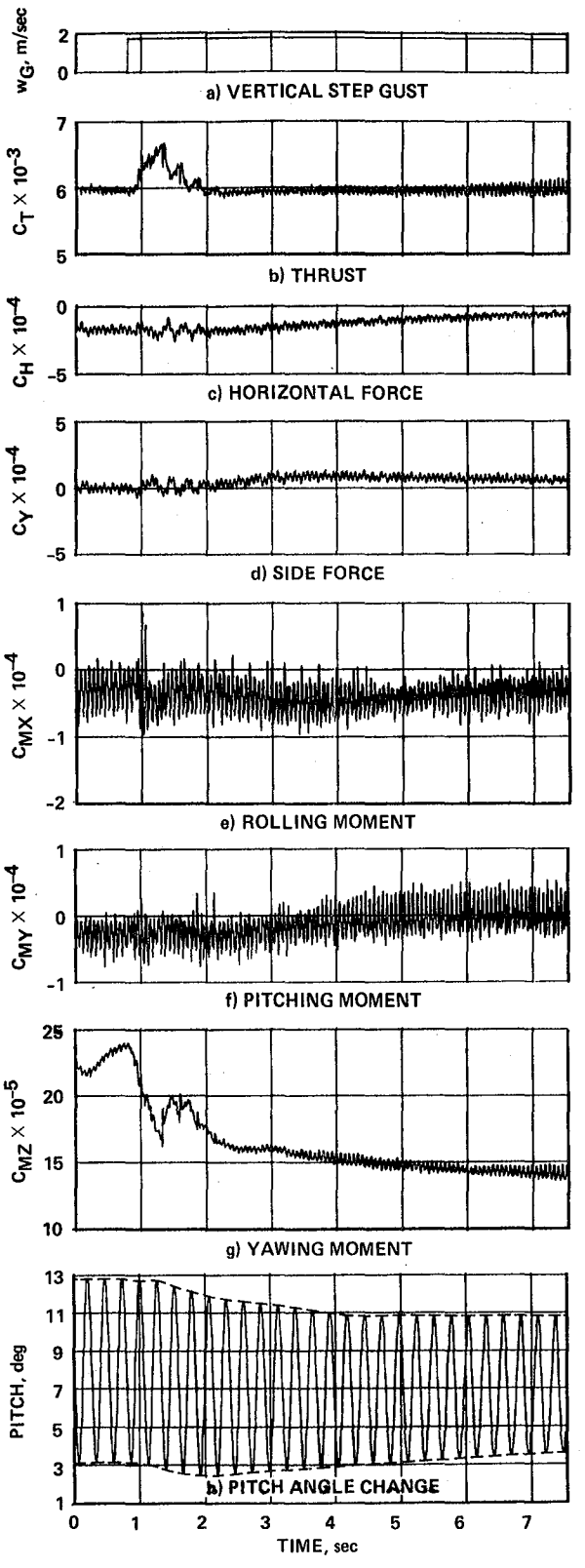

Figure 24.- Time history of hub gust responses with adaptive blade pitch control for a vertical step gust. Adaptive closed-loop regulator without caution (three inputs, three outputs): w_{Go} = 1.8 m/sec, μ = 0.18, Ω = 226 rpm.

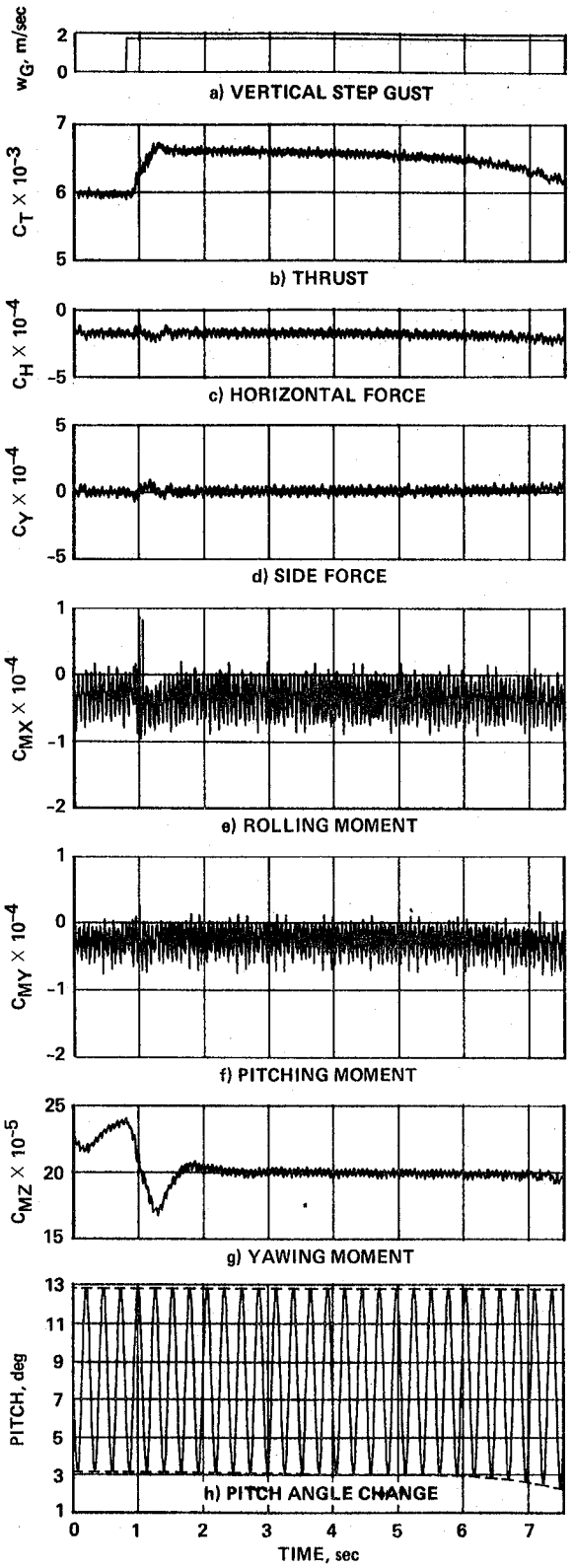

Figure 25.- Time history of hub gust responses with adaptive blade pitch control for a vertical step gust. Adaptive closed-loop regulator without caution (three inputs, three outputs): w_{Go} = 1.8 m/sec, μ = 0.18, Ω = 226 rpm.

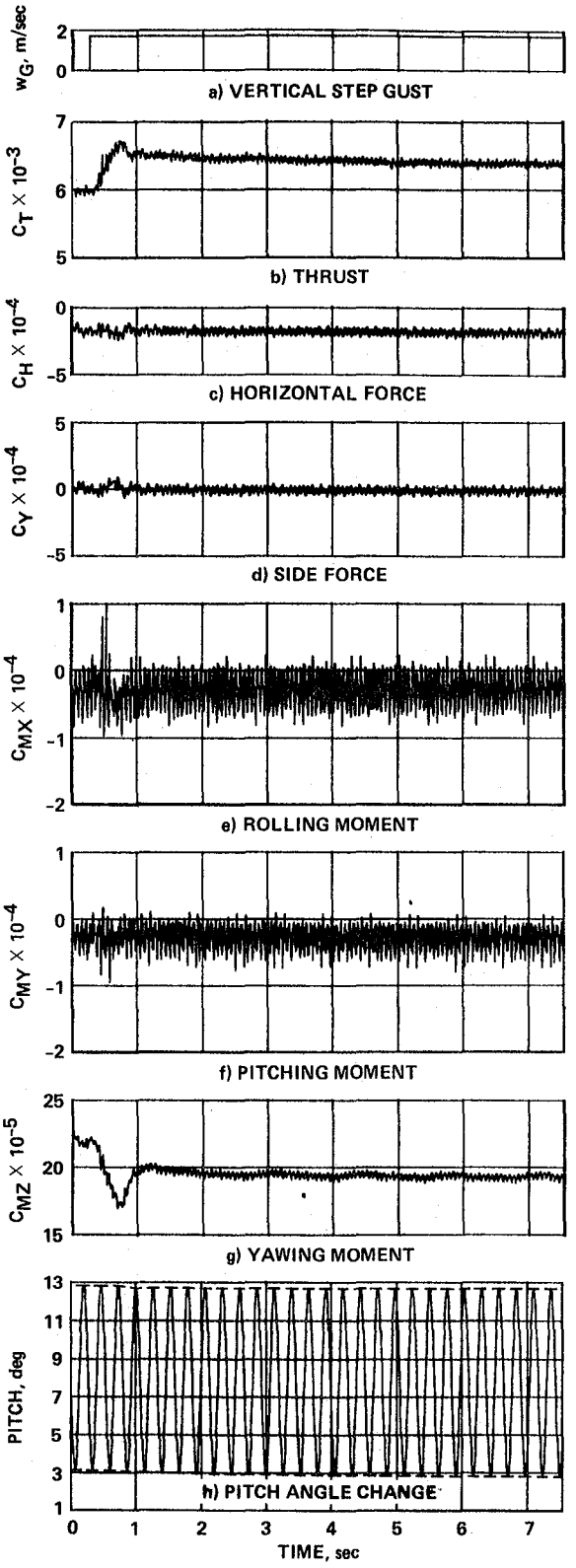

Figure 26.- Time history of hub gust responses with adaptive blade pitch control for a vertical step gust. Adaptive open-loop regulator without caution (three inputs, six outputs): w_{Go} = 1.8 m/sec, μ = 0.18, Ω = 226 rpm.

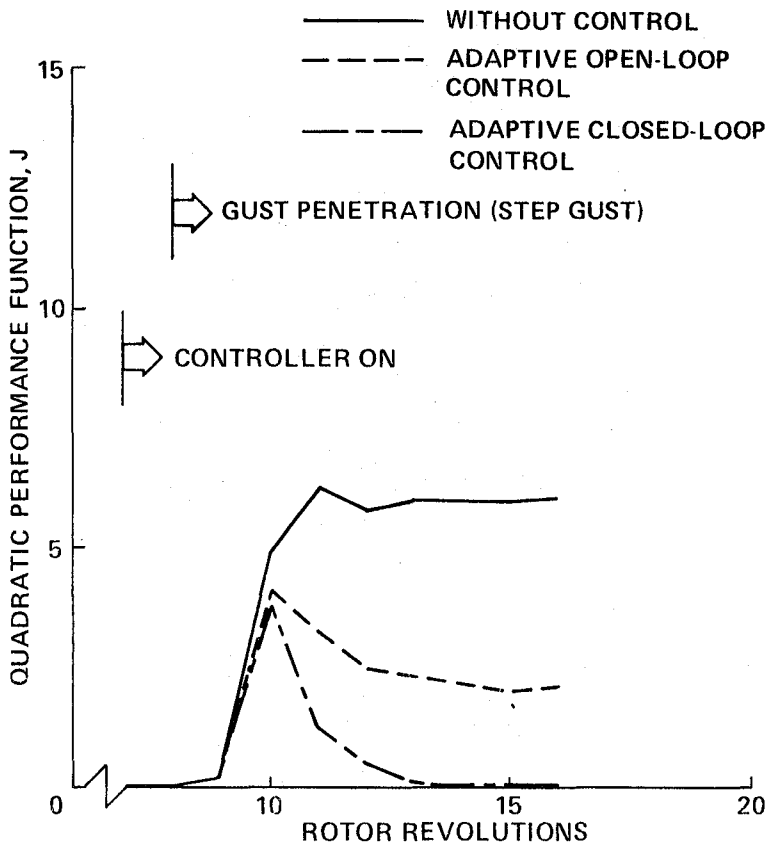

Figure 27.- Time history of quadratic performance function J: w_{Go} = 1.8 m/sec.

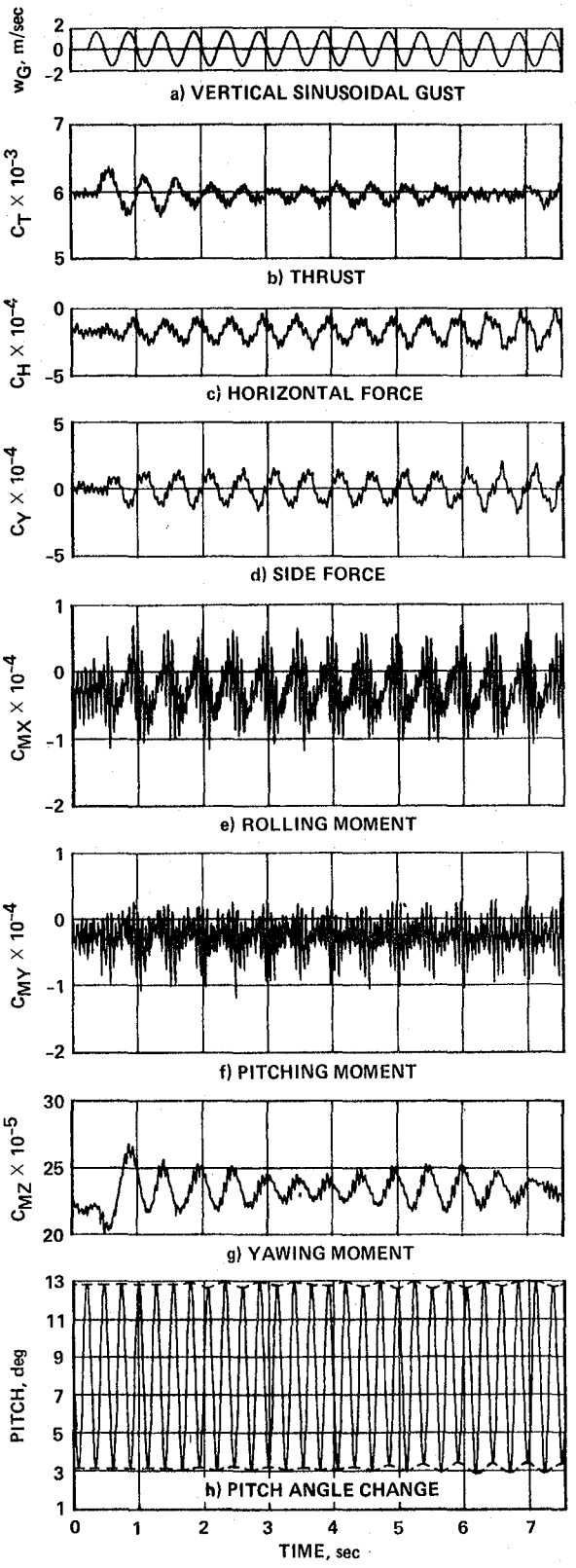

Figure 28.- Time history of hub gust responses with adaptive blade pitch control for a vertical sinusoidal gust. Adaptive open-loop regulator with caution (six inputs, 12 outputs): w_{Go} = 1.8 m/sec, f_G = 2.0 Hz, μ = 0.18, Ω = 226 rpm.

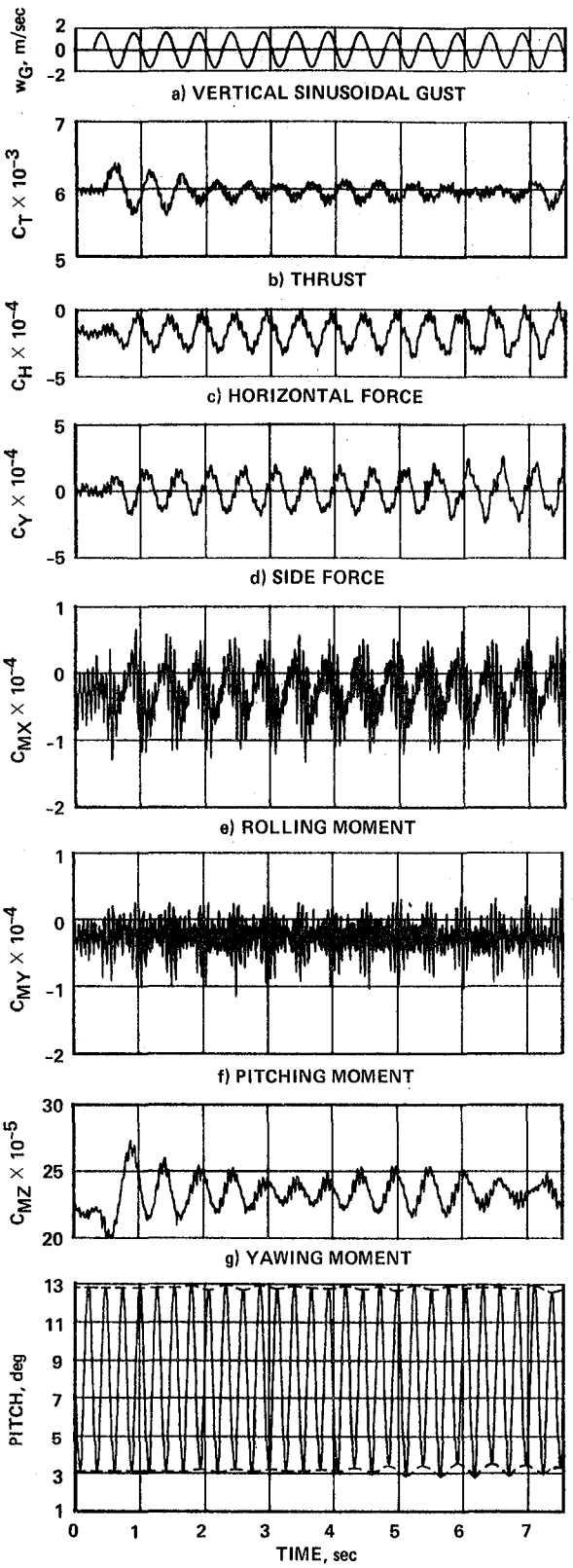

Figure 29.- Time history of hub gust responses with adaptive blade pitch control for three dimensional gust. Adaptive open-loop regulator without caution (six inputs, 12 outputs): u_{Go} = 3.0 m/sec, v_{Go} = 2.0 m/sec, w_{Go} = 1.8 m/sec, f_G = 2.0 Hz, μ = 0.18, Ω = 226 rpm.

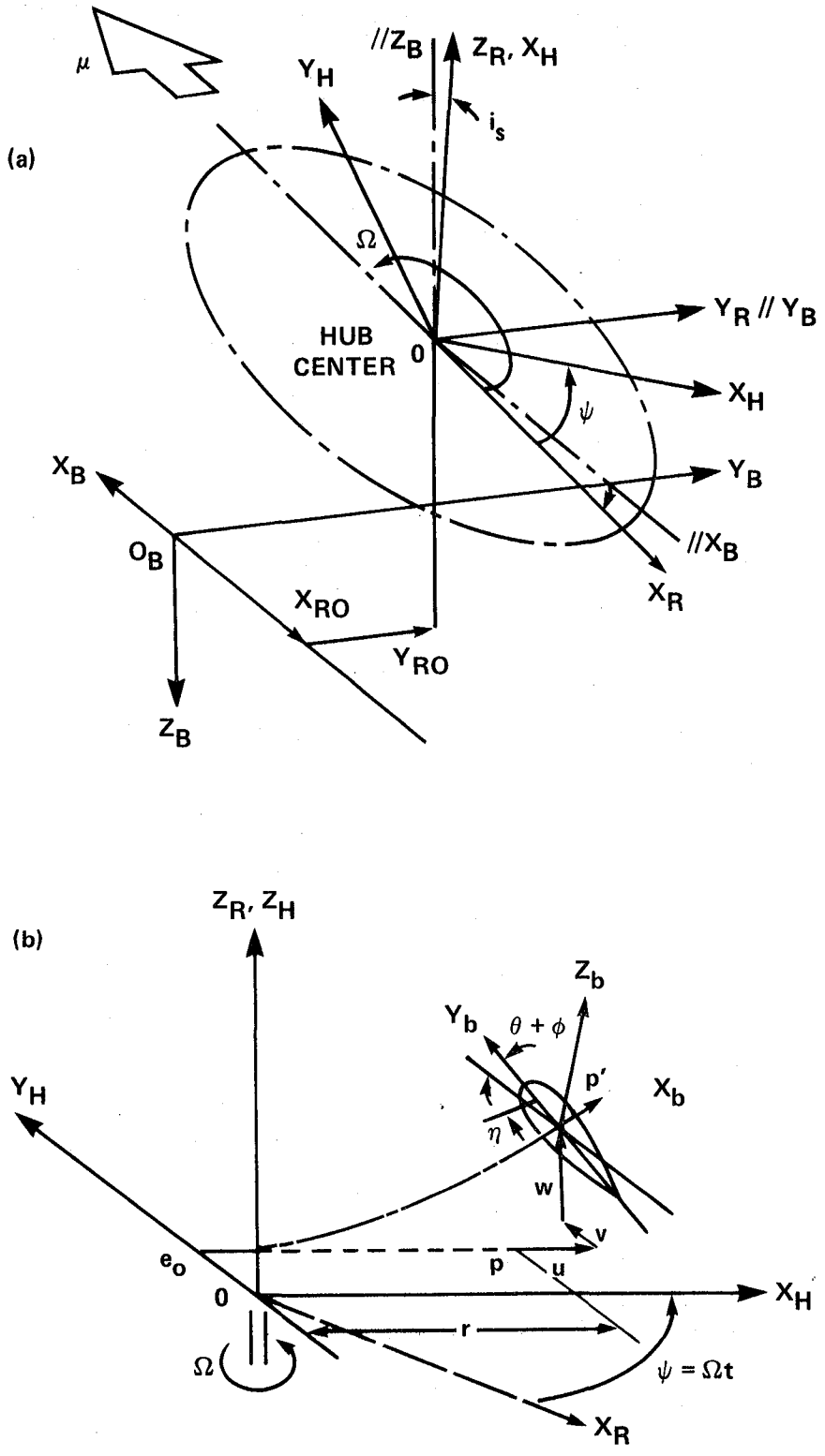

Figure 30.- Coordinate systems.

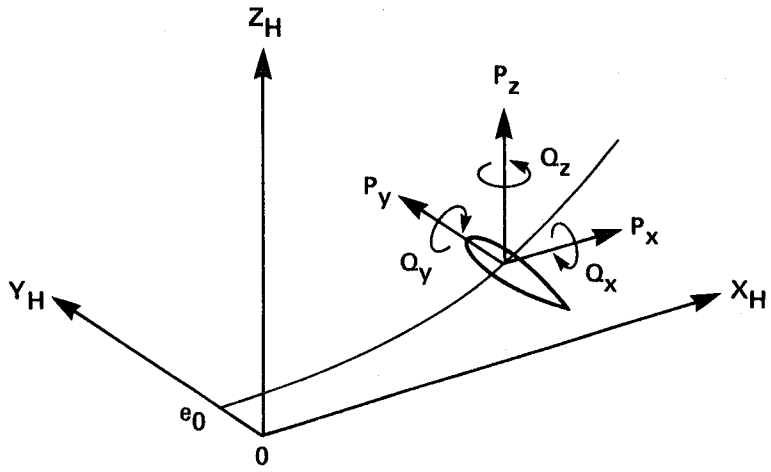

Figure 31.- Blade section loads.

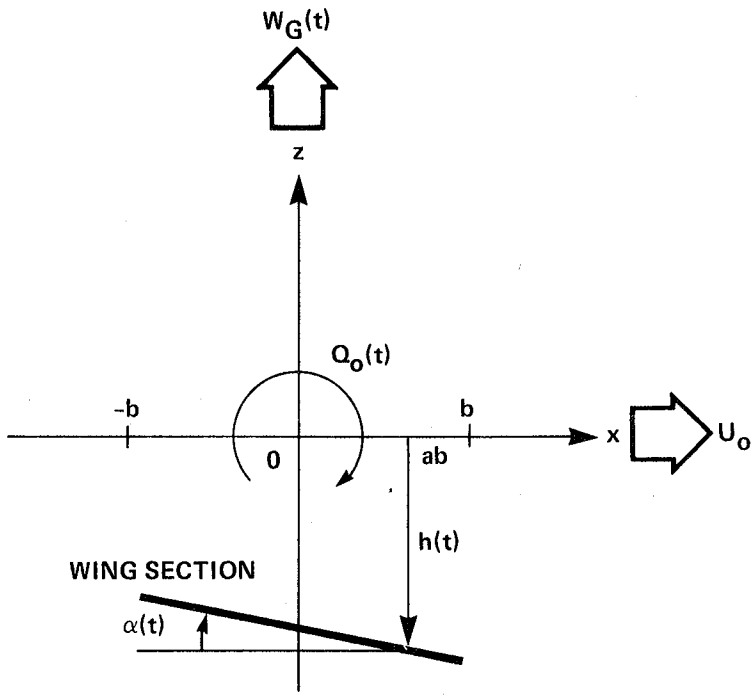

Figure 32.- Two dimensional thin airfoil theory.

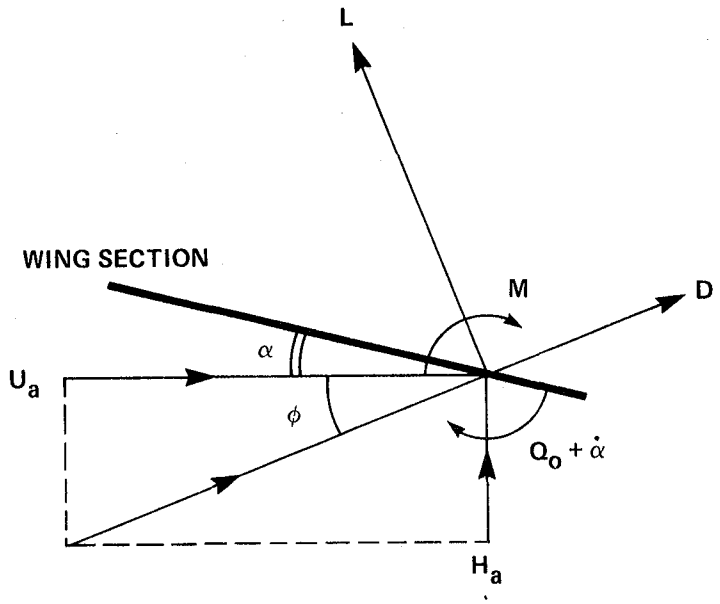

Figure 33.- Schematic view of lift and drag.

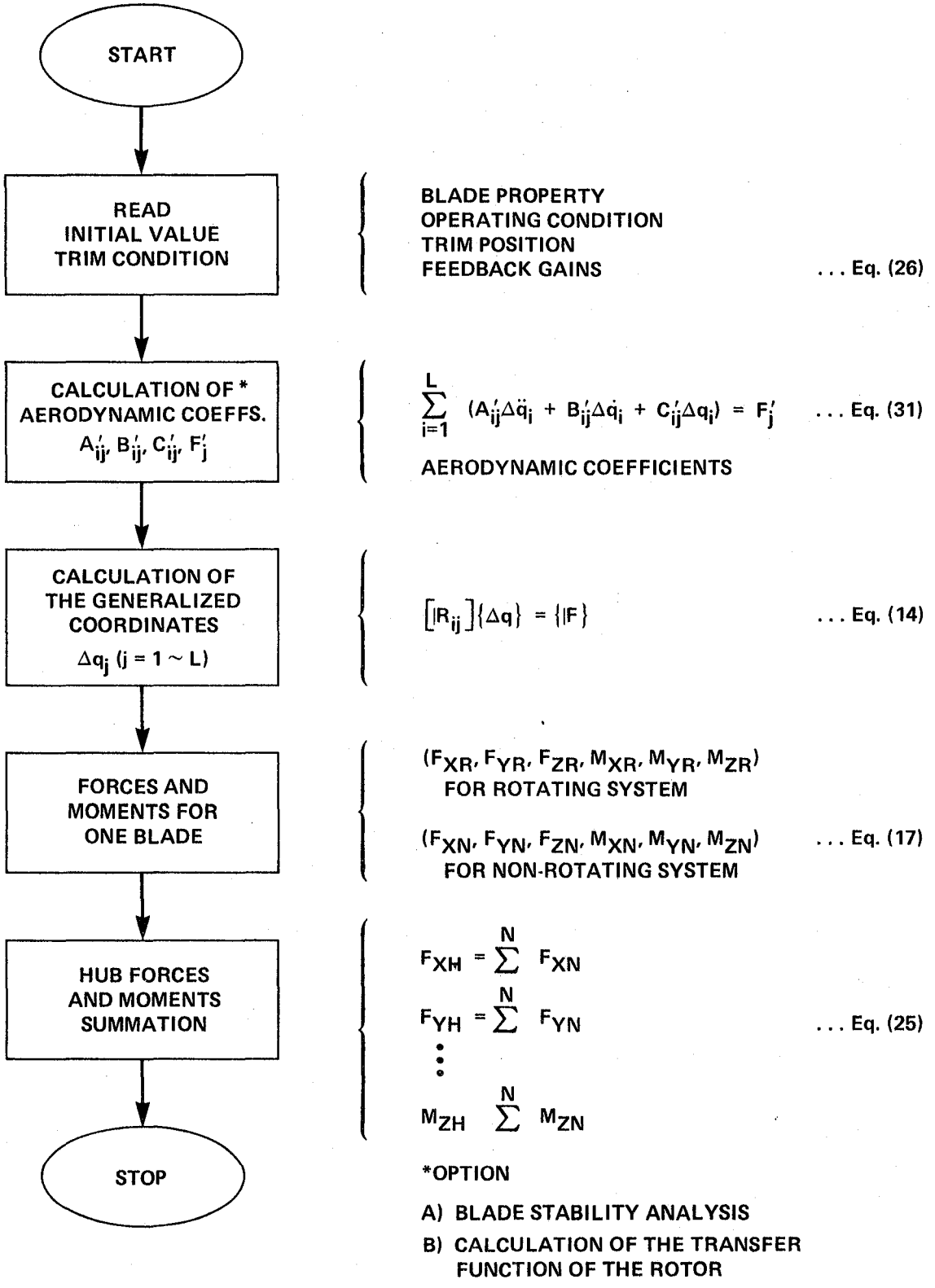

Figure 34.- Flowchart of the programming code.

1. Report No.	2. Government Accession No.	3. Recipient's Catalog No.
NASA TM 85870		

4. Title and Subtitle	5. Report Date
A Study of Helicopter Gust Response Alleviation by Automatic Control	December 1983
	6. Performing Organization Code: ATP

7. Author(s)	8. Performing Organization Report No.
Shigeru Saito	A-9578
	10. Work Unit No.: T-5484A

9. Performing Organization Name and Address	11. Contract or Grant No.
Ames Research Center Moffett Field, California 94035	
	13. Type of Report and Period Covered: Technical Memorandum

12. Sponsoring Agency Name and Address	14. Sponsoring Agency Code
National Aeronautics and Space Administration Washington, DC, 20546	505-42-11

15. Supplementary Notes

Point of contact: William G. Warmbrodt, Ames Research Center, MS 247-1, Moffett Field, CA (415) 965-5642 or FTS 448-5642

16. Abstract

Two control schemes designed to alleviate gust-induced vibration are analytically investigated for a helicopter with four articulated blades. One is an individual blade pitch control scheme. The other is an adaptive blade pitch control algorithm based on linear optimal control theory. In both controllers, control inputs to alleviate gust response are superimposed on the conventional control inputs required to maintain the trim condition. A sinusodial vertical gust model and a step gust model are used. The invidual blade pitch control, in this research, is composed of sensors and a pitch control actuator for each blade. Each sensor can detect flapwise (or lead-lag or torsionwise) deflection of the respective blade. The actuator controls the blade pitch angle for gust alleviation. Theoretical calculations to predict the performance of this feedback system have been conducted by means of the harmonic method. The adaptive blade pitch control system is composed of a set of measurements (oscillatory hub forces and moments), an identification system using a Kalman filter, and a control system based on the minimization of the quadratic performance function. Calculations for the individual blade pitch control system show that the thrust fluctuation can be reduced by more than 50% in the low gust frequency range. In addition, it was found that the adaptive bladepitch control system can also be useful for high frequency gusts.

17. Key Words (Suggested by Author(s))	18. Distribution Statement
Individual blade pitch control and stability analysis Adaptive blade pitch control Gust model	Unlimited Subject Category: 08

19. Security Classif. (of this report)	20. Security Classif. (of this page)	21. No. of Pages	22. Price*
Uncl	Uncl	58	A04

*For sale by the National Technical Information Service, Springfield, Virginia 22161